THE UNIVERSITY OF QUEENSLAND

AUSTRALIA

Mixed Matrix Membranes for Gas Separation

Tuan Manh Vu

Bachelor of Engineering, Master of Science

A thesis submitted for the degree of Doctor of Philosophy at

The University of Queensland in 2019

School of Chemical Engineering

Abstract

Mixed matrix membranes (MMMs) are hybrid membranes, which have been intensively studied and expected to overcome the drawbacks of both polymeric and inorganic counterparts. In fact, MMMs are still facing great challenges, mostly due to the poor compatibility and adhesion between the fillers and polymer matrix, which considerably reduce MMMs separation performance. To address that issue, the work in this thesis focus on modification methods in order to improve the interfacial adhesion between polymer/fillers in the MMMs and consequently enhance the gas separation efficiency of the MMMs.

In the first part of experiment, a non-porous nano-size filler, nanodiamond (ND) was introduced into Pebax copolymer to fabricate the MMM. While being promising filler, the non-porous structure and susceptible to agglomeration of ND are still the issues in gas separation membrane. This chapter proposes an efficient approach as grafting polyethyleneimine (PEI) onto the surface of ND before embedding into the polymer matrix to fabricate the MMMs for CO_2/N_2 separation. The presence of PEI layer on ND surface significantly improved the interfacial adhesion and dispersion of ND in the Pebax matrix, which were clearly indicated by SEM and FIB-SEM observation. The improvement of interfacial interaction led to the increment in CO_2/N_2 selectivity compared to the pristine polymer membranes and the non-PEI MMMs as well. The CO_2/N_2 selectivity of the Pebax/oxND-PEI 0.5 wt.% increased 25% compared to the neat polymer and 43.66% compared to the Pebax/oxND. This chapter has contributed to a simple but effective method to improve the dispersion of the non-porous nanofiller, as well as enhance the gas separation performance of the MMMs.

The next chapter studied the effects of different morphologies of filler on the dispersion, interfacial interaction and gas separation performance of the MMMs. Three types of filler morphologies: conventional polyhedral (P-ZIF), nanorod (R-ZIF) and leaf-shaped nanosheet (L-ZIF) were introduced and investigated. The change in morphology can alter the interfacial interaction between polymer and fillers due to the different aspect ratio and surface structure. The L-ZIF and R-ZIF showed better compatibility with the 6FDA-durene polymer matrix compared to the polyhedral ZIF. L-ZIF improved the gas selectivity of CO_2/N_2 (30.3%), CO_2/CH_4 (40%) compared to the neat polymer, while the R-ZIF enhance the CO_2 permeability (41%) with comparable gas selectivity to the neat polymer. This chapter's results suggested that the nanorod and nanosheet morphologies are more effective in enhancing the interfacial adhesion between polymer/filler and contributed to the guidance in filler morphology selection to achieve improved gas separation performance.

In the following chapter, ZIF nanorod (R-ZIF) was further investigated as the filler and was coated with two types of ILs before incorporated in the the 6FDA-durene matrix. In the previous chapter, while showing compatibility with the 6FDA-durene matrix at low filler loading (10 wt.%), R-ZIF still formed aggregates in the membrane at high loading (20 wt.%) which decrease the gas separation performance of the MMMs. The ionic liquid decoration improved the interfacial interaction between R-ZIF and the polymer matrix leading to the enhancement in gas separation performance of the PR/IL MMMs which was intensively investigated by conventional SEM, FTIR, single and mix gas tests. The most significant improvements were the increment of 50% in CO_2/CH_4 selectivity, while maintaining the CO_2 permeability of the 10 wt.% R-ZIF/IL MMM. The improvement in gas separation efficiency of the IL-incorporated MMMs compared to the non-IL MMMs was still observed even at high loading of filler (20 wt.%). The contribution in this part is to confirm that IL-decoration is an effective approach to enhance the interfacial issues and improve the gas separation efficiency of the MMMs.

In the last experiment section, micron size polyhedral shape ZIF (P-ZIF) was coated with 3 different ILs and dispersed in 6FDA-durene matrix to prepare the MMMs. As investigated in previous experiment section, P-ZIF exhibited the worst interfacial interaction with the polymer matrix among 3 different morphologies. Thus, it is more challenging to obtain excellent filler/polymer contact between micron-sized P-ZIF and polymer matrix and achieve improvement in gas separation efficiency. Acting as the interfacial binder, IL layer has effectively reduced the non-selective interfacial voids in the MMM and enhanced the polymer/P-ZIF adhesion. The vol.% of interfacial voids of the pristine PZ MMM has been reduced from 1.17% to 0.35%, 0.33% and 0.49% with the PZ/IL1, PZ/IL2 and PZ/IL3 MMM, respectively, leading to a significant improvement in gas separation performance, particularly with the CO_2/CH_4 separation performance surpassing the 2008 upper bound. Additionally, the PZ/IL MMMs also showed enhancement in gas separation performance for the CO_2 - CH_4 mix gas (50:50) compared to the non-IL MMMs and the neat polymer membrane. The contribution of this chapter is that it further evidenced the effectiveness of using IL as a interfacial binder to minimize the interfacial defects in MMMs as well as enhance the gas separation performance in both ideal and real conditions.

Declaration by author

This thesis is composed of my original work, and contains no material previously published or written by another person except where due reference has been made in the text. I have clearly stated the contribution by others to jointly-authored works that I have included in my thesis.

I have clearly stated the contribution of others to my thesis as a whole, including statistical assistance, survey design, data analysis, significant technical procedures, professional editorial advice, financial support and any other original research work used or reported in my thesis. The content of my thesis is the result of work I have carried out since the commencement of my higher degree by research candidature and does not include a substantial part of work that has been submitted to qualify for the award of any other degree or diploma in any university or other tertiary institution. I have clearly stated which parts of my thesis, if any, have been submitted to qualify for another award.

I acknowledge that an electronic copy of my thesis must be lodged with the University Library and, subject to the policy and procedures of The University of Queensland, the thesis be made available for research and study in accordance with the Copyright Act 1968 unless a period of embargo has been approved by the Dean of the Graduate School.

I acknowledge that copyright of all material contained in my thesis resides with the copyright holder(s) of that material. Where appropriate I have obtained copyright permission from the copyright holder to reproduce material in this thesis and have sought permission from co-authors for any jointly authored works included in the thesis.

Publications included in this thesis

No publications included

Submitted manuscripts included in this thesis

Manh-Tuan Vu, Rijia Lin, Hui Diao, Zhonghua Zhu, Suresh Bhatia, Simon Smart, EFFECT OF IONIC LIQUIDS ON MOFS/POLYMER INTERFACIAL ENHANCEMENT IN MIXED MATRIX MEMBRANES, Journal of Membrane Science - incorporated as Chapter 6

Contributor	Statement of contribution
Author Manh-Tuan Vu (Candidate)	Concept and designed (60%) Conducted experiment (95%) Analyzed and interpreted data (75%) Wrote and edited the paper (70%)
Author Rijia Lin	Concept and designed (15%) Conducted experiment (5%) Analyzed and interpreted data (20%) Wrote and edited paper (15%)
Author Hui Diao	Analyzed and interpreted data (5%)
Author Zhonghua Zhu	Wrote and edited the paper (5%)
Author Suresh Bhatia	Concept and designed (10%)
Author Simon Smart	Concept and designed (15%) Wrote and edited the paper (10%)

Other publications during candidature

No other publications.

Contributions by others to the thesis

Contributions by A/Prof. Simon Smart, Prof. Suresh Bhatia, Dr. Rijia Lin in concept proposal, experimental design, research data analysis as well as interpretation, drafting revising in the advisory capacity.

Statement of parts of the thesis submitted to qualify for the award of another degree

No works submitted towards another degree have been included in this thesis.

Research Involving Human or Animal Subjects

No animal or human subjects were involved in this research.

Acknowledgements

I would like to express my appreciations to my supervisors, A/Prof. Simon Smart, Prof. Suresh Bhatia and Dr. Rijia Lin for all of their support, encouragement and academic guidance in the past 4 years.

I also would like to express my regards to all other people who supported me during my study

I appreciate the technical support and training by the friendly staffs of The Centre for Microscopy and Microanalysis.

The financial support from Australian Research Council (ARC) Discovery Project and post-graduate scholarship from The University of Queensland are all greatly appreciated.

Many thanks to all my friends in Australia for helping me during my time here. Most of all, I would like to thank all members of my small family: my Mom, my partner, my little baby for their long time encourage, support and love. All my achievements cannot be made without you.

Financial support

This research was supported by an Australian Government Research Training Program Scholarship and Australian Research Council Discovery Project (Grant No. 150101996).

The candidate also acknowledges The University of Queensland postgraduate scholarship.

Keywords

mixed matrix membrane, metal-organic framework, gas separation, interfacial interaction, interfacial voids, focused ion beam scanning electron microscopy

Australian and New Zealand Standard Research Classifications (ANZSRC)

ANZSRC code: 090404, Membrane and Separation Technologies, 60%

ANZSRC code: 091202, Composite and Hybrid Materials, 30%

ANZSRC code: 090401, Carbon Capture Engineering, 10%

Fields of Research (FoR) Classification

FoR code: 0904, Chemical Engineering, 70%

FoR code: 0912, Material Engineering, 30%

Table of Contents

List of Figures

List of Tables

List of abbreviations

PSF : Polysulfone

MOF : Metal organic framework

ZIF : Zeolitic imidazole framework

BET : Brunauer, Emmett, and Teller theory of gas adsorption

6FDA : 4,4' - (hexafluoroisopropylidene)diphthalic anhydride

Durene : 2,3,5,6-tetramethyl-1,3-phenyldiamine

Hmim : 2-methyl imidazole

MMMs : Mixed matrix membranes

SEM : Scanning electron microscopy

FIB-SEM : Focused ion beam scanning electron microscopy

FTIR : Fourier Transform Infrared Spectroscopy

XPS : X-ray Photoelectron Spectroscopy

XRD : X-ray Diffraction

XLPEO: Cross-linked polyethylene oxide

CHAPTER 1. INTRODUCTION

1.1 Background

Membranes are selectively permeable barriers that are used to separate mixtures by allowing the passage of certain components and hindering the passage of others. They have been used very successfully at an industrial scale in water and gas purification for many decades [1]. They typically have a small plant footprint, do not involve a phase change and have lower energy requirements than comparable separation technologies [2]. However, they can be capital intensive and experience a performance trade-off between flux and selectivity which has limited their deployment to specific industrial separations. This is particularly true for polymeric gas separation membranes, where the trade-off is referred to as the Robeson Upper Bound [3]. For the majority of polymers this trade-off is diffusion controlled, although the solubility coefficients are very important in certain classes of polymers such as perfluropolymers [4,5]. One way of 'breaking' the upper bound is to incorporate porous or non-porous fillers into the polymer matrix to improve the gas permeability without sacrificing the selectivity for the components of a gas mixture. [6]. Such membranes were first discussed in the literature in the 1960's but rose to prominence in the late the 1980's where they were commonly termed mixed matrix membranes (MMMs) [7,8]. Since then there has been an explosion of research activities with more than 3000 publications related to MMMs in the Journal of Membrane Science alone. Yet, despite the promise and research MMMs have generally failed to realise their potential to improve the flux / selectivity trade-off [9].

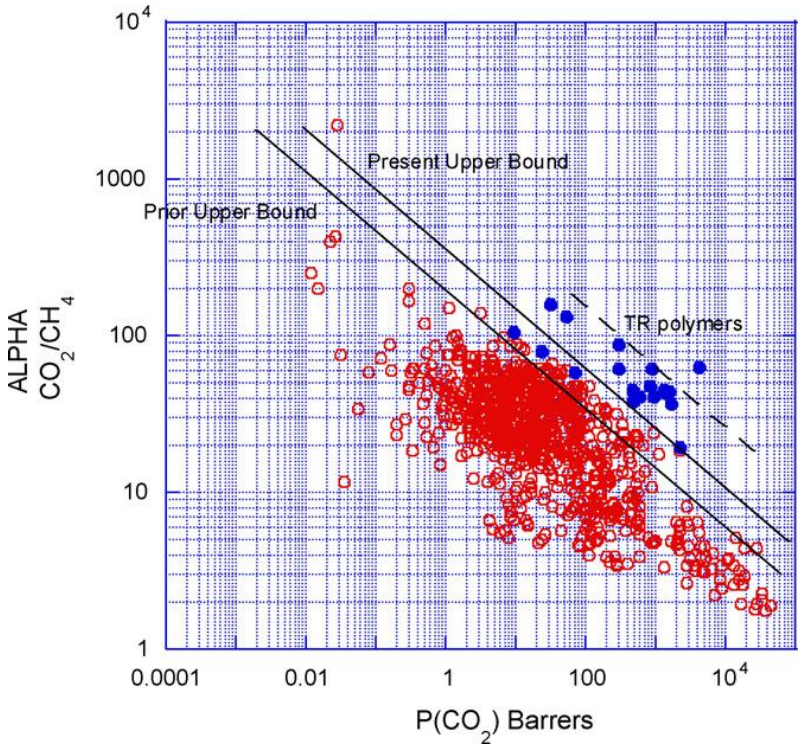

Figure 1.1. Upper bound correlation for CO_2/CH_4 separation [3]

Much of the research activity has focused on choosing or engineering the appropriate filler for a particular gas separation; however, filler dispersion and a poor polymer / filler interface are frequently cited as the largest challenge in making high quality MMMs. There are a myriad of strategies (discussed in detail in Chapter 2) used to overcome these issues but they usually fall into one of two categories: filler compatibilization either through coatings or chemical grafting or the synthesis techniques used to make the MMM, that is the way in which the filler and polymer are mixed prior to casting or spinning [10,11]. This thesis takes the former approach by deploying effective surface coatings on both porous and non-porous fillers. The gas separation pairs of interest relate to the energy and chemicals sectors namely CO_2/N_2 for CO_2 capture in power and industrial applications to mitigate climate change; CO_2/CH_4 for natural gas cleanup and C_3H_6/C_3H_8 which is one of the most important separations for the chemicals industry [1,12–15].

1.2 Research objectives

This project aims to develop mixed matrix membranes with excellent filler/polymer compatibility and high gas separation performance for gas pairs of interest in the energy (CO_2/N_2 and CO_2/CH_4) and chemicals (C_3H_6/C_3H_8) fields. The specific research objectives were to:

- Explore filler compatibilisation strategies to improve the polymer/filler interfacial interactions in MMMs;

- Quantify the degree of dispersion and interfacial void formation for each filler / polymer combination; and
- Evaluate the effects of the various modifications on MMM gas separation performance for both single and mixed gas testing.

1.3 Significance and Contributions to the Field

The significance of this work contained in this thesis lies in the approach taken to improve the compatibility between the filler and polymer matrix in the fabrication of MMM for gas separation applications. The approach was to use relatively inexpensive fillers (nanodiamond and micron-sized MOFs) and explore how the surface decoration and filler morphology affected the filler dispersion, interfacial interactions and gas separation performance of the MMM. An effective strategy which utilized ionic liquids to coat ZIF-67 was developed which improved both the single and mixed gas separation performance of the 6FDA-durene host polymer. There are two key contributions to the field of membranes and gas separation that arise from the work:

- The first relates to how the morphology of the filler affects both the dispersion, interfacial interactions and performance. Whilst the impact of filler aspect ratio on dispersion and mechanical properties in polymer composites has been known in both the material science and MMM fields for some time, it is rare to be able to systematically study a porous filler with different filler morphologies but the same underlying pore size and distribution. As the ZIF-67 filler changes from the traditional polyhedral structure to a rod shape and leaf-sheet shape there are varying edge and aspect ratio effects that altered the way in which the filler and polymer interacted. The rod-like shape (R-ZIF) MMM and leaf-sheet shape (L-ZIF) were more compatible with the 6FDA-durene polymer matrix than the polyhedral shape (P-ZIF). The L-ZIF MMM displayed the best gas separation performance, closely followed by R-ZIF which also had the best dispersion and fewest interfacial voids. Even with no surface modifications the L-ZIF enhanced CO_2/CH_4 selectivity by 20% and the R-ZIF enhanced CO_2 permeability by 40% over the neat polymer.
- The second contribution relates to the use of surface decorations to enhance filler dispersion and improve interfacial interactions in MMMs. Ionic liquids have been used previously with MMM, both as a filler and to help compatibilise another filler into a polymeric matrix. The novelty here is in the choice of filler (micron sized ZIF-67) and the fact that two distinct morphologies of ZIF67 were trialed with ionic liquid decoration. In all cases the ionic liquids trialed improved the dispersion and performance of the MMM at high filler loadings

(ie. 20 wt.%), although the improvement was greater for the R-ZIF MMM (50% for CO_2/CH_4 selectivity) compared to the P-ZIF (41%). The combination of FIB-SEM, single and gas mixture testing results confirmed this was an appropriate method to enhance ZIF67 dispersion in the polymer matrix. This is the first report of ionic liquid decorated micron sized ZIF67 in the public literature.

1.4 Structure of the Thesis

This thesis consists of seven chapters as outlined below. It is structured as a complete thesis although several of the chapters have been or will be submitted for publication. Where this has happened it is noted in the initial "Contribution to the Field" section at the beginning of each research chapter.

Chapter 1 – introduces the relevant background to the thesis, highlighting the critical issues that will be addressed in the form of research objectives. This chapter also contains a summary of the significance of the work and the main contributions to the field.

Chapter 2 – starts with a brief overview of gas separation before exploring the literature regarding mixed matrix membranes. Here the focus is on the choice of filler, synthesis techniques and the state of the art regarding interface modification and MMM performance.

Chapter 3 – describes the preparation and characterization of oxidized and PEI coated nanodiamond for use as a filler in a Pebax polymeric matrix. The resultant MMM was extensively characterized by conventional and FIB-SEM so that the level of filler dispersion and interfacial adhesion could be tied to the CO_2/N_2 gas separation performance for single gas tests.

Chapter 4 – describes the preparation and characterization of three different morphologies of a cobalt based MOF – ZIF67. The morphologies: polyhedral shape (P-ZIF), rod shape (R-ZIF) and leaf-sheet shape (L-ZIF), were extensively characterized for their crystallinity, pore size and distribution before being incorporated into a 6FDA-durene polymer matrix. The resultant MMM was characterized by conventional SEM and FIB-SEM to examine filler dispersion and interfacial adhesion as well as single gas permeation for CO_2/N_2, CO_2/CH_4 and C_3H_6/C_3H_8 single gas tests.

Chapter 5 – furthers the investigation of the rod shaped ZIF67 fillers which proved effective at enhancing MMM performance in chapter 4. Here the R-ZIF filler is coated with two ionic liquids to enhance the interfacial interactions between the polymer and filler. The resultant filler is again extensively characterized before being incorporated into a 6FDA-durene polymer matrix. The

resultant MMM is examined for filler dispersion and interfacial interactions via conventional SEM. Single gas tests for CO_2/N_2, CO_2/CH_4 and C_3H_6/C_3H_8 and a gas mixture test using a 50:50 mixture of CO_2:CH_4 were performed to evaluate the impact of the ionic liquids on membrane performance.

Chapter 6 – is the final research chapter wherein the hypothesis developed at the end of chapter 5, that coating ZIF67 with small quantities of ionic liquids enhances dispersion, improves interfacial interactions and gas performance, is further tested with the polyhedral shaped ZIF67 (P-ZIF). In this instance 3 ionic liquids are trialed to compatibilise the P-ZIF with the 6FDA-durene polymer matrix. Conventional SEM and FIB-SEM are used to evaluate filler dispersion and interfacial interactions whilst single (CO_2/N_2, CO_2/CH_4 and C_3H_6/C_3H_8) and mixed gas (50:50 mixture of CO_2:CH_4) tests were performed to evaluate the impact on membrane performance.

Finally, **Chapter 7** presents the overall conclusions and recommendations for possible future works.

Reference

[1] M. Galizia, W.S. Chi, Z.P. Smith, T.C. Merkel, R.W. Baker, B.D. Freeman, 50th Anniversary Perspective: Polymers and Mixed Matrix Membranes for Gas and Vapor Separation: A Review and Prospective Opportunities, Macromolecules. 50 (2017) 7809–7843.

[2] Z. Low, P.M. Budd, N.B. Mckeown, D.A. Patterson, Gas Permeation Properties , Physical Aging , and Its Mitigation in High Free Volume Glassy Polymers, Chem. Rev. 118 (2018) 5871–5911.

[3] L.M. Robeson, The upper bound revisited, J. Memb. Sci. 320 (2008) 390–400.

[4] I.P. T.C. Merkel R. Prabhakar, B.D. Freeman, Gas and Vapor Transport Properties of Perfluoropolymers, in: I.P. B.D. Freeman Y. Yampolskii (Ed.), Mater. Sci. Membr. Gas Vap. Sep., John Wiley & Sons, New York, 2006.

[5] V.B. T.C. Merkel K. Nagai, B.D. Freeman, Hydrocarbon and Perfluorocarbon Gas Sorption in Poly(dimethylsiloxane), Poly(1-trimethylsilyl-1-propyne), and Copolymers of Tetrafluoroethylene and 2,2-Bis(trifluoromethyl)-4,5-difluoro-1,3-dioxole, Macromolecules. 32 (1999) 370–374.

[6] W.J. Koros, C. Zhang, Materials for next-generation molecularly selective synthetic membranes, Nat. Mater. 16 (2017) 289–297.

[7] R.M. Barrer, J.A. Barrie, N.K. Raman, Solution and Diffusion in Silicone Rubber I - A comparison with natural rubber, Polymer 3 (1962) 595–603.

[8] R.M. Barrer, J.A. Barrie, N.K. Raman, Solution and diffusion in silicone rubber II-The influence of fillers, Polymer (Guildf). 3 (1962) 605–614.

[9] M.R.A. Hamid, H. Jeong, Recent advances on mixed-matrix membranes for gas separation : Opportunities and engineering challenges, Korean J. Chem. Eng., 35(8) (2018) 1577–1600.

[10] M. Rezakazemi, A. Ebadi Amooghin, M.M. Montazer-Rahmati, A.F. Ismail, T. Matsuura, State-of-the-art membrane based CO 2 separation using mixed matrix membranes (MMMs): An overview on current status and future directions, Prog. Polym. Sci. 39 (2014) 817–861.

[11] G. Dong, H. Li, V. Chen, Challenges and opportunities for mixed-matrix membranes for gas

separation, J. Mater. Chem. A. 1 (2013) 4610–4630.

[12] T.C. Merkel, H. Lin, X. Wei, R. Baker, Power plant post-combustion carbon dioxide capture : An opportunity for membranes, J. Memb. Sci. 359 (2010) 126–139.

[13] J.K. Adewole, A.L. Ahmad, S. Ismail, C.P. Leo, Current challenges in membrane separation of CO2 from natural gas: A review, Int. J. Greenh. Gas Control. 17 (2013) 46–65.

[14] K.A. Lokhandwala, I. Pinnau, Z. He, K.D. Amo, A.R. Dacosta, J.G. Wijmans, R.W. Baker, Membrane separation of nitrogen from natural gas : A case study from membrane synthesis to commercial deployment, J. Membr. Sci. 346 (2010) 270–279.

[15] R.L. Burns, W.J. Koros, Defining the challenges for C3H6/C3H8 separation using polymeric membranes, J. Membr. Sci. 211 (2003) 299–309.

CHAPTER 2. LITERATURE REVIEW

This chapter contains a literature review which focuses on membranes for gas separation. A brief state of the art review relevant to the specific topic is also provided as an introduction to each research chapter. In this chapter, an initial overview of current gas separation techniques leads into an overview of membranes for gas separation which explores the theory of gas transport through polymeric membranes. Mixed matrix membranes are introduced with detailed sections on filler types, synthesis techniques and the current state of the art performance. CO_2 separation from N_2 or CH_4 is the primary focus of the membranes discussed in this chapter, although other target gas pairs are also discussed. Finally the challenges associated with mixed matrix membranes are discussed with a specific focus on improving polymer/filler interfacial interactions. The chapter concludes with a summary that outlines the research gaps and highlights the areas to which this thesis contributes.

2.1 Current techniques for gas purification

The separation and purification of gas mixtures is one of the most critical processes in many industrial applications including the production of energy, chemicals and petroleum products. There are a wide range of gas purification technologies that have been commercially deployed: absorption, adsorption, cryogenic distillation and membrane separation (Figure 2.1).

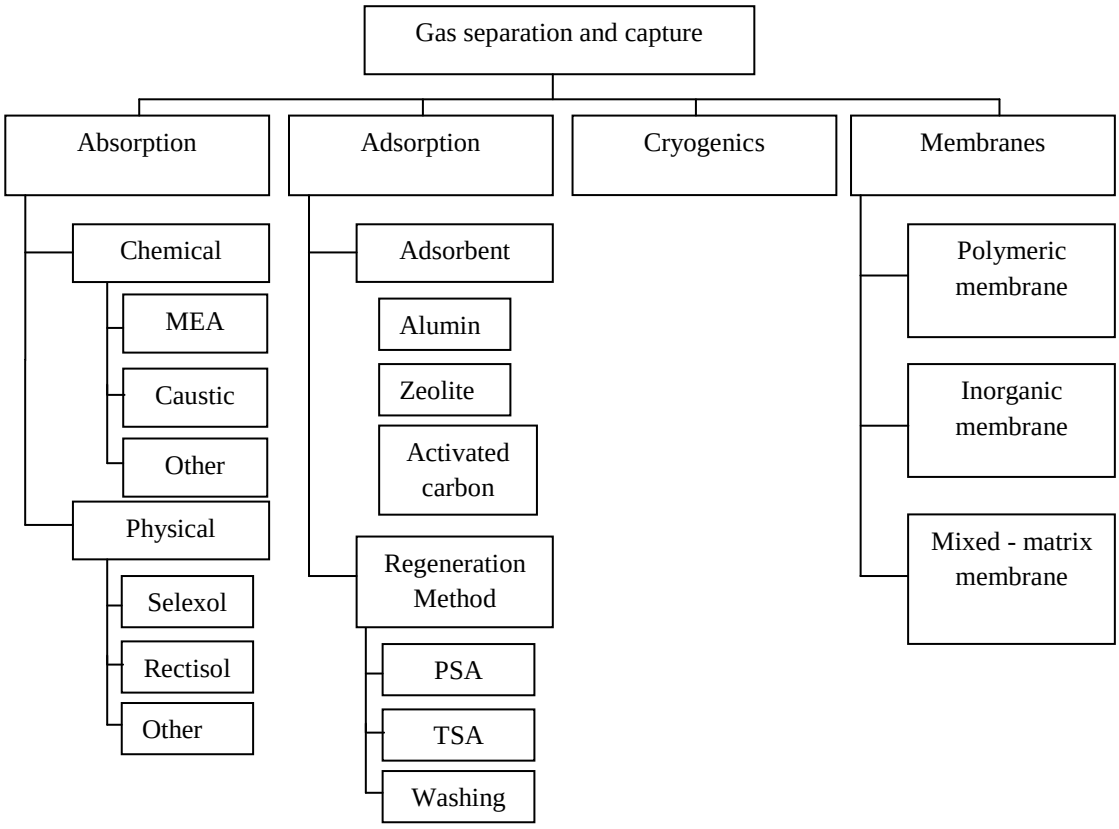

Figure 2.1. **Technology options for gas separation and capture**

2.1.1 Absorption

Absorption is perhaps the primary gas separation technique, widely applied in both the chemical and petroleum industries [1]. This involves the physical dissolution of gases in solvents or by combining dissolution with chemical reaction in the liquid phase [2]. Amine compounds are among the more common absorbents used although aqueous ammonia, Selexol and Rectisol have also been used commercially for acid gas removal or CO_2 capture from natural gas or flue gas streams [2–4]. Recently, ionic liquids have attracted attention with great potential in gas absorption with less environmental impacts [5,6]. The key benefit of the absorption processes is that it is a widely applied technology which can minimize the hydrocarbon loss. Gas absorption comprises at about 70% of the techniques used for natural gas treatment [7]. However, while aqueous amine solutions are effective for gas absorption under a variety of conditions, this process often suffers from issues with corrosion, amine degradation and solvent losses as well as being very energy intensive [8]. Moreover, the organic solvents used in the absorption processes can cause serious environmental problems if the recycle processes and post - absorption solvent treatment are not carefully executed.

2.1.2 Adsorption

Adsorption is a circular process which flows the gas mixture through a packed bed of solid porous adsorbents such as zeolites or activated carbon, on the surface of which the gas is adsorbed. The solid is then regenerated using either pressure (vacuum and pressure swing adsorption), temperature (thermal swing adsorption) or electrical swing adsorption while the desorbed gases are compressed for storage or vented [9]. Some common solid adsorbents include activated carbon, silica gel, ion-exchange resins, zeolites and mesoporous silicates. Recently, metal-organic frameworks (MOFs), a promising new type of adsorbent have been developed for the gas separation. Though adsorption has been currently applied in some large-scale gas separations such as air separation using pressure swing adsorption, the low adsorption capacity and/or slow kinetics of many of the adsorbents are still a huge challenge [9], which leads to high capital costs and operational costs.

2.1.3 Cryogenic

Cryogenic separation, which largely takes the form of distillation of liquefied gas mixtures has been implemented industrially for decades. This type of technique is widely used for separating light alkanes, O_2 / N_2 from air, and in more recent years for CO_2 capture from gas mixtures with high CO_2 concentration (>90%), but not for more dilute CO_2 streams [10]. One benefit of cryogenic separation is that it can directly produce liquified gas, which is the requirement in some specific transport options. A major drawback of cryogenic separation is that it is energy intensive which make it less desirable for commercial and industrial applications. Water vapor, which exists in some gas mixtures, need to be removed before carrying out the process to avoid blockages [10].

2.2 Gas separation by membranes

Membranes separate gas mixtures based on the different interactions of each gas with the membrane materials and are driven by the chemical potential gradient, which manifests as the partial pressure difference between the feed and permeate sides of the membrane. This allows some components to preferentially permeate through the membranes while excluding the others based on size (kinetics) and/or affinity (thermodynamics) [11]. Membrane technology is a powerful method for gas separation which offer many advantages, including: a reduced energy intensity, simple design with a relatively small footprint providing easy set-up and scale-up, and a lack of hazardous chemicals (such as amine in adsorbtion process) [12].

In the last few decades, gas separation membranes have been applied at the industrial scale in various processes, including: nitrogen separation from air, natural gas sweetening, vapor/liquid

separations as well as hydrogen recovery and purification from refineries and petrochemical plants [13–15]. In fact, most of the current applied membranes are made from only a limited number of materials, which have been used for decades. This is despite an enormous amount of research which has resulted in many new materials being synthesized and evaluated [13]. Conventionally, membrane materials can be commonly classified into classes as organic (polymers) and inorganic (ceramics, carbons and molecular sieves). Polymeric membranes have been successfully established in gas clean-up operations for a long time but there are still a lot of challenges related to the large scale applications. These include the inevitable trade-off between permeability and selectivity of the membrane, low chemical and thermal resistance, weak performance under low driving force (polymeric membrane), and difficulty in thin film manufacture (inorganic membrane) [1]. Of these, the inherent permeability / selectivity trade-off have received the most research attention, but this has not necessarily translated into improved commercial outcomes.

Currently, the vast majority of commercial membranes are polymeric which separate gases by the solution diffusion mechanism [13]. Theoretically, polymeric membranes are applicable for separation of most gas mixtures, however, only a few large industrial applications can be carried out, named as below: [14,16–20]

- O_2/N_2 separation
- Hydrogen separations (petrochemical industry)
- CO_2 capture from CO_2/CH_4 mixtures (natural gas sweetening) and CO_2/N_2 (treatment of flue gas, etc.)
- Vapor/gas separations

Various of polymers have been studied so far for membrane fabrication, however, only those presented in Table 2.1, have found application in industrial gas separation plants. There are also research works published with excellent results where membrane materials with extremely high performance for some gas mixtures separation (for instance, CO_2/CH_4) were synthesized [21–27]. Cellulose acetate is still the most successfully applied polymeric membrane, which were installed in 1980s for CO_2 removal [28], and upgrade to hollow fiber membrane in 2006 for expanding the facilities with gas feed of 87 mol% CO_2. Separation performance of some commercial membranes are presented in Figure 2.2.

Table 2.1. Membrane companies and their products [14,15,17]

Company	Principal membrane materials
Permea (Air Products)	Polysulfone
MEDAL (Air Liquid)	Polyimides
Generon	Tetrabromopolycarbonate
Separex (UOP)	Cellulose acetate
Aquila	Poly(phenylene oxide)
Ube	Polyimide
MTR	Silicon rubber
Helmholtz Centrum (formerly GKSS)	Silicon rubber
Kryogenmash	Poly(vinyltrimethylsilane)
Air Liquid	Ethyl cellulose
OPW Vaposaver	Poly(trimethylsilyl propyne)

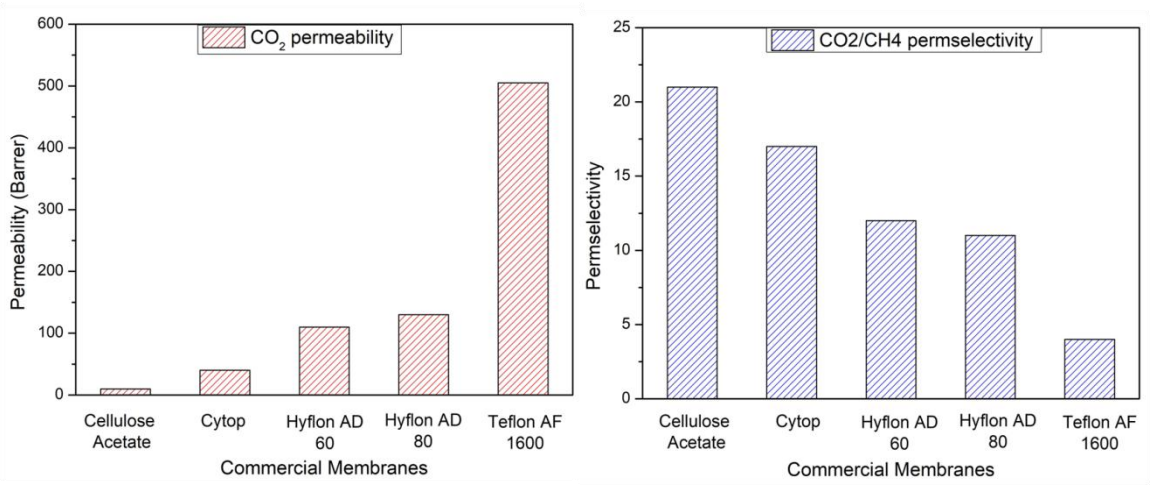

Figure 2.2. CO_2 permeability and CO_2/CH_4 permselectivity for pure gases of polymer membranes at 3.5 bar [29]

2.3 Overview of Mixed Matrix Membranes

2.3.1 Introduction

Despite being extensively applied in gas separation industry together with many efforts to improve the gas separation efficiency of polymeric membrane, the enhancements rarely surpass the well-known Robeson upper bound, which represents the trade-off between permeability and selectivity

[30]. In contrast, some inorganic membrane materials exhibit exceptional separation performance [31–37] along with superior chemical and thermal stabilities compared to polymers [38]. However, inorganic membranes suffer from several major issues including high fabrication associated with their low processability and difficulty in effectively scaling up for large scale industry [39]. In order to overcome those limitations, a new class of membranes have been developed over the last 50 years, namely mixed matrix membranes (MMM) which combine inorganic fillers into a polymeric matrix (Figure 2.3). Theoretically, MMMs can inherit some advantages from inorganic particles, especially their superior separation performance, while still retain the low fabrication cost and high processability of the polymeric materials due to the flexibility of polymer chains [40].

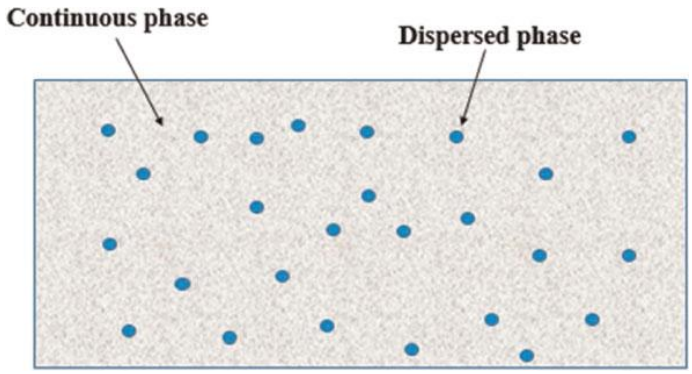

Figure 2.3 Schematic diagram of mixed matrix membranes [41]

Similar synthesis routes for polymeric membranes can be applied to fabricate MMMs which means they should be suitable for scaling up for industrial applications. The synthesis techniques are typically categorized in three ways: (1) Forming filler suspension prior to adding and dissolving the polymer, (2) prepare the polymer solution before dispersing filler in, (3) prepare separate polymer solution and filler suspension before mixing them together [42,43]. These different fabrication methods are summarized in Fig 2.4. The obtained polymer/filler mixture is then typically cast on flat surface and evaporating the solvent, although wet spinning phase inversion techniques have been used for hollow fibre MMMs. The membranes are finally dried at particular temperature (based on the polymer thermal properties and solvent boiling point) to remove the remaining solvent.

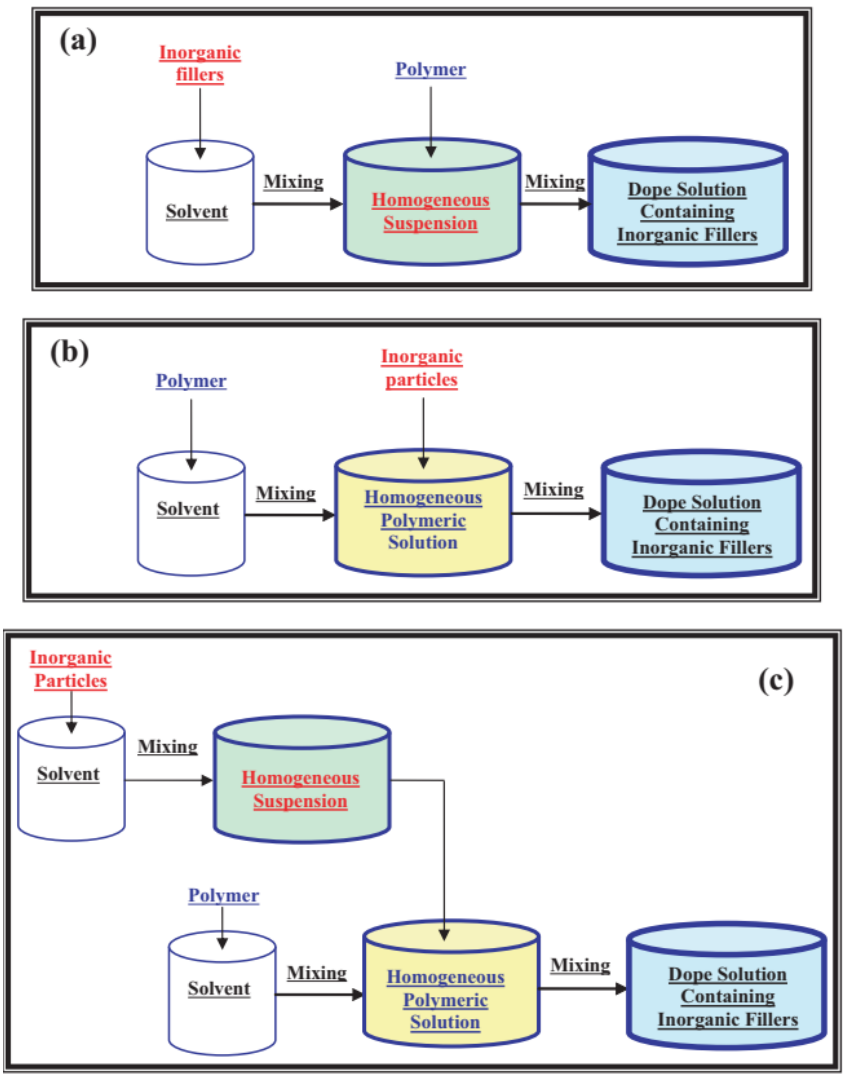

Figure 2.4. Different methods for mixed matrix membrane fabrication [43]

2.3.2 Gas transport mechanism in polymer membranes

The way gases permeate through membranes depends on the membrane material and gas components. Two models were commonly used to describe the mechanism of permeation as presented in Figure 2.5. In the pore-flow model (porous membrane) (Figure 2.5a), gases travel in the membrane through pores and are separated due to the size – exclusion. In dense membrane (Figure 2.5b), the dominant mechanism is solution – diffusion model, which include three steps: absorption (dissolve), diffusion and desorption. Assuming that the gas dissolves in the membrane material similar to a liquid, the dissolve gas then diffuses through membrane by random diffusion down a concentration gradient [44].

The solution-diffusion model describes the permeation of gas molecules through polymeric membranes based on the diffusivity coefficient (D) and the solubility coefficient (S) [44]. The permeability (P) of a gas molecule is defined as below:

$$P_i = D_i S_i$$

Permeability is commonly measured in barrer (1 barrer = 1 x 10^{-10} cm^3(STP)cm/(cm^2 s cm Hg) = 7.5005 x 10^{-18} m^2 s^{-1} Pa^{-1})).

The membrane selectivity for a gas pair (A/B) is calculated based on the ratio of the permeability of gas A (in isolation) over the permeability of gas B (in isolation):

$$\alpha_{AB} = \frac{P_A}{P_B} = \frac{D_A}{D_B}\frac{S_A}{S_B}$$

Where P_A and P_B are the singe gas permeability coefficients of gases A and B, respectively.

For a gas mixture, the separation factor α_{AB} is defined as:

$$\alpha_{AB} = \frac{\gamma_{A,permeate}}{\gamma_{A,retentate}}\frac{\gamma_{B,permeate}}{S_{B,retentate}}$$

where $\gamma_{permeate}$ is the molar ratios of each components in the permeate side, $\gamma_{retentate}$ is the molar ratio of each components in the retentate side [45].

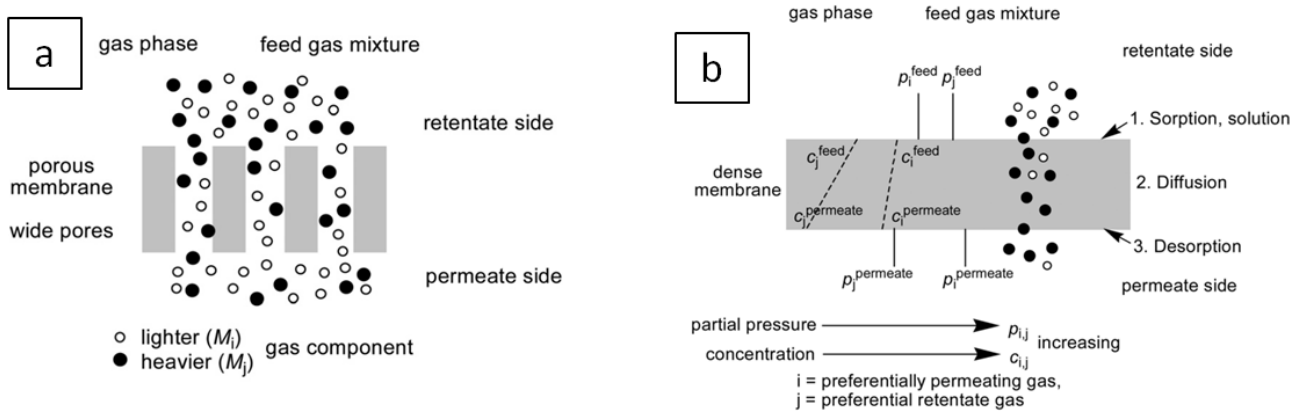

Figure 2.5. Comparison of permeation through a porous membrane (a) and a dense membrane (b) [44]

In dense polymeric materials, ideally a high gas selectivity is achieved when the desired component is both smaller and more condensable than the non-desired counterpart, as in case of CO_2/CH_4 separation. CO_2 is both smaller and more condensable than CH_4, leading to the more preferential permeation of CO_2 through the membrane. However, in some application, the sorption selectivity and diffusion selectivity are opposed. For instance, the separation of H_2 from CO_2 in hydrogen production. CO_2 with boiling point (bp) at -56°C is more condensable than hydrogen (bp = -253°C), so sorption selectivity favors permeation of CO_2. On the other hand, CO_2 (kinetic diameter = 3.3 A°) is larger than H_2 (2.9 A°), so the diffusion is in favor of the smaller hydrogen [46]. In this case, the nature of polymer materials will decide the dominant transport mechanism and hence what governs the selectivity. Polar polymers with highly flexible molecular chains will favor the sorption selectivity of CO_2 due to the higher free volume and polar interaction between CO_2 and the polymer chains, while in membrane made of polymers with rigid chains the diffusion of hydrogen will dominate the separation process, thus the overall selectivity of H_2 will be maximized.

For hollow fiber membranes, the separation performance is calculated in term of permeance [29].

$$Permeance = \frac{P_A}{L}$$

where P_A is permeability of A in the membrane, and L is the membrane thickness

Permeance unit is GPU (1 GPU = $1x10^{-6}$ cm^3(STP)/(cm^2 scmHg) = 7.5005 x 10^{-12} m s^{-1} Pa^{-1}).

2.3.3 Morphologies of Mixed Matrix Membranes

One approach to MMM fabrication is to take advantage of the superior gas transport properties of porous inorganic particles. Hence, the morphology in ideal MMM should allow the preferential gas to be transported through the inorganic phase, whereas the other gases in the mixture must travel through the polymer phase. Other approaches use dense inorganic particles to alter the polymeric structure around the filler thereby again altering the preferred diffusion pathway. MMMs are commonly fabricated in two morphologies including symmetric and asymmetric membrane (Figure 2.6) [47].

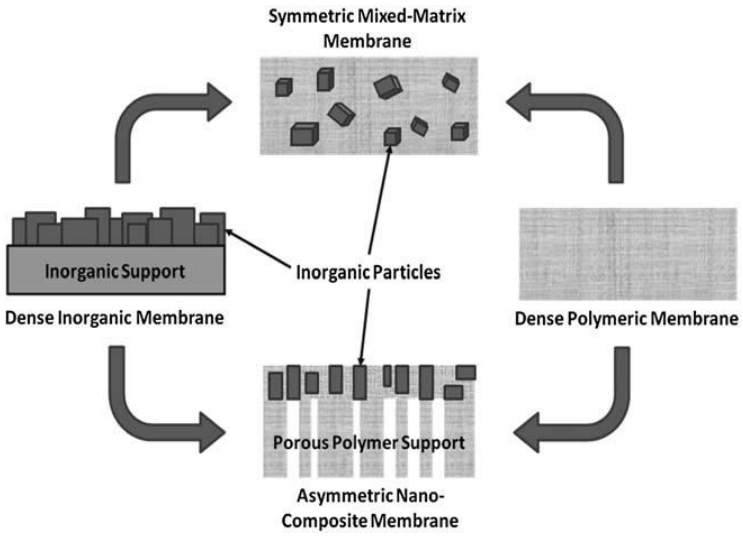

Figure 2.6. Two morphology types of MMMs [48]

The symmetric dense morphology has been intensively studied for MMM due to the simple fabrication process. A critical drawback with this morphology type is that there is a filler loading threshold (usually lower than 50%) due to the filler agglomeration, which deteriorate the membrane performance [48]. For this reason, the polymer phase still remains the dominant gas transport mechanism through the membrane, which hinders the advantages of inorganic fillers. Additionally, symmetric MMM are typically thicker (>50 μm) in order to maintain mechanical stability of the membrane, which also create diffusion resistance for gas transportation and decreases the permeability of the membrane.

On the other hand, asymmetric membranes are fabricated with ultra-thin, dense selective layer on top of a porous support layer, which is suitable for industrial applications. This morphology (with selective layer thickness <1 μm), can significantly reduce overall membrane resistance compared to the dense membrane. However, the particle loading threshold still exists as a challenge for these types of membrane [49].

2.3.4 Types of polymers

There are two categories of polymers that are commonly used for gas separation membranes: rubbery and glassy polymers. Rubbery polymers possess flexible segments that can rotate freely around the main chain while their counterparts exhibit rigid structures with restricted segmental motion. Rubbery polymers with their high flexibility can provide strong interaction with inorganic fillers which contribute to formation of defect-free interface of the membranes. However, rubbery polymers are also highly gas permeable which means the polymer phase dominates the gas transport

in the membrane reducing the impact of the inorganic phase and subsequently the gas separation performance [48]. On other hand, glassy polymers will often exhibit superior gas separation efficiency, but their rigid structure also hinders the polymer/filler interaction, which causes the formation of non-selective voids which usually form at the polymer/filler interface. This provides alternative passages for gas transportation and deteriorates the separation performance.

Another approach, a combination of rubbery and glassy polymers – the block copolymers containing both rigid and flexible segments – have been synthesized and investigated with the idea of both improving interfacial adhesion without sacrificing selectivity. Despite this being a promising approach, research has been somewhat limited [13,17].

Beside the size – selective polymers, there is another type of "reserve – selective polymers", for example poly 1 – trimethylsilyl – 1 – propyne (PTMSP) and poly (tert – butylacetylene) (PTBA), which favors the permeation of more condensable gas (e.g. CO_2) over smaller size gas (e.g. H_2). This type of polymers possesses bulky size group (e.g. isopropyl group) that reduce the polymer chain packing density and create very high fractional free volume [53]. Such high fractional free volume shifts the gas transport mechanism from diffusivity controlled to solubility favored and they no longer display size exclusion behavior [51]. As a result, higher permeability of more condensable species is observed over the smaller gases. Furthermore, introduction of non – porous inorganic particles into the polymer matrix could substantially disrupt the chain packing, further increasing the free volume as well as the solubility selectivity [52]. Some common polymeric membranes used in MMM are listed in Table 2.2.

Table 2.2 CO_2 permeability and CO_2/CH_4 selectivity of some polymeric membranes [45]

Polymer	P_{CO2} (Barrer)	$\alpha_{CO2/CH4}$
Polyethersulfone	2.8	28
Polysulfone	3.7	23
Cellulose acetate	6.0	29
Matrimid 5218	6.5	34
Polyimide (6FDA-ODA)	14.4	44.1
Polyimide (6FDA-DAF)	24.1	51

Polyimide (6FDA-6FpDA)	63.9	39.9
Poly(4-methyl-1-pentene)	63.5	5.7
PPO	90	16.7
Polyimide (6FDA-DAM)	370	21
Poly(tert-butylacetylene)	1020	8.5
Silicone rubber (PDMS)	4553	3.4

2.3.5 Type of filler particles

The selection of inorganic fillers in mixed matrix membranes is based on several factors such as adsorption capacity, filler size and pore system. Inorganic materials are divided into porous and non-porous materials at the most basic level. Porous inorganic particles have dominated the research field with the majority of studies on microporous particles (with pore size < 2 nm). More recently non-porous lamellar inorganic particles have attracted more attention [53]. As the main focus of this thesis is on the polymer/filler interfacial design and optimization, only a limit number of exemplary fillers in each typical filler class were reviewed below.

a. Zeolites

Zeolites are historically the most common inorganic materials used for MMM fabrication due to their thermal stability and outstanding adsorption properties [54]. Their highly defined pore structure (Figure 2.7) make good contribution to the size – selective and even diffusivity selective mechanism in MMM performance. Ceramic composite membrane using zeolite has been reported, however, the low packing density make such membranes less favored in gas separation [55].

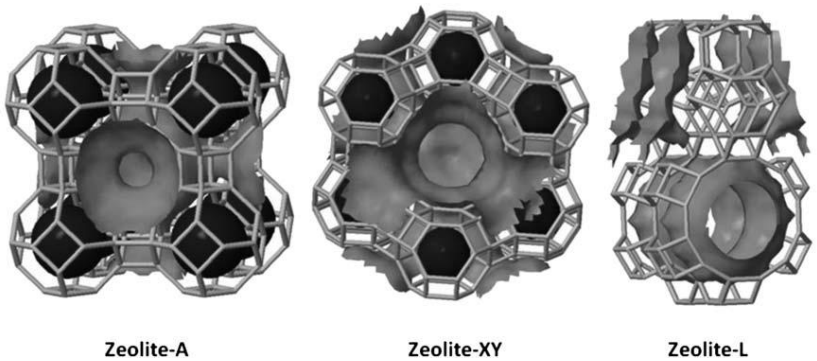

Figure 2.7. Structure of some common zeolites [54]

Embedding zeolites into a polymer matrix was supposed to be a promising approach to enhance the gas separation efficiency of polymeric membranes [54]. Zeolite-4A was introduced into PES matrix to fabricate the MMMs, which showed almost 4 times increment of the CO_2 permeability increased almost 4 times with 2 times increase in CO_2/N_2 selectivity [56]. Beiragh et al. incorporated ZSM-5 zeolite in a Pebax matrix, which showed good interaction with ZSM-5 due to the high chain mobility of poly ethylene oxide (PEO) soft segment in Pebax [57]. Thus, the increment of 78% in CO_2 permeability and 15% in CO_2/CH_4 selectivity were achieved at 5 wt.% loading of ZSM-5. Sanaeepur et al. examined NH_2-NaY/cellulose acetate (CA) MMMs where the permeability of CO_2 increased about 122% with NaY loadings up to 20 wt.% accompanied with no decrease in CO_2/N_2 selectivity [58]. In another work, the presence of zeolite-L in 6FDA-6FPDA-PDMS substantially improved the permeability of O_2 (from 4 Barrer with pure polymer to 44 Barrer with MMM), however the gas selectivity was significantly reduced [55]. The incorporation of zeolites in glassy polymers potentially exhibits higher mechanical stability and gas separation performance compared to rubbery polymers. However, MMMs based on zeolites and glassy polymers are more likely to form interfacial non-selective voids due to poor adhesion at the zeolite/polymer interface, leading to the reduction of gas selectivity of the MMMs. In many cases, modification of both the zeolite surface and polymer are necessary in order to overcome the interfacial defects and improve the gas separation performance of the MMMs.

b. Carbon molecular sieves (CMS)

Carbon molecular sieves (CMS), a highly porous carbonaceous material, have been extensively investigated as fillers for gas separation membranes [59,60]. Along with high porosity and well defined micropores which provide high gas permeability, the aperture size of CMS is of the same order as the size of gas molecules, allowing size-exclusion mechanism for particular gas species. Several works have investigated the potential of fabricating mixed-matrix membranes with CMS [61–66]. Vu and coworker examined the gas separation performance of Matrimid/CMS MMMs, which showed considerable increase of 45% in CO_2/CH_4 selectivity at 20 wt.% loading of CMS [67]. In many works, CMS also exhibited better interfacial adhesion with polymers compared to zeolites, however interfacial voids are still prevalent.

c. Activated carbon (AC)

Activated carbon is promising inorganic filler candidature for MMM due to its large surface area (BET surface area > 500 m^2g^{-1}). MMM of ABS (acrylonitrile butadiene styrene) copolymer incorporated with AC was investigated with 10 times higher permeability and 2 times higher selectivity compare to pure ABS membrane [68]. This improvement, according to the authors, was attributed to: (1) the superior CO_2/CH_4 selectivity of ABS itself, (2) selective adsorption of CO_2 by AC, and (3) good adhesion between AC and ABS.

d. Carbon nanotubes (CNTs)

CNTs possess unique tubular structure with a nano-scale diameter which can be synthesized as single-walled nanotubes (SWCNTs) or multi-walled nanotubes (MWCNTs) [51]. CNTs have been considered promising filler materials for MMMs due to the desirable physical and chemical properties. One of the main challenges with using CNTs for MMM is the dispersion of the nanotubes. CNTs showed poor dispersion in the polymer matrix due to the strong inter-tube van der Waals force, leading to the formation of aggregates in the membranes [61]. Functionalization seems to be an effective strategy to improve the dispersion quality of CNTs. These functional groups could provide better dispersion of CNTs in the solvent and enhance the interfacial interaction with the polymers. Moreover, proper alignment of CNTs in the polymer matrix can improve the gas permeability compared to the non-aligned CNT based MMMs [69].

e. Metal oxides

Metal oxide nanoparticles exhibit good potential for applications in membrane based gas separation although this area has not been widely explored. In some investigations, metal oxides provided special interactions with particular types of gases, which was thus attributed to the separation performance. Some metal oxides (e.g. MgO) possess larger pore size than the kinetic diameters of gas molecules, which contributed to the increase in permeability of the membrane [48].

f. Metal organic frameworks (MOFs)

MOFs is a new class of hybrid porous crystalline materials which possess large surface area (BET surface area: >1000 m^2g^{-1}), as well as high porosity and affinity towards certain gases. Furthermore, the pore structure in MOFs, particle size and shape can be tailored by changing the combination of metals source and organic ligands or alternating the other fabrication conditions [70]. MOFs are also expected to show better interaction with the polymer matrix due to the presence of organic linkers in their structure which is compatible with the polymers [71]. With these benefits, MOF

have been considered a promising material for gas separation with numerous of MOF structures studied in the past decade. However, only a small number of them have been used in MMM fabrication so far [72]. Some of the common MOFs which have been used for MMMs were showed in Figure 2.8.

- Zirconium-based MOFs (UiO-66) possess exceptional stabilities as each Zr-metal center is connected to the benzene-1,4-dicarboxylate (BDC) linkers to form the crystal framework. UiO-66/PEBA MMMs were investigated by Shen et al., which showed enhancement in both CO_2 permeability (80-90%) and CO_2/N_2 selectivty (40-65%) compared to the neat PEBA membrane [73]. Anjum et al. fabricated MMMs by embedding amino and carboxylic group containing UiO-66 MOF into a PIM-1 matrix. UiO-66 and NH_2-UiO-66 exhibited higher CO_2 permeability at 1100 and 1600 barrer, respectively, without much improvement in CO_2/CH_4 selectivity. In the mean time, COOH-UiO-66 decreased the CO_2 permeability (300 barrer) and 25% of CO_2/CH_4 selectivity compared to neat PIM-1 due to the presence of carboxylic groups, which reduced the intrinsic microporosity and free volume in PIM-1 [74].
- Zeolitic imidazole framework (ZIF) is a sub-class of MOFs with zeolite topology and tunable pore structures. Different ZIFs can be prepared by varying the organic linkers and metal ions. MMMs based on ZIF-8 and polysulfone (PSf) was fabricated by Nordin et al., which displayed an increase in both CO_2 permeation and selectivity up to 1.37 and 1.19 times with 0.5 wt.% loading of ZIF-8 [75]. Nevertheless, at higher loading of ZIF-8 (10 wt.%), the gas selectivity of the MMMs drastically diminished due to large number of agglomerations, causing non-selective channels in the MMMs. In another work, Hao et al. investigated the ZIF-71/PIM MMM which showed superior CO_2 permeability of 5042 barrer with the same CO_2/CH_4 selectivity of pure PIM membrane at the loading of 30 wt.% of ZIF-71 [76]. Chi et al. prepared MMMs based on ZIF-8 and the matrix of poly(vinyl chloride-g-poly(oxyethylene methacrylate) (PVC-g-POEM), which showed an increase of 9.80 times in CO_2 permeability as well as 14.4% in CO_2/N_2 selectivity compared to neat PVC-g-POEM due to good interfacial interaction of ZIF-8 and POEM phases [77].
- MIL is another series of MOFs with metal ion (Al, Cr, Ti) connected to organic linkers to form crystal structure. MILs exhibit some potential characteristics in gas separation membranes such as large pore volume, high surface area and superior gas adsorption capacity. The incorporation of NH_2-MIL-53 (Al) into PSf matrix was studied, which showed improvement in CO_2/CH_4 selectivity by 7 times compared to the pure polymer [78]. Other

work by Anjum et al. studied the MMMs base on MIL-125(Al) and NH_2-MIL-125(Al) with polyimide matrix, which displayed enhanced permeability of 20% and 38%, respectively, over the pure polymer while the CO_2/CH_4 selectivity increased up to 23% [79].

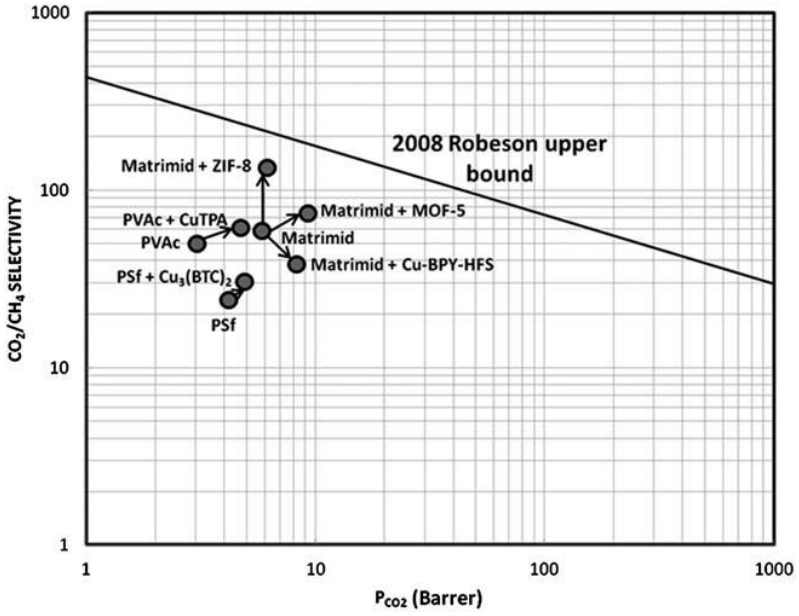

Figure 2.8. Comparison of the gas separation performance between pure polymeric membranes and the MMM incorporated with MOFs [51]

g. Mesoporous materials

The larger pore size of this filler (from 2-50 nm) can allow the penetration of the polymer chains, which promote good polymer/filler interaction and dispersion of fillers as well, potentially leading to improvement in gas separation properties [80]. The major drawback of mesoporous materials is that their pore sizes are too large for the size exclusion mechanism, which requires chemical modification facilitate selective adsorption as have been proposed by some research groups [80–82].

h. Non – porous materials

Mixing non – porous particles with the polymer matrix can improve the permeability of the MMMs due to the packing disruption of the polymer chains, which is a promising candidate for the reverse – selective membranes [52]. Though lacking the separation ability based on kinetic size discrimination, this type of materials can still bring benefit for some particular separation processes

as the functional groups on the surface of these materials may interact with polar gases (such as CO_2, SO_2), thus improving the solubility of these gas molecules in the membrane [83,84].

i. Lamellar inorganic materials

Recently, inorganic fillers with a sheet – shape have attracted the attention due to the unique shape and properties of these materials. The most noticeable advantage of the lamellar materials for MMM fabrication is that with proper orientation of the particles in the polymer matrix an ultra – thin membrane can be obtained with improvement in gas selectivity compared to other filler morphologies [85–89]. The challenges with using lamellar materials is to minimize the membrane thickness and ensure proper filler orientation in the polymer matrix to achieve optimal gas separation performance (Figure 2.9) [48].

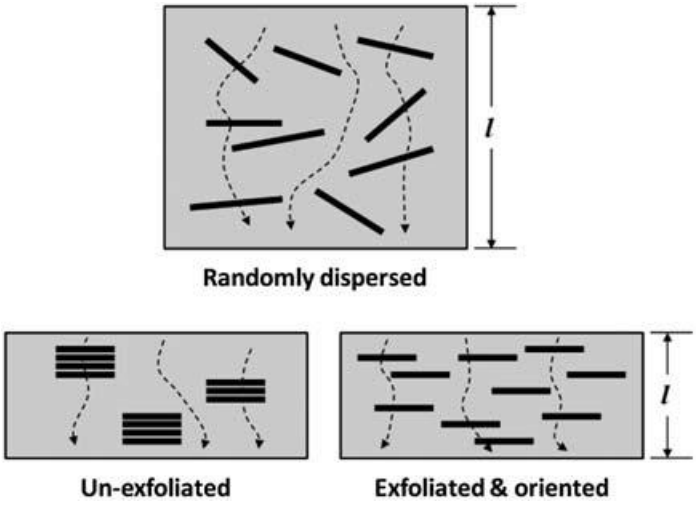

Figure 2.9. Schematic representation of different lamellar inorganic filler dispersion in MMM [51]

k. Graphene oxide

Graphene oxide (GO) is used widely as nanofillers in various applications including gas separation due to the abundant number of polar groups (-OH, -COOH) on the surface of GO which allow potential surface modification as well as benefiting transportation of some specific gas through the membranes. The presence of polar groups also increases the compatibility of GO with the polymer matrix due to the high number of interaction sites. Also, as mentioned above, the 2D structure of GO nanosheet is very promising for fabricating mixed matrix membranes. Shen et al. [91] studied the MMMs of GO nanosheets and Pebax polymer for CO_2/N_2 separation. The Pebax/GO MMMs showed improvement of CO_2 permeability up to 100 barrer and CO_2/N_2 selectivity of 91 and the

performance enhancement was retained for up to 100 h. In another work, MMMs were developed by dispersing GO in cross-linked PEO, which showed good interfacial. The CO_2 permeability improved from 250 barrer to 450 barrer, while the CO_2/N_2 selectivity increased from 48 to 55 [92]. However, at higher loading of GO than 1 wt.%, a significant decrease in gas permeability through the MMMs was observed. The functionalization of GO with amino acid compounds and consequently incorporated into sPEEK polymer were reported by Xin et al. [93]. The presence of amines and carboxylic groups increased the CO_2 solubility in humid conditions as the CO_2 permeability increased from 565 barrer to 1247 barrer while the CO_2/N_2 and CO_2/CH_4 selectivity simultaneously enhanced at 8 wt.% loading of GO. Porous GO was also reported in the literature as another potential filler selection for MMMs. Dispersion of tuned porous GO in Pebax matrix showed 2-fold enhancement of CO_2 permeability (60 to 119 barrer) and CO_2/N_2 selectivity increased from 55 to 104 at 5 wt.% of GO loading [94]. Another approach to utilize GO in MMMs is as a scaffold for other nanofillers. Dong et al. grew ZIF-8 on reactive sites of GO before dispersing the ZIF-8/GO fillers into Pebax matrix [95]. The resultant MMMs showed improvement in CO_2 permeability and CO_2/N_2 selectivity of 190% and 175%, respectively. The high microporosity and CO_2 adsorption capacity of ZIF-8 was claimed to increase the solubility selectivity of the MMMs while the high aspect ratio of GO contributed to the enhancement in diffusivity selectivity.

2.4 Factors influencing the MMM structure and performance

In order to obtain the desired morphology, gas separation properties and mechanical/chemical stability of the MMM, several challenges named here need to be addressed, including: (1) to achieve a homogeneous dispersion of fillers in the polymer matrix to prevent filler agglomeration, (2) obtain a defect-free polymer/filler interface to optimize the separation performance, and (3) proper selection of polymers and fillers with compatibility and good separation properties [43,96]. Several strategies have been proposed to overcome these issues as demonstrated in Figure 2.10

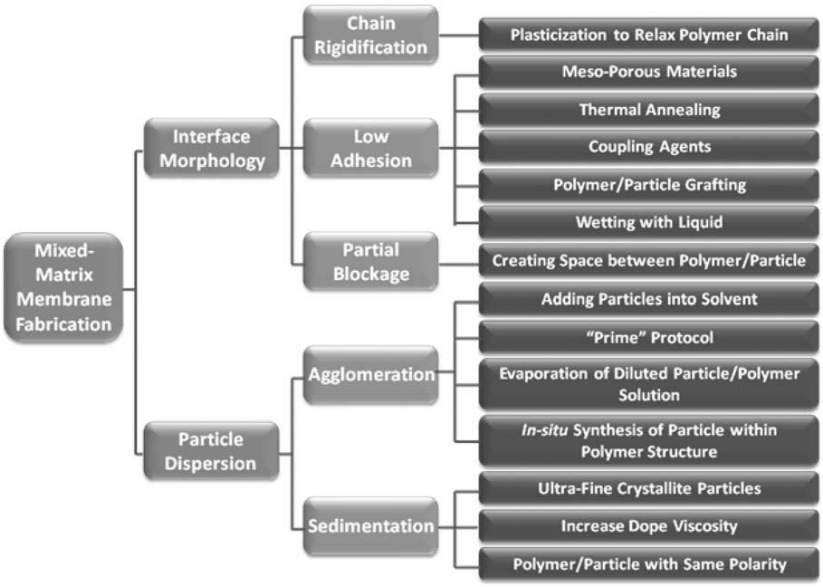

Figure 2.10. Some strategies to overcome challenges for MMMs fabrication [51]

2.4.1 Selection of filler and polymer matrix for MMMs

Proper selection of polymeric/filler materials for membranes can considerably contribute to the gas separation performance of the MMMs. In a defect-free mixed matrix membrane, the filler properties may predominantly determine the improvement in gas separation efficiency of the MMMs [97,98]. Because of this the properties of fillers in MMMs should match with the desired gas, including chemical structure, surface chemistry, pore size distribution and the compatibility between filler and polymer matrix. The fillers possessing similar functional groups with the polymer chain are more likely to be compatible with the polymer. For instance, fillers containing amino groups may improve the interaction with the polymers such as polysulfone and polyimide [99−101]. Some reports in literature showed that zeolitic imidazole frameworks (ZIFs) are a suitable choice as fillers for some specific polymers such as polybenzimidazole (PBI) due to the good compatibility and interaction formed by similar linkers in both ZIF and PBI structure [94, 118, 119]. In another work, Nik et al. prepared MMMs by embedding five different MOFs: UiO-66, NH_2-UiO-66, UiO-67, MOF-199, and NH_2-MOF-199 into 6FDA-ODA polyimide and investigated the gas separation performance on CO_2/CH_4 [102]. It was found that the presence of amine groups in those MOFs improved the interfacial interaction of polymer/MOFs, leading to the enhancement of both the CO_2 permeability and ideal selectivity.

2.4.2 Dispersion of particles

As aforementioned, the introduction of filler into polymer matrix is usually constrained by a threshold, above which the aggregation of filler occurs. This agglomeration of filler can form non-selective voids which cannot be covered by polymer segments. Consequently, the voids will be extra space for gas molecules to transport through, which deteriorate the separation efficiency of the membrane (Figure 2.11).

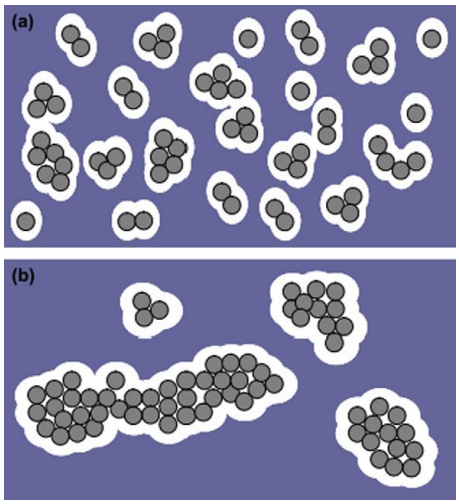

Figure 2.11. The possible distribution of inorganic filler in MMMs: (a) dispersed filler and voids, (b) agglomerated and voids [103]

Among the approaches to avoid aggregation or agglomeration, the most common one is priming. In this approach the filler particles are coated with a thin layer of polymer by introducing a small amount of polymer solution into the filler suspension, before mixing with the remaining bulk of polymer solution [104,105]. Another way is to disperse the fillers and dissolve the polymer in separated solvents before mixing together. The dilute filler suspension has low viscosity that the vigorous stirring can reduce the agglomeration of the inorganic particles [106,107]. Another technique is to prepare the dilute filler – polymer mixture suspension, following by solvent evaporation with continuous sonication/stirring until the suspension reaches a suitable viscosity. This method can then suppress aggregation due to the high viscosity of the suspension [108].

Another factor affect the dispersion of the inorganic filler is sedimentation, which often occurs with larger, high density particles. This issue can be avoided by choosing suitable filler particle size as well as increase the viscosity of the filler suspension, or if possible, choose polymer and inorganic filler with similar polarity [52,109].

The dispersion of inorganic fillers can also be improved by applying the interfacial polymerization processes. In this approach, the inorganic filler is dispersed along with the organic monomer and the polymerization will occurred on the interface between filler and monomer. In reverse, the membrane can also be prepared by growing filler particles directly on a porous polymer membrane surface, which can exhibit a defect – free top layer with well – dispersed fillers [110].

2.4.3 Filler/polymer interfacial morphology

The polymer – filler interfacial morphology in MMMs is a critical factor which determining the gas separation performance. A poor interaction between polymer and filler particles could cause significant reduction in the performance of the composite membrane and vice – versa. Figure 2.12 represents some common polymer/filler interface structures. Case 1 is an ideal interfacial morphology, while in case 2, the detachment of polymer chains from the filler surface can be observed, which causes the formation of interfacial voids. In case 3, the introduction of filler with strong interaction with the polymer chains at the interface caused the interfacial rigidification. Case 4 is where the filler surface pores has been partially sealed by the rigidified polymer chains. There are three factors commonly control the interfacial morphology: the adhesion of polymer and particle, the pore blockage by polymer chain and interfacial rigidification [48,96].

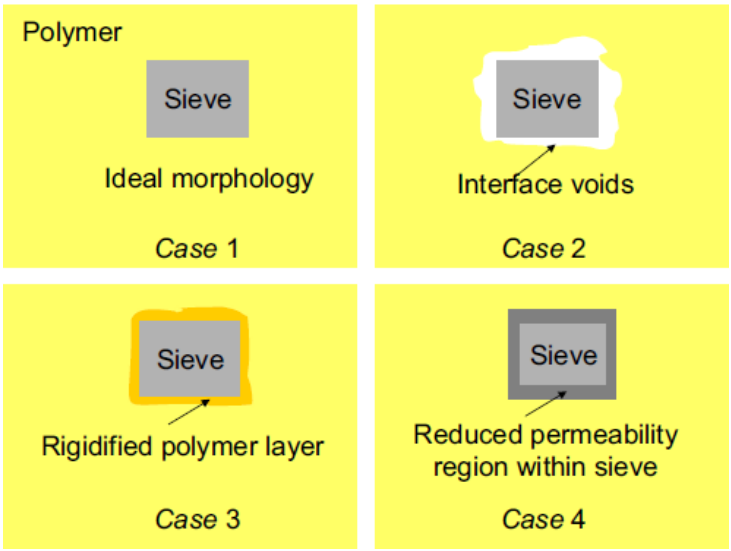

Figure 2.12. The schematic diagram of various nanoscale morphology of the MMMs [111]

Low adhesion between polymer matrix and fillers could form non selective voids at the interface region [112,113]. The most common method to overcome this issue is the use of silane coupling agents to form “interfacial bridges” between the polymer and inorganic particle surface as

represented in Figure 2.13 with some good results have been reported [103,114]. However, the introduction of coupling agents could potentially cause the pore blockage by polymer chain due to the short distance of the interface. Besides, even without coupling agents, the polymer chains could still partial block the filler pores and affect the membrane performance. In some cases, the partial blockage still improves the gas selectivity if the reduced pore size is suitable for the molecular sieving mechanism to occur [114,115], but most of the time, it will decrease the permeability of the particles and the membrane. In such cases, the proper choice of coupling agents with suitable chain size and structure to create enough space between polymer chain and particles without forming non – selective voids is critical in order to improve the separation performance.

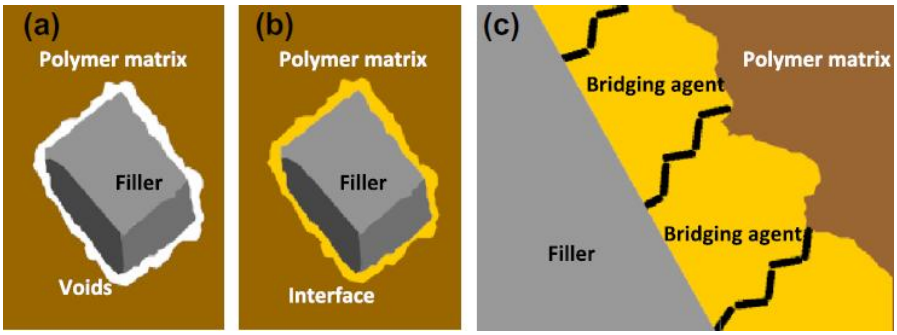

Figure 2.13. Interfacial of MMMs: (a) void formation at the interface, (b) and (c) bridging of the filler and polymer matrix upon surface modification [103]

The interface rigidification is the result of the polymer chain mobility inhibition due to the introduction of filler into the composite. The interaction between polymer and particles reduces the flexibility and mobility of polymer chains in the interfacial regions and thus alter the gas transport behavior of the particles. Normally, this phenomenon could improve or decline the separation performance based on the nature of the gas mixture. A method to mitigate this issue is introducing the plasticizers to increase the mobility of the polymer chains [116].

2.4.4 Plasticization and physical aging

Plasticization in polymeric membranes for gas separation occurs when the membrane is working under high pressure for long time. The dissolution of certain penetrants into polymer matrix during the separation process can disrupt the chain packing and increase the molecular chain mobility of the polymer [117]. Various studies have been carried out to investigate the impact of plasticization phenomena on membrane separation performance when being exposed to a highly soluble feed gas stream [40, 47,118-120].

In gas separation, plasticization is commonly caused by condensable gases including CO_2, hydrocarbons and other organic vapors, which is a serious problem in such processes involving high feeding pressures like for instance in natural gas cleaning [56,59]. At low pressure, the permeability of polymers usually decreases with increase in pressure due to gradual occupation of free volume in the membrane [60]. At high pressure, condensable gas as CO_2 increase the free space and mobility of polymer chain segments, thus increasing the diffusivity of all gases in the membrane [121,122]. This phenomenon increases the gas permeability along with decrement in gas selectivity at a critical point of partial pressure of plasticizing penetrant, which is referred as the plasticization pressure (Figure 2.14).

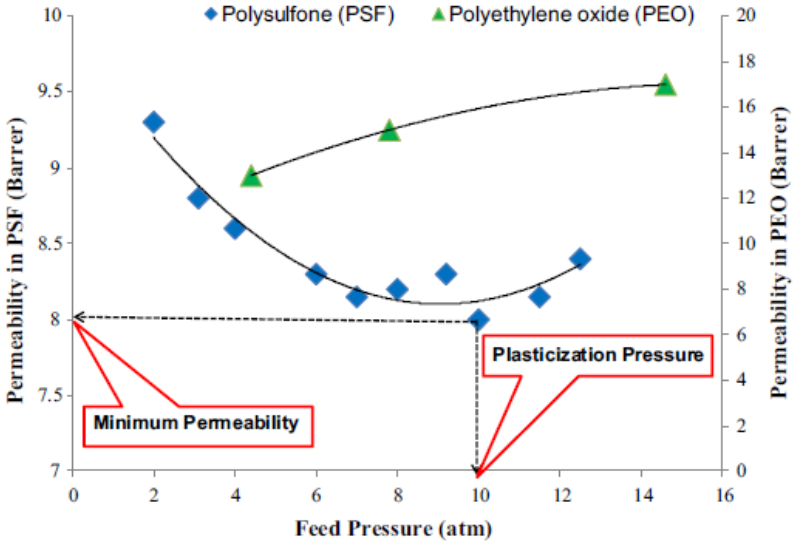

Figure 2.14. Permeability of CO_2 as a function of feed pressure in glassy PSF and rubbery PEO [29]

The state of polymers at the temperature below their glass transition point are known to be in a non-equilibrium state. In this state, a gradual rearrangement of polymer chains occurs to attain equilibrium state and this process is referred to as physical aging [49]. This process can affect the density, free volume and gas permeability of the membranes. In thin films, physical aging can be more significant due to the more rapid change toward the equilibrium state. Physical aging of thin films are mostly observed as densification [53], which decrease the free volume and gas permeabilities of the membranes. This phenomena is expected to affect productivity of commercial polymer membranes and the reliability of the membrane performance in the long term as well.

2.5 Modification methods for MMMs

All the important factors previously mentioned need to be taken into account in order to achieve high performance MMMs. Among those factors, the dispersion of fillers and the interfacial interaction between polymer matrix and fillers are the most critical, considerably affecting the gas separation efficiency of the MMMs [67,102,123]. Poor interfacial adhesion in MMMs may greatly reduce the gas selectivity and integrity of the membrane structure as well. Variety of modification techniques have been studied in order to enhance the polymer/filler compatibility and interaction and to enhance the membrane separation performance as well.

2.5.1 Filler size, shape and loading adjustment

Introducing filler with suitable size into polymer matrix can significantly contribute to the achievement of favorable interfacial property in MMMs. Generally, smaller sizes of MOFs exhibit better interfacial interaction with the polymeric matrix due to the large surface area which provide more polymer/particle interfacial interaction [124]. Bae and co-workers [125] applied sub-micrometer-sized ZIF-90 into 6FDA-DAM polyimide to prepare the MMMs which showed defect-free interface with high gas separation performance. The CO_2 permeability of the MMMs reach 720 Barrer at 15 wt.% loading of ZIF-90 while CO_2/CH_4 selectivity increase from 24 to 37 compared to the pure polymer, which surpasses the 1991 Robeson upper bound. In contrast to nano-fillers, it is very challenging for some micron-sized fillers to achieve good compatibility and affinity with the polymeric matrix due to the poor interfacial adhesion. One feasible modification way is physical treatment applied by Lei and coworkers, reducing the size of Cu-BTC by using sonication after filler fabrication, which enhanced the interfacial interaction between MOF/polymer [126].

Tailoring the shape of fillers is another approach that can improve the membrane interfacial interaction and membrane gas separation performance as well. Rodenas et al. prepared the MMMs with CuBDC nanosheets in polyimide and compared with MMMs using different morphologies of CuBDC fillers [127]. The results showed that the CuBDC nanosheets exhibited much better dispersion in the polymer matrix and the MMMs showed higher gas selectivity than the other MMMs in their study. Yang et al. synthesized ZIF-8 with five different shapes and compared their effects on the gas separation efficiency of the cross-linked PEO (XLPEO) based membranes. Among those different morphologies, the nanorod crystals showed the best compatibility with the polymer matrix and the XLPEO/ZIF-8 nanorod exhibited significant improvement in both C_3H_6 permeability and C_3H_6/C_3H_8 selectivity in a 50:50 gas mixture [128].

2.5.2 Crosslinking

Crosslinking is an effective modification method to improve interfacial adhesion. Typically this is done by using a crosslinkable polymer (*e.g.* copolyimides) and then initiating the crosslinking after casting the MMMs [129] or by using crosslinking agents [130]. Askari and co-workers [129] fabricated high ZIF-8 loading MMMs fabricated by mixing ZIF-8 suspension with the cross-linkable co-polyimides 6FDA-Durene/DABA solution and carried out the cross-linking reaction at 400°C. Significant enhancement in CO_2/CH_4 and C_3H_6/C_3H_8 selectivity of the MMM was observed along with improvement in plasticization resistance. In another study, high loading ZIF-8/6FDA-duren MMMs were fabricated and surface cross-linking by exposing the membrane to ethylenediamine (EDA) vapor [130]. After the crosslinking activated by EDA, the MMM gas separation performance improved by an order of magnitude in H_2/CO_2, H_2/N_2, and H_2/CH_4 selectivities compared to pure 6FDA-durene membrane, which surpassed the 2008 Robeson upper bound for those gas pairs. Tien-Binh et al. investigated membranes based on Mg-MOF-74 as filler and PIM-1 as polymer matrix. The membrane fabrication included the chemical crosslinking between the hydroxyl groups of Mg-MOF-74 with the fluoride in PIM-1 chain under optimized conditions which effectively eliminate interfacial defects [131]. Compared to the pure PIM-1 membrane, significant enhancement in CO_2 permeability (from 6500 Barrer to 21000 Barrer) and CO_2/CH_4 selectivity (from 12.3 to 19.1) were observed with the Mg-MOF-74/PIM-1 mixed matrix membranes. In another work by Zhang et al. [132], UiO-66-NH_2 MOF was firstly modified with polymerizable methacrylamide groups and consequently mixed with the butyl methacrylate (BMA) monomer and the photoinitiator. The photo-copolymerization between the methacrylamide groups on the MOFs and the BMA was carried out under UV light, resulting in the covalently-linked composite network between the MOF and polymer chains. Improved MOF dispersion with less agglomeration were observed with those membranes due to the enhanced interaction between MOF and polymer matrix."

2.5.3 Adding additives

Adding other components into mixed matrix membranes (beside polymer and filler phases) has also been shown to be an effective method and has been widely used for enhancing the MMMs integrity and separation performance. Ionic liquids, when use as additive can behave like a compatibilizer to improve the polymer/filler interface and separation efficiency of MMMs. Hao et. al [133] added ZIF-8 into miscible ionic liquid blend systems and study the MMMs used for CO_2 capture in natural gas mixture. Results showed that the presence of free ionic liquids contributed to the uniform

dispersion of ZIF-8 in the MMMs, which exhibited significantly enhanced permeability for CO_2 with minor reduction in the CO_2/N_2 and CO_2/CH_4 selectivity.

2.5.4 Filler surface modification

Surface modification of filler is also a common route to enhance the interfacial adhesion between fillers and polymer matrix. Adding suitable functional groups on the surface of filler particles can improve the interaction with the polymer chains, thus minimizing the formation of non-selective interfacial voids. A study by Venna et al [134] coated the surface of MOF UiO-66-NH_2 with phenyl acetyl groups before incorporating with Matrimid® to fabricate the MMMs. Significant improvements were observed with the CO_2 permeability of the MMM increased by 200% with 25% increment in CO_2/N_2 selectivity along with enhanced thermal and mechanical properties. It is hypothesized that the hydrogen bondings have been formed between amide-imide groups of the modified MOF and the polymer, which eliminated the non-selective voids at the interface and enhance the interactions between MOF and polymer. In another work, Xin and coworkers [135] decorated MIL-101(Cr) MOF with polyethylenimine, which was consequently embedded into sulfonated poly(ether ether ketone) matrix. The presence of PEI layer on the surface of the modified MOF is believed to improve the filler/polymer interfacial adhesion due to the specific interaction between sulfonic acid groups and PEI, providing significant increment in CO_2 permeability along with CO_2/CH_4 selectivities of 71.8.

2.5.5 In-situ synthesis of MMM

One final method to uniformly disperse filler particles and minimize filler aggregation is to synthesize fillers in the same solution that can dissolve the polymer matrix. Seoane and coworker [136] synthesized MIL-68(Al) in THF solvent together with dissolving polysulfone (PSF) at the same time to prepare MOF/polysulfone (PSF) MMMs. Their in-situ synthesis method significantly improved the dispersion of MIL-68(Al) in PSF matrix. The results showed that the in-situ fabricated MMMs can achieve much better dispersion of MOFs and the filler/polymer morphology than those of conventional MMM. However, the residue precursors of MOF synthesis remained in the membranes and their impact on the separation performance of MMMs have not been addressed.

2.6 Summary

Mixed matrix membrane have been considered promising candidates for improved gas separation performance in industrial settings. This type of membranes combines the processability and flexibility of polymers with high gas separation performance of inorganic particles.. Although many reports have been published in the literature regarding MMMs, the gas separation performance and stability of these membranes still need to be further improved. Most of the studies on MMMs up to now only focus on porous nano-sized fillers and their performance with MMMs and ignore their non-porous or micron-sized counterparts, which are inherently cheaper and more readily available. The weakness of those larger fillers is the lack of gas size-exclusion properties (non-porous fillers) or the large size (micron-sized porous fillers) that caused the poor adhesion with the polymer matrix. With proper modifications, the gas separation performance of the MMM containing those fillers can be enhanced. Among those factors that affect the MMMs performance, the polymer/fillers interfacial properties play the most crucial role. Thus, appropriate design and control the interfacial morphology and how these modifications affect the gas separation performance of those MMMs need further investigation and will be the subject of this thesis.

References

[1] D.Y. S.D. Kenarsari G. Jiang, S. Zhang, J. Wang, A.G. Russell, Q. Wei and M. Fan, Review of recent advances in carbon dioxide separation and capture, RSC Adv. 3 (2013) 22739.

[2] C.M. White, B.R. Strazisar, E.J. Granite, J.S. Hoffman, H.W. Pennline, Separation and capture of CO_2 from large stationary sources and sequestration in geological formations—coalbeds and deep saline aquifers, J. Air Waste Manag. Assoc. 53 (2003) 645–715.

[3] K.P.R. J.T. Yeh K. Rygle, H.W. Pennline, Semi-batch absorption and regeneration studies for CO_2 capture by aqueous ammonia, Fuel Process. Technol. 86 (2005) 1533–1546.

[4] D.R.L. H.W. Pennline K.L. Jones, C.R. Myers, B.I. Morsi, Y.J Heintz, J.B. Ilconich, Progress in carbon dioxide capture and separation research for gasification -based power generation point sources, Fuel Process. Technol. 89 (2008).

[5] M.S. M. Hasib-ur-Rahman F. Larachi, Ionic liquids for CO_2 capture - Development and progress, Chem. Eng. Process. Process Intensif. 49 (2010) 313–322.

[6] G.G. D. Wappel R. Kalb, J. Draxler, Ionic liquids for post-combustion CO_2 absorption, Int. J. Greenh. Gas Control. 4 (2010) 486–494.

[7] A.V. B.D. Bhide S.A. Stern, Hybrid processes for the removal of acid gases from natural gas, J. Memb. Sci. 140 (1998) 27–49.

[8] G.W.M. L.M. Galan Sanchez A.B. de Haan, Solvent Properties of Functionalized Ionic Liquids for CO2 Absorption, Chem. Eng. Res. Des. 85 (2007) 31–39.

[9] J.H.D. S. Choi C.W. Jones, Adsorbent materials for carbon dioxide capture from large anthropogenic point sources, ChemSusChem. 2 (2009) 796–854.

[10] N.G. A. Hart, Cryogenic CO_2 capture in natural gas, Energy Procedia. 1 (2009) 697–706.

[11] Y.M. J.R. Li M.C. McCarthy, J. Sculley, J. Yu, H.K. Jeong, P.B. Balbuena, H.C. Zhou, Carbon dioxide capture-related gas adsorption and separation in metal-organic frameworks, Coord. Chem. Rev. 255 (2011) 1791–1823.

[12] R.W. Baker, B.T. Low, Gas separation membrane materials: A perspective, Macromolecules. 47 (2014) 6999–7013.

[13] B.T.L. R.W. Baker, Gas Separation Membrane Materials: A Perspective, Macromolecules. 47 (2014) 6999–7013.

[14] E.D. P. Bernado G. Golemme, Membrane Gas Separation: A Review/State of the Art, Ind. Eng. Chem. Res. 48 (2009) 4638–4663.

[15] R.W. Baker, Future Directions of Membrane Gas Separation Technology, Ind. Eng.Chem. Res. 41(6) (2002) 1393–1411.

[16] R.W. Baker, Future Directions of Membrane Gas Separation Technology, Ind. Eng. Chem. Res. 41 (2002) 1393–1411.

[17] Y. Yampolskii, Polymeric Gas Separation Membranes, Macromolecules. 45 (2012) 3298–3311.

[18] T.M.N. N.W. Ockwig, Membranes for Hydrogen Separation, Chem. Rev. 107 (2007) 4078–4110.

[19] E.D. P. Bernado, Membrane gas separation progresses for process intensification strategy in the petrochemical industry, Pet. Chem. 50 (2010).

[20] K.K. R.W. Baker, Natural Gas Processing with Membranes: An Overview, Ind. Eng. Chem. Res. 47 (2008) 2109–2121.

[21] Y.X. M. Askari P. Li, T.S. Chung, Natural gas purification and olefin/paraffin separation using cross-linkable 6FDA-Durene/DABA copolyimides grafted with a, b, and g - cyclodextrin, J. Membr. Sci. 390–391 (n.d.) 141–151.

[22] T.Y. M. Askari T.S. Chung, Natural gas purification and olefin/paraffin separation using cross-linkable dual-layer hollow fiber membranes comprising b-cyclodextrin, J. Membr. Sci. 423–424 (n.d.) 392–403.

[23] S.H.H. S. Kim Y.M. Lee, Thermally rearranged (TR) polybenzoxazole hollow fiber membranes for CO_2 capture, J. Membr. Sci. 403–404 (2012) 169–178.

[24] J.E.L. S.H. Han J.K. Lee, H.B. Park, Y.M. Lee, Highly gas permeable and microporous polybenzimidazole membrane by thermal rearrangement, J. Membr. Sci. 357 (2010) 143–151.

[25] L.S. Y. Yampolskii N. Belov, M. Gringolts, E. Finkelshtein, V. Shantarovich, Addition-type polynorbornene with Si(CH3)3 side groups: detailed study of gas permeation free volume and thermodynamic properties., John Wiley & Sons, Ltd, West Sussex, 2010.

[26] S.J.P. C.L. Staiger A.J. Hill, C.J. Cornelius, Gas separation, free volume distribution, and physical aging of a highly microporous spirobisindane polymer, Chem. Mater. 20 (2008) 2606–2608.

[27] T.N. T. Nakagawa A. Higuchi, Morphology and gas permeability in copolyimides containing polydimethylsiloxane block, J. Membr. Sci. 206 (2002) 149–163.

[28] S.H.H. H.B. Park C.H. Jung, Y.M. Lee, A.J. Hill, Thermally rearranged (TR) polymer membranes for CO_2 separation, J. Membr. Sci. 359 (2010) 11–24.

[29] J.K. Adewole, A.L. Ahmad, S. Ismail, C.P. Leo, Current challenges in membrane separation of CO_2 from natural gas: A review, Int. J. Greenh. Gas Control. 17 (2013) 46–65.

[30] R.W.B. J.G. Wijmans, The solution-diffusion model: a review, J. Membr. Sci. 107 (1995) 1–21.

[31] W. Shusen, Z. Meiyun, W. Zhizhong, Asymmetric molecular sieve carbon membranes, J. Membr. Sci. 109 (1996) 267–270.

[32] H. Suda, K. Haraya, Molecular Sieving Effect of Carbonized Kapton Polyimide Membrane, J. Chem. Soc., Chem. Commun. 3 (1995) 1179–1180.

[33] X. Ning, W.J. Koros, Carbon molecular sieve membranes derived from Matrimid® polyimide for nitrogen/methane separation, Carbon N. Y. 66 (2014) 511–522.

[34] C.W. Jones, W.J. Koros, Membranes-I . Preparation and Characterization Based on Polyimide Precursors, Science 32 (1994) 1419–1425.

[35] B. Shimekit, H. Mukhtar, F. Ahmad, S. Maitra, Ceramic membranes for the separation of carbon dioxide—a review, Trans. Indian Ceram. Soc. 68 (2009) 115–138.

[36] H.A. Meinema, R.W.J. Dirrix, H.W. Brinkman, R.A. Terpstra, J. Jekerle, P.H. Kösters, Ceramic membranes for gas separation - Recent developments and state of the art, Int. Ceram. Rev. 54 (2005) 86–91.

[37] J. Sunarso, S. Baumann, J.M. Serra, W.A. Meulenberg, S. Liu, Y.S. Lin, J.C. Diniz da Costa, Mixed ionic-electronic conducting (MIEC) ceramic-based membranes for oxygen separation, J. Membr. Sci. 320 (2008) 13–41.

[38] B.T.L. Y. Xiao S.S. Hosseini, T.S. Chung, D.R. Paul, The strategies of molecular architecture and modification of polyimide-based membranes for CO_2 removal from natural gas - a review, Prog. Polym. Sci. 34 (2009) 561–580.

[39] M.H.K. B.J.M. Flaconneche, Permeability, diffusion and solubility of gases in polyethylene, polyamide 11 and poly(vinylidene fluoride), Oil Gas Sci. Technol. 56 (2001) 261–278.

[40] D.R.P. N.R. Horn, Carbon dioxide plasticization and conditioning effects in thick vs. thin glassy polymer films, Polymer (Guildf). 52 (2011) 1619–1627.

[41] M.N. Nejad, M. Asghari, M. Afsari, Investigation of Carbon Nanotubes in Mixed Matrix Membranes

for Gas Separation: A Review, ChemBioEng Rev. 3 (2016) 276–298.

[42] I. Erucar, G. Yilmaz, S. Keskin, Recent Advances in Metal-Organic Framework-Based Mixed Matrix Membranes, Chem. - An Asian J. 8 (2013) 1692–1704.

[43] M.A. Aroon, A.F. Ismail, T. Matsuura, M.M. Montazer-Rahmati, Performance studies of mixed matrix membranes for gas separation: A review, Sep. Purif. Technol. 75 (2010) 229–242.

[44] H.B. Tanh Jeazet, C. Staudt, C. Janiak, Metal-organic frameworks in mixed-matrix membranes for gas separation, Dalt. Trans. 41 (2012) 14003–14027.

[45] R. Lin, MOFs-based Mixed Matrix Membranes for Gas Separation, 2016.

[46] R.W. Baker, B.T. Low, Gas Separation Membrane Materials: A Perspective, Macromolecules 47 (20) (2014) 6999-7013.

[47] D.R.P. N.R. Horn, Carbon dioxide plasticization of thin glassy polymer films, Polymer (Guildf). 52 (n.d.) 5587–5594.

[48] G. Dong, H. Li, V. Chen, Challenges and opportunities for mixed-matrix membranes for gas separation, J. Mater. Chem. A. 1 (2013) 4610–4630.

[49] W.Q. L. Cui D. Paul, W. Koros, Responses of 6FDA-based polyimide thin membranes to CO_2 exposure and physical aging as monitored by gas permeability, Polymer (Guildf). 52 (2011) 5528–5537.

[50] I.P. A. Morisato, Synthesis and gas permeation properties of poly(4-methyl-2-pentyne), J. Membr. Sci. 121 (1996) 243–250.

[51] H.L. G. Dong V. Chen, Challenges and opportunities for mixed-matrix membranes for gas separation, J. Mater. Chem. A. 1 (2013) 4610.

[52] B.D.F. T.C. Merkel R.J. Spontak, Z. He, I. Pinnau, P. Meakin, A.J. Hill, Ultrapermeable, Reverse-Selective Nanocomposite Membranes, Science 296 (2002) 519–522.

[53] T.S.C. J. Xia P. Li, R.N. Horn, D.R. Paul, Aging and carbon dioxide plasticization of thin polyetherimide films, Polymer (Guildf). 53 (2012) 2099–2108.

[54] D. Bastani, N. Esmaeili, M. Asadollahi, Polymeric mixed matrix membranes containing zeolites as a filler for gas separation applications: A review, J. Ind. Eng. Chem. 19 (2013) 375–393.

[55] T.W. Pechar, S. Kim, B. Vaughan, E. Marand, V. Baranauskas, J. Riffle, H.K. Jeong, M. Tsapatsis, Preparation and characterization of a poly(imide siloxane) and zeolite L mixed matrix membrane, J.

Membr. Sci. 277 (2006) 210–218.

[56] C.C.C. W. Qiu L. Xu, L. Cui, D.R. Paul, W. Koros, Sub-Tg cross-linking of a polyimide membrane for enhanced CO_2 plasticization resistance for natural gas separation, Macromolecules. 44 (2011) 6046–6056.

[57] H.H. Beiragh, M. Omidkhah, R. Abedini, T. Khosravi, S. Pakseresht, Synthesis and characterization of poly (ether-block-amide) mixed matrix membranes incorporated by nanoporous ZSM-5 particles for CO_2/CH_4 separation, Asia-Pac. J. Chem. Eng 11 (2016) 522–532.

[58] H. Sanaeepur, A. Kargari, B. Nasernejad, Aminosilane-functionalization of a nanoporous Y-type zeolite for application in a cellulose acetate based mixed matrix membrane for CO_2/N_2 separation, RSC Adv. 4 (2014) 63966–63976.

[59] D.R.P. J.D. Wind W.J. Koros, Natural gas permeation in polyimide membranes, J. Membr. Sci. 228 (2004) 227–236.

[60] R.J. S.R. Reijerkerk K. Nijmeijer, M. Wessling, Highly hydrophilic, rubbery membranes for CO_2 capture and dehydration of flue gas, Int. J. Greenh. Gas Control. 5 (n.d.) 26–36.

[61] T.S.C. P.S. Tin S. Kawi, M.D. Guiver, Novel approaches to fabricate carbon molecular sieve membranes based on chemical modified and solvent treated polyimides, Microporous Mesoporous Mater. 73 (2004) 151–160.

[62] A. Singh-Ghosal, Air separation properties of flat sheet homogeneous pyrolytic carbon membranes, J. Membr. Sci. 174 (2002) 177–188.

[63] T.A.C. A.B. Fuertes, Preparation of supported asymmetric carbon molecular sieve membranes, J. Membr. Sci. 144 (1998) 105–111.

[64] T.A.C. A.B. Fuertes, Preparation of supported carbon molecular sieve membranes, Carbon N. Y. 37 (1999) 679–684.

[65] J.M.L. Y.K. Kim H.B. Park, Y.M. Lee, The gas separation properties of carbon molecular sieve membranes derived from polyimides having carboxylic acid groups, J. Membr. Sci. 235 (2004) 139–146.

[66] Y.K.K. H.B. Park J.M. Lee, S.Y. Lee, Y.M. Lee, Relationship between chemical structure of aromatic polyimides and gas permeation properties of their carbon molecular sieve membranes, J. Membr. Sci. 229 (2004) 117–127.

[67] W.J.K. D.Q. Vu S.J. Miller, Mixed matrix membranes using carbon molecular sieves: I. Preparation

and experimental results, J. Membr. Sci. 211 (2003) 311–334.

[68] J.M. M. Anson E. Garis, N. Ochoa, C. Pagliero, ABS copolymer-activated carbon mixed matrix membranes for CO_2/CH_4 separation, J. Membr. Sci. 243 (2004) 19–28.

[69] J.J. J.H. Choi W.N. Kim, Modification of Performances of Various Membranes Using MWNTs as a Modifier, Macromol. Symp. 249–250 (2007) 610–617.

[70] R. Lin, B. Villacorta Hernandez, L. Ge, Z. Zhu, Metal organic framework based mixed matrix membranes: An overview on filler/polymer interfaces, J. Mater. Chem. A. 6 (2018) 293–312.

[71] H.B. Tanh Jeazet, C. Staudt, C. Janiak, Metal-organic frameworks in mixed-matrix membranes for gas separation, Dalt. Trans. 41 (2012) 14003–14027.

[72] B. Zornoza, C. Tellez, J. Coronas, J. Gascon, F. Kapteijn, Metal organic framework based mixed matrix membranes: An increasingly important field of research with a large application potential, Microporous Mesoporous Mater. 166 (2013) 67–78.

[73] J. Shen, G. Liu, K. Huang, Q. Li, K. Guan, Y. Li, W. Jin, UiO-66-polyether block amide mixed matrix membranes for CO_2 separation, J. Membr. Sci. 513 (2016) 155–165.

[74] M.W. Anjum, F. Vermoortele, A.L. Khan, B. Bueken, D.E. De Vos, I.F.J. Vankelecom, Modulated UiO-66-Based Mixed-Matrix Membranes for CO_2 Separation, ACS Appl. Mater. Interfaces. 7 (2015) 25193–25201.

[75] N.A.H.M. Nordin, A.F. Ismail, A. Mustafa, R. Surya Murali, T. Matsuura, Utilizing low ZIF-8 loading for an asymmetric PSf/ZIF-8 mixed matrix membrane for CO_2/CH_4 separation, RSC Adv. 5 (2015) 30206–30215.

[76] L. Hao, K.S. Liao, T.S. Chung, Photo-oxidative PIM-1 based mixed matrix membranes with superior gas separation performance, J. Mater. Chem. A. 3 (2015) 17273–17281.

[77] W.S. Chi, S.J. Kim, S.J. Lee, Y.S. Bae, J.H. Kim, Enhanced Performance of Mixed-Matrix Membranes through a Graft Copolymer-Directed Interface and Interaction Tuning Approach, ChemSusChem. 8 (2015) 650–658.

[78] B. Zornoza, A. Martinez-Joaristi, P. Serra-Crespo, C. Tellez, J. Coronas, J. Gascon, F. Kapteijn, Functionalized flexible MOFs as fillers in mixed matrix membranes for highly selective separation of CO_2 from CH_4 at elevated pressures, Chem. Commun. 47 (2011) 9522–9524.

[79] M. Waqas Anjum, B. Bueken, D. De Vos, I.F.J. Vankelecom, MIL-125(Ti) based mixed matrix membranes for CO_2 separation from CH_4 and N_2, J. Membr. Sci. 502 (2016) 21–28.

[80] Y. Zhang, K.J. Balkus, I.H. Musselman, J.P. Ferraris, Mixed-matrix membranes composed of Matrimid® and mesoporous ZSM-5 nanoparticles, J. Membr. Sci. 325 (2008) 28–39.

[81] B. Zornoza, C. Téllez, J. Coronas, Mixed matrix membranes comprising glassy polymers and dispersed mesoporous silica spheres for gas separation, J. Membr. Sci. 368 (2011) 100–109.

[82] S. Kim, E. Marand, J. Ida, V. V. Guliants, Polysulfone and mesoporous molecular sieve MCM-48 mixed matrix membranes for gas separation, Chem. Mater. 18 (2006) 1149–1155.

[83] J. Ahn, W.J. Chung, I. Pinnau, M.D. Guiver, Polysulfone/silica nanoparticle mixed-matrix membranes for gas separation, J. Membr. Sci. 314 (2008) 123–133.

[84] J. Ahn, W.J. Chung, I. Pinnau, J. Song, N. Du, G.P. Robertson, M.D. Guiver, Gas transport behavior of mixed-matrix membranes composed of silica nanoparticles in a polymer of intrinsic microporosity (PIM-1), J. Membr. Sci. 346 (2010) 280–287.

[85] F. Xue, P. Kumar, W. Xu, K.A. Mkhoyan, M. Tsapatsis, Direct Synthesis of 7 nm-Thick Zinc(II)-Benzimidazole-Acetate Metal-Organic Framework Nanosheets, Chem. Mater. 30 (2018) 69–73.

[86] F. Xue, P. Kumar, W. Xu, K.A. Mkhoyan, M. Tsapatsis, Supporting Information Direct Synthesis of 7 nm-Thick Zinc (II) − Benzimidazole − Acetate Metal − Organic Framework Nanosheets, (n.d.).

[87] M. Zhao, Y. Huang, Y. Peng, Z. Huang, Q. Ma, H. Zhang, Two-dimensional metal–organic framework nanosheets: synthesis and applications, Chem. Soc. Rev. (2018).

[88] Y.-H. Luo, C. Chen, C. He, Y.-Y. Zhu, D.-L. Hong, X.-T. He, P.-J. An, H.-S. Wu, B.-W. Sun, Single-Layered 2-D MOF Nanosheets as In-Situ Visual Test Paper for Solvents, ACS Appl. Mater. Interfaces. 10 (34) (2018) 28860-28867.

[89] L. Huang, X. Zhang, Y. Han, Q. Wang, Y. Fang, S. Dong, In situ synthesis of ultrathin metal-organic framework nanosheets: A new method for 2D metal-based nanoporous carbon electrocatalysts, J. Mater. Chem. A. 5 (2017) 18610–18617.

[90] H.J.L. W. Cho M. Oh, Growth-Controlled Formation of Porous Coordination Polymer Particles, J. Am. Chem. Soc. 130 (2008) 16943–16946.

[91] J. Shen, G. Liu, K. Huang, W. Jin, K.R. Lee, N. Xu, Membranes with fast and selective gas-transport channels of laminar graphene oxide for efficient CO_2 capture, Angew. Chemie - Int. Ed. 54 (2015) 578–582.

[92] S. Quan, S.W. Li, Y.C. Xiao, L. Shao, CO_2-selective mixed matrix membranes (MMMs) containing graphene oxide (GO) for enhancing sustainable CO_2 capture, Int. J. Greenh. Gas Control. 56 (2017)

22–29.

[93] Q. Xin, Z. Li, C. Li, S. Wang, Z. Jiang, H. Wu, Y. Zhang, J. Yang, X. Cao, Enhancing the CO_2 separation performance of composite membranes by the incorporation of amino acid-functionalized graphene oxide, J. Mater. Chem. A. 3 (2015) 6629–6641.

[94] G. Dong, J. Hou, J. Wang, Y. Zhang, V. Chen, J. Liu, Enhanced CO_2/N_2 separation by porous reduced graphene oxide/Pebax mixed matrix membranes, J. Membr. Sci. 520 (2016) 860–868.

[95] L. Dong, M. Chen, J. Li, D. Shi, W. Dong, X. Li, Y. Bai, Metal-organic framework-graphene oxide composites: A facile method to highly improve the CO_2 separation performance of mixed matrix membranes, J. Membr. Sci. 520 (2016) 801–811.

[96] T.S. Chung, L.Y. Jiang, Y. Li, S. Kulprathipanja, Mixed matrix membranes (MMMs) comprising organic polymers with dispersed inorganic fillers for gas separation, Prog. Polym. Sci. 32 (2007) 483–507.

[97] S. Kim, Y.M. Lee, Rigid and microporous polymers for gas separation membranes, Prog. Polym. Sci. 43 (2015) 1–32.

[98] M. Rezakazemi, A. Ebadi Amooghin, M.M. Montazer-Rahmati, A.F. Ismail, T. Matsuura, State-of-the-art membrane based CO 2 separation using mixed matrix membranes (MMMs): An overview on current status and future directions, Prog. Polym. Sci. 39 (2014) 817–861.

[99] T. Rodenas, M. Van Dalen, E. García-Pérez, P. Serra-Crespo, B. Zornoza, F. Kapteijn, J. Gascon, Visualizing MOF mixed matrix membranes at the nanoscale: Towards structure-performance relationships in CO_2/CH_4 separation over NH_2-MIL-53(Al)@PI, Adv. Funct. Mater. 24 (2014) 249–256.

[100] B. Zornoza, A. Martinez-Joaristi, P. Serra-Crespo, C. Tellez, J. Coronas, J. Gascon, F. Kapteijn, Functionalized flexible MOFs as fillers in mixed matrix membranes for highly selective separation of CO_2 from CH_4 at elevated pressures, Chem. Commun. 47 (2011) 9522–9524.

[101] B. Seoane, C. Téllez, J. Coronas, C. Staudt, NH_2-MIL-53(Al) and NH_2-MIL-101(Al) in sulfur-containing copolyimide mixed matrix membranes for gas separation, Sep. Purif. Technol. 111 (2013) 72–81.

[102] O.G. Nik, X.Y. Chen, S. Kaliaguine, Functionalized metal organic framework-polyimide mixed matrix membranes for CO_2/CH_4 separation, J. Membr. Sci. 413–414 (2012) 48–61.

[103] A.F.I. P.S. Goh S.M. Sanip, B.C. Ng, M. Ariz, Recent advances of inorganic fillers in mixed matrix

membrane for gas separation, Sep. Purif. Technol. 81 (2011) 243.

[104] R.B. R. Mahajan M. Schaeffer, W.J. Koros, Challenges in forming successful mixed matrix membranes with rigid polymeric materials, J. Appl. Polym. Sci. 86 (2002) 881–890.

[105] W.J.K. R. Mahajan, Factors Controlling Successful Formation of Mixed-Matrix Gas Separation Materials, Ind. Eng. Chem. Res. 39 (2000) 2692–2696.

[106] T.S.C. L.Y. Jiang C. Cao, Z. Huang, S. Kulprathipanja, Fundamental understanding of nano-sized zeolite distribution in the formation of the mixed matrix single-and dual-layer asymmetric hollow fiber membranes, J. Membr. Sci. 252 (2005) 89–100.

[107] T.D. Kusworo, A.F. Ismail, A. Mustafa, T. Matsuura, Dependence of membrane morphology and performance on preparation conditions: The shear rate effect in membrane casting, Sep. Purif. Technol. 61 (2008) 249–257.

[108] J.D.P. M. Das W.J. Koros, Gas-Transport-Property Performance of Hybrid Carbon Molecular Sieve-Polymer Materials, Ind. Eng. Chem. Res. 49 (2010) 9310–9321.

[109] K.V.P. M.D. Jia R.D. Behling, Preparation and characterization of thin-film zeolite-PDMS composite membranes, J. Membr. Sci. 73 (1992) 119–128.

[110] T.S. C. Kong T. Tsuru, "Pre-seeding"-assisted synthesis of a high performance polyamide-zeolite nanocomposite membrane for water purification, New J. Chem. 34 (2010) 2101–2104.

[111] P.S. Goh, A.F. Ismail, S.M. Sanip, B.C. Ng, M. Aziz, Recent advances of inorganic fillers in mixed matrix membrane for gas separation, Sep. Purif. Technol. 81 (2011) 243–264.

[112] C.S. A. Car K.V. Peinemann, Hybrid membrane materials with different metal-organic frameworks (MOFs) for gas separation, Desalination. 200 (2006) 424–426.

[113] W.J.K. S. Husain, Mixed matrix hollow fiber membranes made with modified HSSZ-13 zeolite in polyetherimide polymer matrix for gas separation, J. Membr. Sci. 288 (2007) 195–207.

[114] H.M.G. Y.Li T.S. Chung, S. Kulprathipanja, Effects of novel silane modification of zeolite surface on polymer chain rigidification and partial pore blockage in polyethersulfone (PES)-zeolite A mixed matrix membranes, J. Membr. Sci. 275 (2006) 17–28.

[115] R. Mahajan, W.J. Koros, Factors controlling successful formation of mixed-matrix gas separation materials, Ind. Eng. Chem. Res. 39 (2000) 2692–2696.

[116] T.S.C. Y.Li C. Cao, S. Kulprathipanja, The effects of polymer chain rigidification, zeolite pore size

and pore blockage on polyethersulfone (PES)-zeolite A mixed matrix membranes, J. Membr. Sci. 260 (2005) 45–55.

[117] J.L. J.S. Lee R.P. Choudhury, R.M. Kriegel, H.W. Beckham, W.J. Koros, Antiplasticization-based enhancement of poly(ethylene terephtalate) barrier properties, Polymer (Guildf). 53 (n.d.) 213–222.

[118] L.A.P. N.M. Larocca, Effect of antiplasticization on the volumetric, gas sorption and transport properties of polyetherimide, J. Membr. Sci. 218 (2003) 69–92.

[119] W.M. J.S. Lee W.J. Koros, Antiplasticization and plasticization of Matrimid asymmetric hollow fiber membranes - Part A. Experimental, J. Membr. Sci. 350 (n.d.) 232–241.

[120] W.M. J.S. Lee W.J. Koros, Antiplasticization and plasticization of Matrimid asymmetric hollow fiber membranes - Part B. Modelling, J. Membr. Sci. 350 (n.d.) 242–251.

[121] G.T.O. T.M. Murphy D.R. Paul, Fundamentals of membrane gas separation, in: L.G. E. Drioli (Ed.), Membr. Oper. Innov. Sep. Transform., WILEY-VCH Verlag GmbH & Co KGaA, Weinheim, 2009: pp. 63–82.

[122] G.Q.C. C.A. Scholes G. Stevens, S.E. Kentish, Plasticization of ultra-thin polysulfone membranes by carbon dioxide, J. Membr. Sci. 346 (n.d.) 208–214.

[123] H. Ren, J. Jin, J. Hu, H. Liu, Affinity between metal-organic frameworks and polyimides in asymmetric mixed matrix membranes for gas separations, Ind. Eng. Chem. Res. 51 (2012) 10156–10164.

[124] G.M. Shi, T. Yang, T.S. Chung, Polybenzimidazole (PBI)/zeolitic imidazolate frameworks (ZIF-8) mixed matrix membranes for pervaporation dehydration of alcohols, J. Membr. Sci. 415–416 (2012) 577–586.

[125] T.H. Bae, J.S. Lee, W. Qiu, W.J. Koros, C.W. Jones, S. Nair, A high-performance gas-separation membrane containing submicrometer-sized metal-organic framework crystals, Angew. Chemie - Int. Ed. 49 (2010) 9863–9866.

[126] L. Ge, W. Zhou, V. Rudolph, Z. Zhu, Mixed matrix membranes incorporated with size-reduced Cu-BTC for improved gas separation, J. Mater. Chem. A. 1 (2013) 6350–6358.

[127] T. Rodenas, I. Luz, G. Prieto, B. Seoane, H. Miro, A. Corma, F. Kapteijn, F.X. Llabrés I Xamena, J. Gascon, Metal-organic framework nanosheets in polymer composite materials for gas separation, Nat. Mater. 14 (2015) 48–55.

[128] F. Yang, H. Mu, C. Wang, L. Xiang, K.X. Yao, L. Liu, Y. Yang, Y. Han, Y. Li, Y. Pan,

Morphological Map of ZIF-8 Crystals with Five Distinctive Shapes: Feature of Filler in Mixed-Matrix Membranes on C_3H_6/C_3H_8 Separation, Chem. Mater. 30 (2018) 3467–3473.

[129] M. Askari, T.S. Chung, Natural gas purification and olefin/paraffin separation using thermal cross-linkable co-polyimide/ZIF-8 mixed matrix membranes, J. Membr. Sci. 444 (2013) 173–183.

[130] S.N. Wijenayake, N.P. Panapitiya, S.H. Versteeg, C.N. Nguyen, S. Goel, K.J. Balkus, I.H. Musselman, J.P. Ferraris, Surface cross-linking of ZIF-8/polyimide mixed matrix membranes (MMMs) for gas separation, Ind. Eng. Chem. Res. 52 (2013) 6991–7001.

[131] N. Tien-Binh, H. Vinh-Thang, X.Y. Chen, D. Rodrigue, S. Kaliaguine, Crosslinked MOF-polymer to enhance gas separation of mixed matrix membranes, J. Membr. Sci. 520 (2016) 941–950.

[132] Y. Zhang, X. Feng, H. Li, Y. Chen, J. Zhao, S. Wang, L. Wang, B. Wang, Photoinduced postsynthetic polymerization of a metal-organic framework toward a flexible stand-alone membrane, Angew. Chemie - Int. Ed. 54 (2015) 4259–4263.

[133] L. Hao, P. Li, T. Yang, T.S. Chung, Room temperature ionic liquid/ZIF-8 mixed-matrix membranes for natural gas sweetening and post-combustion CO_2 capture, J. Membr. Sci. 436 (2013) 221–231.

[134] S.R. Venna, M. Lartey, T. Li, A. Spore, S. Kumar, H.B. Nulwala, D.R. Luebke, N.L. Rosi, E. Albenze, Fabrication of MMMs with improved gas separation properties using externally-functionalized MOF particles, J. Mater. Chem. A. 3 (2015) 5014–5022.

[135] Q. Xin, J. Ouyang, T. Liu, Z. Li, Z. Li, Y. Liu, S. Wang, H. Wu, Z. Jiang, X. Cao, Enhanced interfacial interaction and CO 2 separation performance of mixed matrix membrane by incorporating polyethylenimine-decorated metal-organic frameworks, ACS Appl. Mater. Interfaces. 7 (2015) 1065–1077.

[136] B. Seoane, V. Sebastián, C. Téllez, J. Coronas, Crystallization in THF: The possibility of one-pot synthesis of mixed matrix membranes containing MOF MIL-68(Al), Cryst.Eng.Comm. 15 (2013) 9483–9490.

CHAPTER 3. APPLICATION OF FUNCTIONALIZED - NANODIAMOND IN MIXED MATRIX MEMBRANES FOR CO_2 SEPARATION

Contribution to the field

Nanodiamonds (ND) recently emerged as excellent candidates for various applications including fillers in mixed matrix membrane technology due to their nano-scale size, non-toxic nature, excellent mechanical and thermal properties, high surface areas and tunable surface structures with functional groups. However, their non-porous structure and tendency to aggregate have hindered their potential in MMM applications for gas separation. To enhance their performance as a filler, this study proposes an efficient modification approach by grafting polyethyleneimine (PEI) onto the surface of ND before embedding into the polymer matrix to fabricate the MMMs. The target here is CO_2/N_2 separation. Acting as both interfacial binder and gas carrier agent, the PEI layer not only enhances the polymer/filler interfacial interaction, minimizing the agglomeration of ND in the polymer matrix, but also effectively improves the CO_2/N_2 selectivity compared to the pristine polymer. The contribution from this work is a simple and effective modification method, which can apply to non-porous nano-fillers in MMMs, to improve interfacial adhesion, decrease aggregation and enhance membrane performance.

3.1. Introduction

Carbon dioxide is the most prominent greenhouse gas contributing to climate change [1], but it is also one of the most serious impurities in natural gas processing, causing operational problems such as pipeline corrosion, gas hydrate formation, high energy consumption and waste of pipeline capacity [2,3]. Therefore, highly efficient and effective approaches for CO_2 capture are urgently needed. Current technologies employed for the separation of CO_2 from N_2 or CH_4 include absorption (amines), adsorption and cryogenic distillation. Membranes have also received considerable attention due to their high energy efficiency, environmental reliability and ease of scale-up [4–6]. Indeed, polymeric membranes are one of the most popular candidates for gas separation at an industrial scale due to their processability and low price [7]. However, polymeric membranes suffer from a trade-off between gas permeability and selectivity which is described by Robeson's upper bound [8]. To overcome this issue, mixed matrix membranes (MMMs) consisting of appropriate polymer and inorganic fillers have been developed as an alternative for gas separation applications [9–11].

One of the main issues affecting the gas separation performance of MMMs is the interfacial interaction and compatibility between polymeric matrix and the embedded fillers. Both glassy and rubbery polymers have been applied to fabricate gas separation MMMs. Generally, glassy polymers show good mechanical stability and CO_2 selectivity but low CO_2 permeability as well as poor interaction and compatibility with conventional inorganic fillers, leading to mediocre gas separation performance [12]. In contrast, rubbery polymeric based MMMs express higher CO_2 permeability along with acceptable polymer-filler compatibility but low CO_2 selectivity and are more susceptible to plasticization effects under pressure [13]. Recently, use of block copolymers as the matrix materials in MMMs fabrication has attracted increasing attention due to the advantage combination of both rubbery and glassy polymers [4]. One of the promising candidates for CO_2 separation is the polyether block amide (Pebax) [2]. Pebax consists of polyamide (PA) as hard segments and polyether (PE) as soft segments in the polymer chains, where the hard crystalline PA block provides mechanical strength and the soft polyether block plays as the gas permeable phase due to its high chain mobility [14]. The structure of Pebax repeating unit is as below:

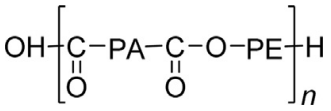

Studies on Pebax-based membranes have been increasingly reported in the literatures. Potreck et al. used Pebax 1074 as the membrane material for water removal from light gases, which showed water/N_2 selectivity increase with increasing water vapor activity [15]. Bondar et al. investigated Pebax membranes and showed strong interaction between soft segment PE block and CO_2 gas [16]. More recently, Bernado et al. fabricated gel membranes based on Pebax (1657 and 2533) and the ionic liquid [Bmim][CF_3SO_3] [17]. Their results indicated that the incorporation of the ionic liquid improved the permeability for CO_2. Zhang et al. used nonionic hydrocarbon surfactant (Tween) as the CO_2 carrier in Pebax based membranes, which improved both permeability and selectivity of CO_2 over N_2 [18]. Azizi's research group investigated the Pebax/poly ethylene glycol (PEG)/nano-size TiO_2 MMM for CO_2/CH_4 separation. They showed that the synthesized MMMs exhibit better separation performance compared to the neat Pebax membranes [4].

Nanodiamonds (ND) are carbon nano-crystalline particles which were first observed after the detonation of explosive mixtures [19,20] and are now being commercially synthesized by a relatively low-cost and large scale process [21]. ND particles have the primary spherical shape with

average diameter of 5 - 10 nm with a narrow particle size distribution, while also possessing a high surface area (more than 200 m^2/g) covered by functional groups formed during detonation process [22,23]. Nanodiamond is popular for its chemical stability, high thermal conductivity, biocompatibility, hardness and electrical insulation, that make them a potential candidates for various applications [24–27]. In term of membrane fabrication, composite membrane based on poly(vinylidene fluoride)/NDs have been applied to water desalination [28]. Other work by Polotskaya et.al selected ND as an inorganic filler for poly(2,6-dimethyl-1,4-phenylene oxide) membranes for gas separation [29]. Recently, Avagimova et al. incorporated ND into poly(phenylene-isophtalamide) matrix to prepare MMMs for gas separation [30]. Their results showed that the selectivity of H_2/N_2 and O_2/N_2 gas pairs increased with the ND concentration up to 3 wt.%. One drawback of ND is its tendency to form aggregates in polymer composites, which is devastating in MMM fabrication for gas separation, as non-selective voids are formed reducing the separation performance of the MMM. One of the effective approaches to prevent ND agglomeration and improve the filler/polymer interfacial interaction is ND surface treatment, which has been reported in the literature such as funtionalization with long alkyl chains [26], fluorine [31], mineral acids [32], acrylates [33] and a silane coupling agent [34]. When acting as filler for gas separation MMMs, another disadvantage of ND is its non-porous nature which does not allow the ND to separate gases base on size discrimination. For this reason, functionalizing ND surface with functional groups that have high affinity for a desired gas is necessary in order to enhance the gas permeability and selectivity of polymer/ND MMMs. A layer of suitable functional groups on the surface of ND may create alternative pathways for the desired gas to permeate through similar to the role of a gas carrier agent in mixed matrix membranes.

This chapter aims to investigate the effects of ND in a Pebax matrix on the separation of CO_2 from N_2. To the best of my knowledge, there are no studies on Pebax/ND MMM for gas separation reported at the time of writing. The pristine ND particles were functionalized with low molecular weight polyethylene imine (PEI), which acts as both a polymer/filler interfacial binder as well as a CO_2 carrier agent, prior to ND incorporation into the Pebax matrix. The results showed that the CO_2/N_2 selectivity of Pebax/ND-PEI MMMs is significantly improved compared to the Pebax/ND MMMs and pristine Pebax membranes. The structural investigation by scanning electron microscopy (SEM) also demonstrated obvious enhancement of polymer/filler interfacial interaction with the presence of PEI in the MMMs.

3.2. Experimental

3.2.1. Materials

Nanodiamond, polyethyleneimine (PEI) was purchased from Sigma-Aldrich. Pebax (MH 1657) was kindly supplied by Arkema. Ethanol was supplied by Sigma-Aldrich.

3.2.2. Nanodiamond oxidation

Neat nanodiamond (ND) was firstly oxidized in order to generate functional groups (hydroxyl or carboxyl groups) on the surface of ND according to method in literature elsewhere [8]. Amount of ND was heated up from room temperature to 400 ^{o}C in air using an oven for 4 h with heating rate of 10°C/min. Obtained oxidized oxND was stored in dessicator under vacuum before use.

3.2.3. Nanodiamond surface modification

Pre-calculated amount 2g of polyethyleneimine (PEI) was dissolve in 15 mL of deionized water and stirred in 30 minutes to form a homogeneous solution. 0.2g of oxidized nanodiamond (oxND) was then dispersed into the PEI contained solution and sonicated for 15 minutes in order to completely dispersed the oxND nanoparticles. The well-dispersed mixture was subsequently heated up to 70 ^{o}C whilst stirring at 250 rpm for 24 h. The mixture was then centrifuged and washed with deionized water for at least three times before drying in vacuum oven at 100 ^{o}C in 24 h and stored under vacuum before use. The loading of PEI was adjusted to obtain the ratio oxND : PEI = 1 : 10 (wt : wt), and the obtained sample was then labelled as oxND-PEI.

3.2.4. Fabrication of nanodiamond incorporated mixed matrix membranes

For the neat Pebax membrane, 0.48 g of Pebax was dissolved in mixture of ethanol/water (70/30 wt.%/wt.%) by heating up to 70 ^{o}C and stirring for 6 h. The resulting solution was then cast on a flat glass surface with a doctor blade at gap setting of 300 µm and dried in vacuum oven at 100 ^{o}C in 24 h. The obtained membrane was then peeled off the glass plate and stored under vacuum before use.

For the mixed matrix membrane fabrication, a quantity of modified nanodiamond (oxND or oxND-PEI) was dispersed into a mixed solution of ethanol/water (70/30 wt.%/wt.%) and sonicated for 15 minutes. Pebax was then slowly added into the mixture while heating up to 70°C along with sonication several times during the process. Amount of Pebax and nanodiamond was calculated in order to form the ratio: Pebax : oxND = 99.9 : 0.1, 99.5 : 0.5, 99 : 1, 98.5 : 1.5 (wt.% : wt.%). The resulting mixture was cast onto a clean glass plate with a doctor blade at gap setting of 300 µm and dried at 100 ^{o}C in 24h before peeling off. The thickness of pure Pebax and MMMs were measured

using a micrometer within the range of 40−50 μm. The membranes were stored with desiccant under vacuum before gas permeation tests and characterization.

3.3. Characterization

The N_2 adsorption isotherms were obtained from a Micromeritics ASAP 2020 at 77 K, after degassing the sample at 180 ^{o}C for 24 h. BET surface area was calculated over the range of relative pressures between 0.005 and 0.05. The CO_2, N_2 adsorption isotherms at 303K were also carried out .

The elemental analysis was carried out by FLASH 2000 CHNS/O Analyzer instrument and the procedure was described elsewhere [35]. In short, samples of approximately 1mg kept in a lightweight tin capsule were dropped at preset intervals of time into a vertical quartz combustion tube maintained at 1020 °C with a constant flow of helium. After introducing the sample, the helium stream was temporarily enriched with pure oxygen to initiate the flash combustion. Quantitative combustion was then achieved by passing the mixture of gases over tungstic oxide. The mixture of gases was passed over copper to remove the excess oxygen and reduce oxides of nitrogen to nitrogen and then travelled through a chromatographic column onto a TC detector. The gases eluted were N_2, CO_2, H_2O, SO_2. For O element determination, the sample was weighed into a silver capsule and heated to 1060 °C, then passing over nickel coated carbon to quantitatively converted to CO. Any other gases are removed with suitable gas traps.

The surface of ND particles and the cross-surface morphologies of the membrane samples were obtained with a JEOL JSM7100 scanning electron microscope (SEM) at 10 kV.

Focused ion beam scanning electron microscopy (FIB-SEM) observation was carried out in a FEI SCIOS FIB/SEM dual beam system to determine the contact of the inorganic phase and polymeric matrix. A trench was firstly milled on the surface of the membrane with a Ga+ focused ion beam (FIB) (Fig 3.1). Numbers of slices with fixed thickness were cut from the specimen by the Ga+ FIB at 30kV and 3nA, while a series of exposed cross-section SEM images were collected in back-scattered electron (BSE) mode at 2kV. The segmentation of the individual phases (e.g. polymer, filler, voids) was conducted by image thresholding based on their different grayscale [29,30]. The whole stack of these SEM images was aligned and reconstructed in three-dimensions using Avizo software (FEI Visualization Sciences Group).

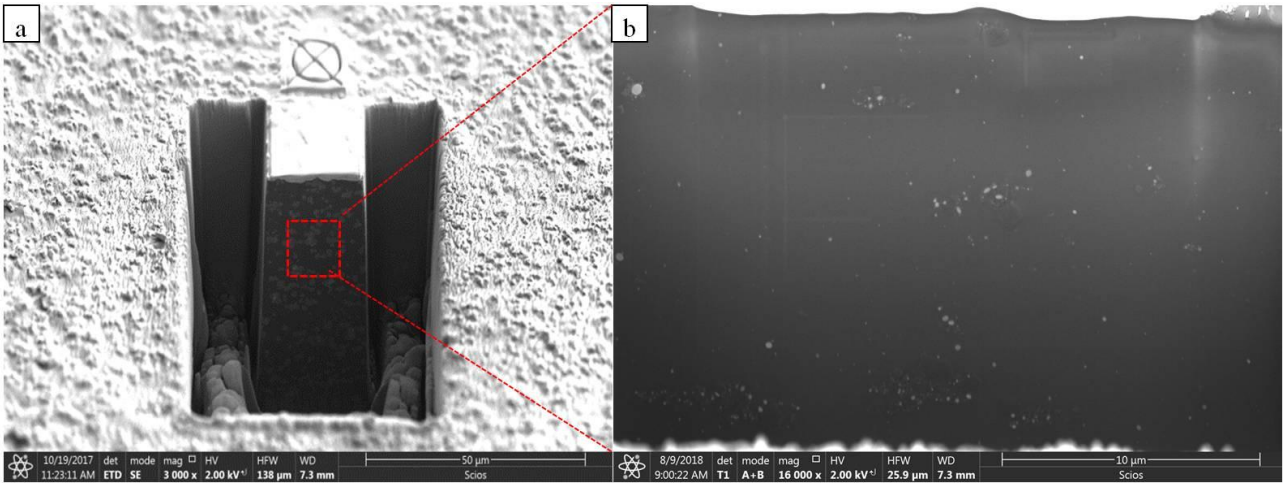

Figure 3.1 Typical FIB-SEM images of Pebax/oxND 1.5 wt.% MMM: (a) FIB milling trend and (b) cross-sectional image in BSE mode

3.3.1. Gas permeation test

The single gas permeation test was conducted as described in detail in the Appendix. The membranes were held under vacuum for 30 min to achieve a steady state before being exposed to the selected gas. The test was held at 30 ^{o}C, 2 atm feed pressure. The permeation coefficient is calculated using the following equation:

$$P = \frac{273.15 \times 10^{10}}{760\mathrm{AT}} \frac{VL}{\frac{P_0 \times 76}{14.7}} \frac{\mathrm{d}p}{\mathrm{d}t}$$

where P is the permeation coefficient in barrer (1 barrer =1×10^{-10} cm^3 (STP) cm cm^{-2} s^{-1} cm Hg^{-1}), A is the effective area of the membrane (cm^2), T is the absolute temperature (K), V is the dead-volume of the downstream chamber (cm^3), L is the membrane thickness (cm), P^0 is the feed pressure (psi), and dp/dt is the steady rate of pressure increase in the downstream side (mm Hg s^{-1}).

The ideal selectivity for two gases is determined as:

$$\alpha = \frac{P_\mathrm{A}}{P_\mathrm{B}}$$

where P_A and P_B are the permeation coefficients of pure gas A and B, respectively.

3.4. Results and discussion

Fig. 3.2 shows the SEM images of oxND and oxND-PEI. The oxND expresses spherical shape crystalline structure with size of around 10 nm. In case of oxND-PEI samples, a similar morphology has been observed which indicated that the grafting process showed negligible effect on the crystalline structure and shape of oxND.

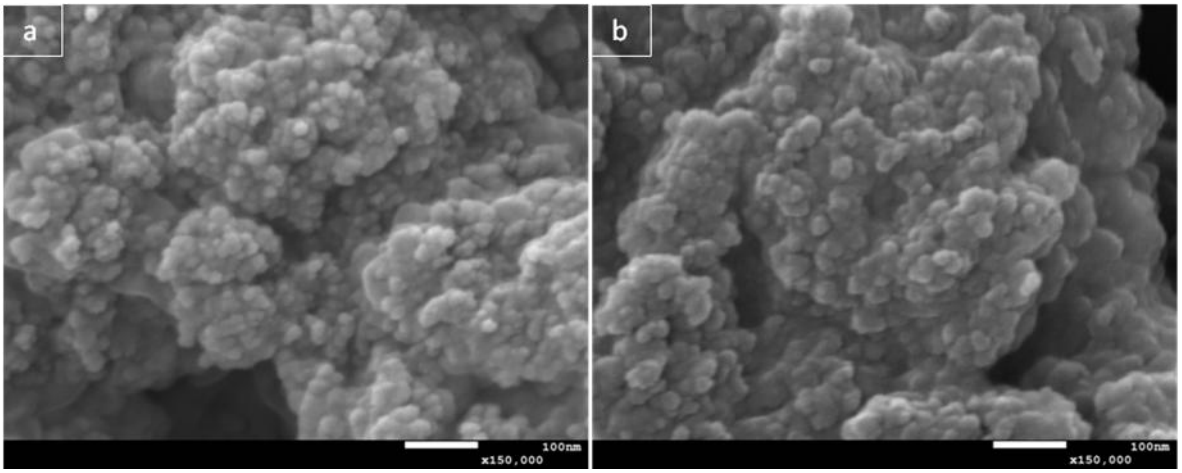

Figure 3.2 SEM images of oxND (a) and oxND-PEI (b)

In order to confirm the success of the surface modification of oxND by PEI, elemental analysis was conducted and the results are shown in Table 3.1. Compared to the oxND, the oxND-PEI particles showed higher concentration of N, C, H and a lower concentration of O. These results provide strong evidence that the PEI has been successfully incorporated on the oxND surface.

Table 3.1 Elemental weight ratio of pristine ND, oxND and oxND-PEI particles

Samples	Elemental ratio (wt.%)			
	N	**C**	**H**	**O**
Pristine ND	1.61	86.27	0.64	11.48
oxND	1.62	81.32	0.26	16.80
oxND-PEI	4.34	83.94	1.25	10.47

N_2 adsorption isotherm at 77K of oxND and oxND-PEI were showed in Fig. 3.3. A sharp increase of adsorption at low relative pressure (< 0.02) was observed due to the textured surface of the nanodiamond. The BET surface areas calculated from the isotherms were 264.36 ± 2.37 m^2/g and 205.59 ± 3.91 m^2/g for oxND and oxND-PEI, respectively, which indicated a reduction in surface area of ND with the presence of PEI. There is an associated decrease in adsorption at low pressure

(<0.02). Both observations are most likely associated with the occupation of free surface area of ND by PEI.

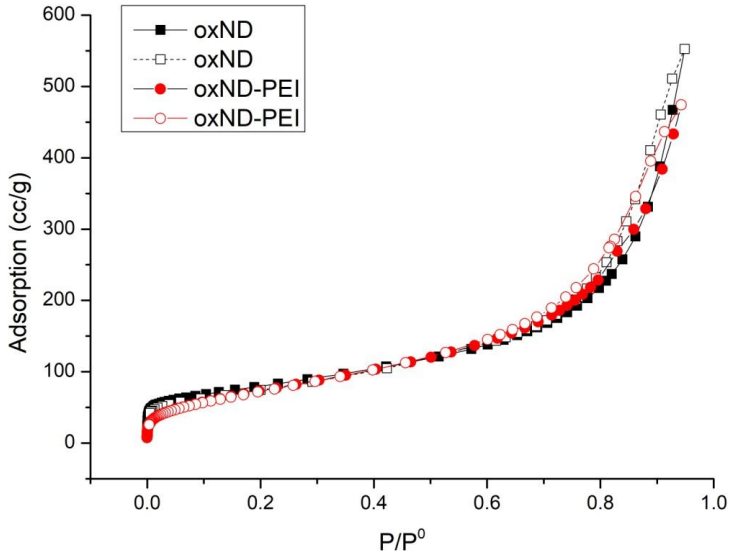

Figure 3.3 N_2 adsorption isotherm of oxND and oxND-PEI at 77K (Full: adsorption, hollow: desorption)

The gas sorption capacity of oxND and oxND-PEI at 303K were also investigated and the results are showed in Fig. 3.4. Similar trends with the N_2 adsorption isotherm at 77K (Fig. 3.3) were observed as the oxND-PEI shows lower adsorption capacity with both CO_2 and N_2 gases compared to the oxND particles. Based on the isotherms, the ideal CO_2/N_2 selectivities of oxND and oxND-PEI at 1 bar were calculated and are shown in Table 3.2. Interestingly, oxND-PEI shows higher CO_2/N_2 selectivity though expressing lower adsorption capacity for both gases. This is hypothesized to be due to the PEI layer on the ND surface. The occupation of the PEI on the surface area of ND leads to lower total gas adsorption. However, the amine functional groups of PEI have affinity to CO_2 meaning the reduction in CO_2 adsorption is less that the reduction in N_2 adsorption capacity, causing a small relative increase in selectivity of CO_2/N_2 at 1 bar for the oxND-PEI particles.

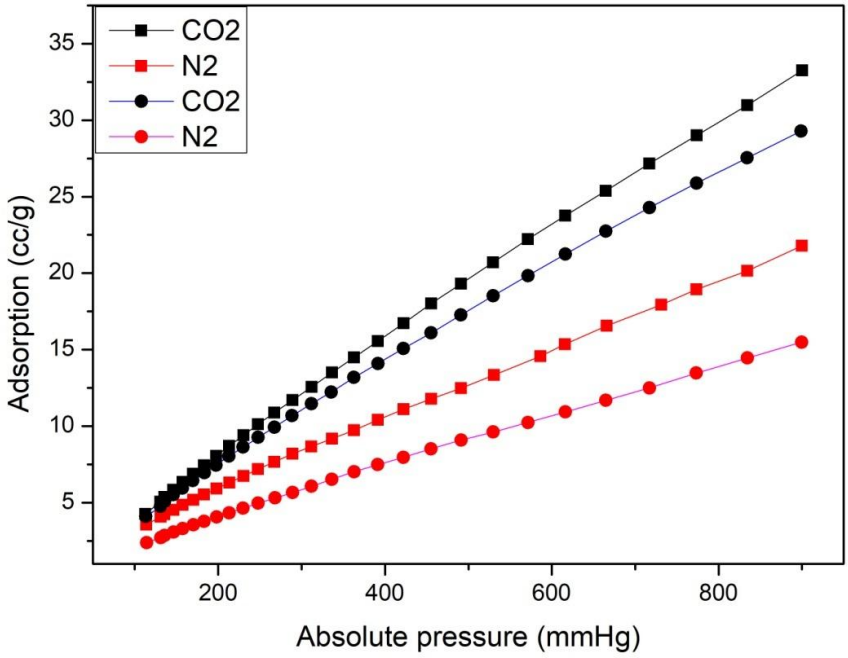

Figure 3.4 Gas sorption capacity of oxND (square) and oxND-PEI (round) at 303K

Table 3.2 Ideal selectivity of oxND and oxND-PEI at 1 bar

Samples	**Gas adsorption capacity at 1 bar (cc/g)**		**Ideal selectivity at 1 bar**
	CO_2	N_2	CO_2/N_2
oxND	29.01	18.94	1.53
oxND-PEI	25.89	13.47	1.92

The transport performance and the integrity of the membrane relies significantly on the filler dispersion and the filler/matrix adhesion. The interfacial morphology of Pebax/oxND MMMs and Pebax/oxND-PEI MMMs were investigated by FESEM technique and the images are displayed in Fig. 3.5 and Fig. 3.6. Compared to the pristine Pebax membrane (Fig. 3.5(a,b)), poor dispersion of oxND in Pebax matrix was clearly observed in the Pebax/oxND MMMs (Fig. 3.5(c) - 3.5(k)), as

indicated by large aggregates of oxND (indicated by arrows) in the matrix. It would appear that the oxygen-containing functional groups on the ND surface do not improve the dispersion of ND in the Pebax matrix. Without further surface modification, the oxND tends to form agglomerations easily, which has also been reported in previous literature [15]. The aggregation of the ND can cause the formation of the non-selective interfacial voids, leading to the deterioration in gas selectivity of the membrane. With further increasing the oxND loading, unsurprisingly, more aggregate clusters with larger size were observed.

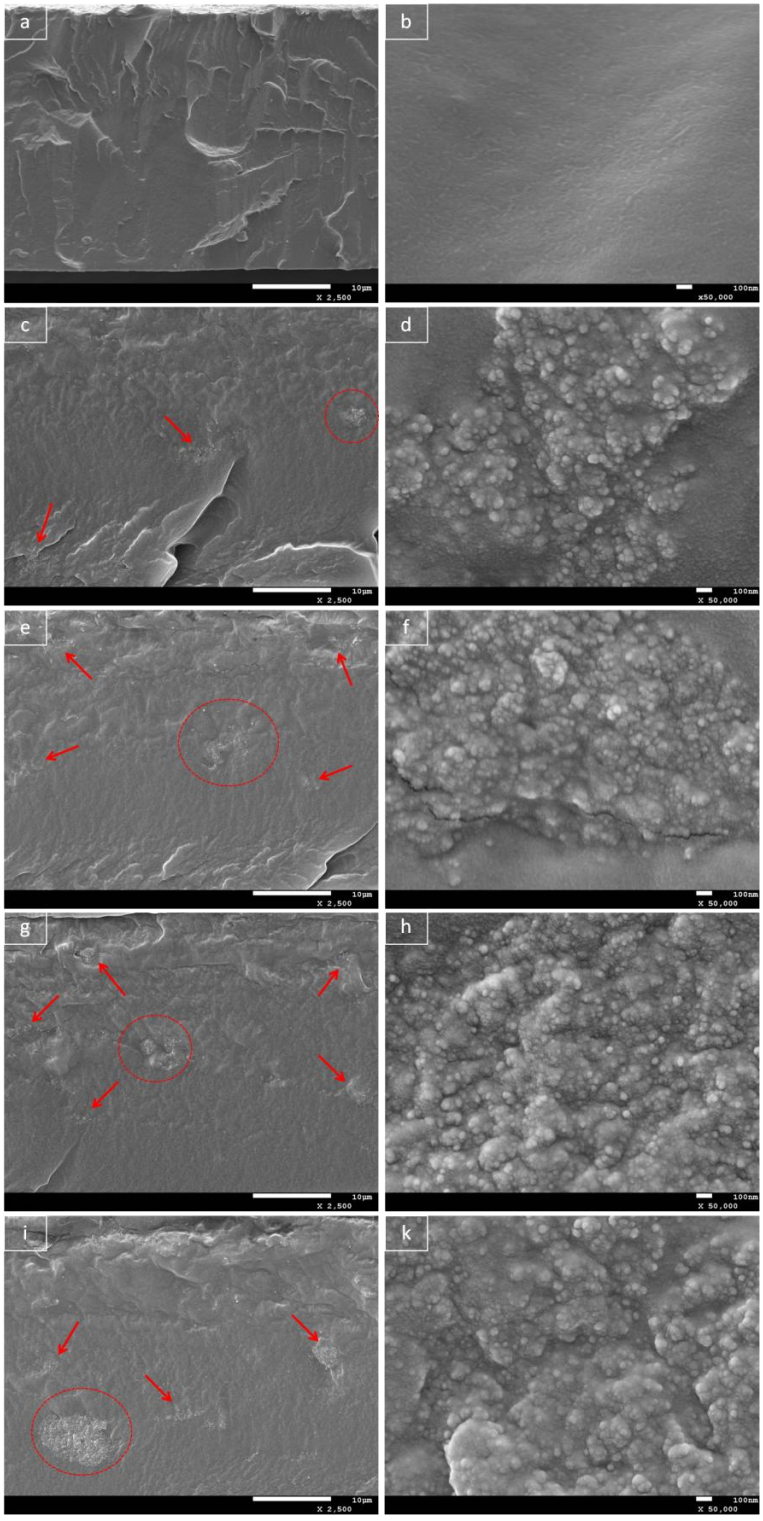

Figure 3.5 SEM images of pristine Pebax membrane (a, b) and Pebax/oxND MMMs with different ND ratio: 0.1 wt.% (c, d), 0.5 wt.% (e, f), 1.0 wt.% (g, h), 1.5 wt.% (i, k) arrows point to ND aggregate clusters in the MMMs.

In the case of Pebax/oxND-PEI MMMs (Fig. 3.6), the cross-surface of the membrane is homogenous and the individual oxND-PEI particles were less visible in the matrix, with

considerably fewer aggregate clusters of oxND-PEI fillers observed. The roughness of the Pebax/oxND-PEI MMMs was also significantly increased compared to the neat Pebax membranes. Both observations indicate improved dispersion of ND in polymer matrix was achieved. The improvement in dispersion and adhesion of oxND-PEI with the polymer matrix, is attributed to the presence of the PEI layer on ND surface. The amino functional groups (-NH- and -NH_2) in PEI molecules may form hydrogen bonding with carboxylic groups (-COO-) on both oxND surface and Pebax molecular chains, resulting in the enhanced interfacial interaction of Pebax and oxND-PEI. Besides, the PEI layer may also acts as the polymeric compatibilizer, which can improve the compatibility between the crystalline carbon structure of ND and the rubbery polymeric nature of Pebax, leading to the increase in dispersibility of ND in the Pebax matrix. However, at higher loading of oxND-PEI (1.5 wt.%), some filler agglomeration were observed, which is probably due to the larger concentration of ND particles preventing the uniform distribution of fillers above a critical threshold. From the SEM images, it can be seen that introducing PEI can contribute to the improvement of filler/polymer interfacial interaction and the prevention of filler aggregation in the MMMs.

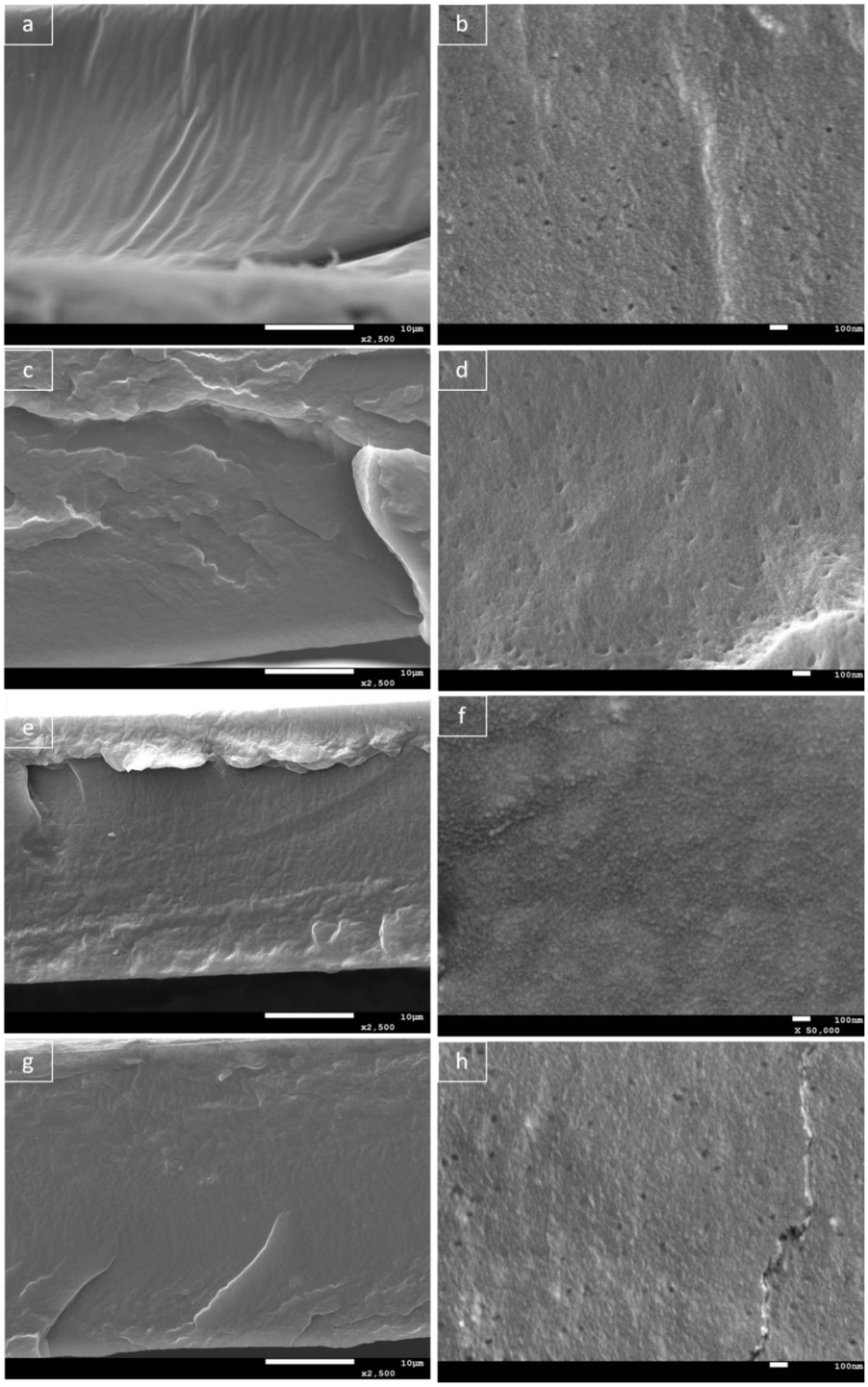

Figure 3.6 SEM images of Pebax/oxND-PEI MMMs with different ND ratio: 0.1 wt.% (a, b), 0.5 wt.% (c, d), 1.0 wt.% (e, f), 1.5 wt.% (g, h)

In order to further investigate the dispersion and interfacial adhesion of oxND and oxND-PEI particles with the Pebax matrix, FIB-SEM was conducted to study the internal structure of the MMM at 1.5 wt.% loading of oxND and oxND-PEI. Fig. 3.7 shows the FIB 3D images of the Pebax/oxND 1.5 wt.% MMM and Pebax/oxND-PEI 1.5 wt.% MMM. The oxND and oxND-PEI

exhibit round shapes which are in agreement with the SEM images in Fig. 3.2. As was observed in the traditional SEM images (Fig. 3.5 and 3.6), the oxND particles formed large aggregates in the MMMs, while in contrast, the oxND-PEI aggregates are less likely to be observed. This is hypothesized to be due to the presence of PEI as discussed previously. Based on the 3D image analysis, the amount of ND particles (based on the particle volume in the MMMs) were calculated and reported in Fig 3.8. For the Pebax/oxND 1.5 wt.% MMMs, a majority of the oxND are large-volume particles (10^4-10^6 nm^3), while the small volume particles only occupy a small fraction. This indicates the aggregation of oxND particles in the MMMs. On the other hand, the oxND-PEI exhibited a greater percentage of smaller volume particles, demonstrating better dispersion of oxND-PEI in the polymer matrix, which can only be due to the incorporation of PEI. Hence, the PEI layer clearly provides compatibility and interfacial interaction between the ND and Pebax matrix.

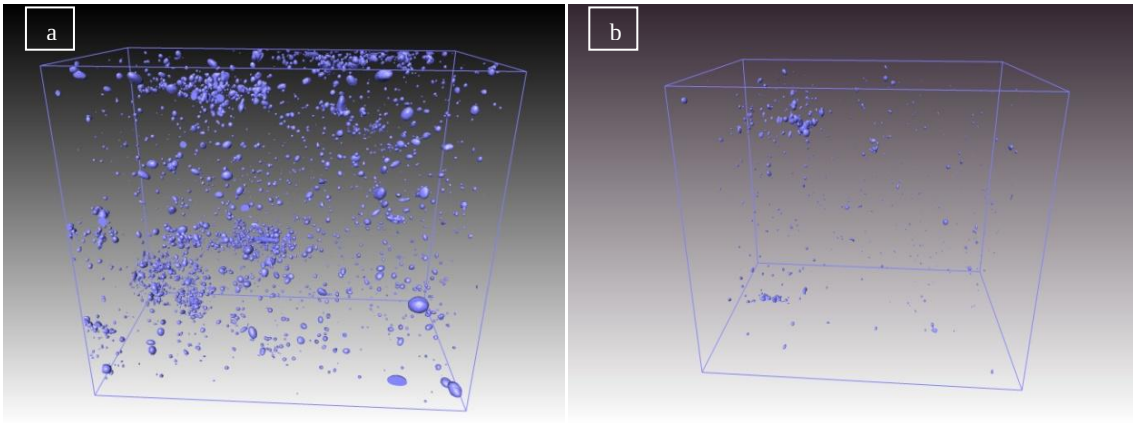

Figure 3.7. The FIB surface rendered view of Pebax/oxND 1.5 wt.% MMM (a) and Pebax/oxND-PEI 1.5 wt.% MMM (b)

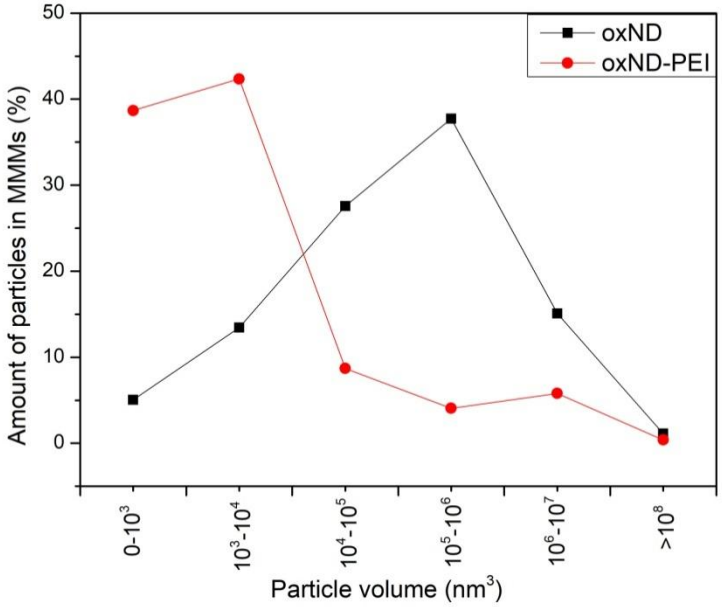

Figure 3.8. Amount of ND particles in Pebax/oxND 1.5 wt.% MMM and Pebax/oxND-PEI 1.5 wt.% MMM based on particle volume

The ideal gas separation performance of the pristine Pebax membranes, Pebax/oxND MMMs and Pebax/oxND-PEI MMMs were investigated by single gas permeability measurement, as shown in Fig. 3.9, Fig. 3.10 and Table 3.3. The pristine Pebax membrane showed CO_2 permeability of 56 barrer with the CO_2/N_2 selectivity of 40.60, which is consistent with previous studies. At lower loading of oxND (0.1 wt.%, 0.5 wt.%, 1 wt.%), the CO_2 and N_2 permeability of oxND MMMs decreased after the introduction of oxND when compared to the neat Pebax membranes, with the CO_2/N_2 selectivity also reduced. The presence of oxND in the polymer matrix may reduce free volume between the polymer chains, which when combined with the non-porous nature of ND, hinders gas diffusion through the membrane, leading to the reduction in gas permeability. Furthermore, the oxND agglomerations and poor filler/polymer interaction as seen in the SEM investigation (Fig. 3.5), led to the formation of non-selective voids, which lowered CO_2/N_2 selectivity of the MMMs. Interestingly, at 1.5 wt.% loading of oxND, the Pebax/oxND MMMs expressed a higher CO_2 permeability and comparable CO_2/N_2 selectivity compared to the lower oxND loading MMMs. This result may be explained as at high loading, the oxND particles tend to form a smaller number of large aggregated clusters with a significant number of non-selective voids, these increase the permeability of both CO_2 and N_2 through the membranes. However, the selectivity of the MMM system is still governed by the polymer matrix which occupies a larger distance between the aggregated oxND clusters. These effect of the two competing mechanisms leads to a sharp increase of CO_2 permeability along with a slight improvement in CO_2/N_2 selectivity.

In case of MMMs with oxND-PEI (Fig. 3.10), at 0.1 wt.% loading of oxND-PEI, the gas permeability of MMMs decreased while the CO_2/N_2 selectivity slightly reduced. In this case, the incorporation of PEI may improved the interfacial adhesion of ND and the Pebax matrix, which results in the reduction of free volume in the MMMs due to the occupation of oxND-PEI particles. This result leads to the deterioration in both CO_2 and N_2 permeability through the MMMs. At lower loading of oxND-PEI, the amount of PEI incorporated in the MMMs may not be enough to enhance the CO_2 permeability to overcome the deterioration above, leading to the slight reduction in CO_2/N_2 selectivity. When the loading of oxND-PEI increased (up to 1 wt.%), both CO_2 permeability and CO_2/N_2 selectivity of the Pebax/oxND-PEI MMMs were improved compared to the pristine Pebax and the Pebax/oxND MMM. The introduction of PEI layer significantly enhanced the interfacial interaction between oxND particles and the polymer matrix, which prevents the agglomeration formation and eliminates the non-selective voids, leading to better CO_2/N_2 separation performance. Furthermore, the PEI layer on the ND surface may acts as the "CO_2 carrier agent" due to the amine functional groups, which further enhances the solubility of CO_2 through the MMMs and subsequently improve the CO_2/N_2 selectivity. At 1.5 wt.% loading of oxND-PEI, the MMMs show higher permeability for both CO_2 and N_2 while the CO_2/N_2 selectivity is decreased (37.09), which can be due to the formation of the ND aggregations caused by the high concentration of ND in the polymer matrix, and it is in agreement with the SEM investigation above.

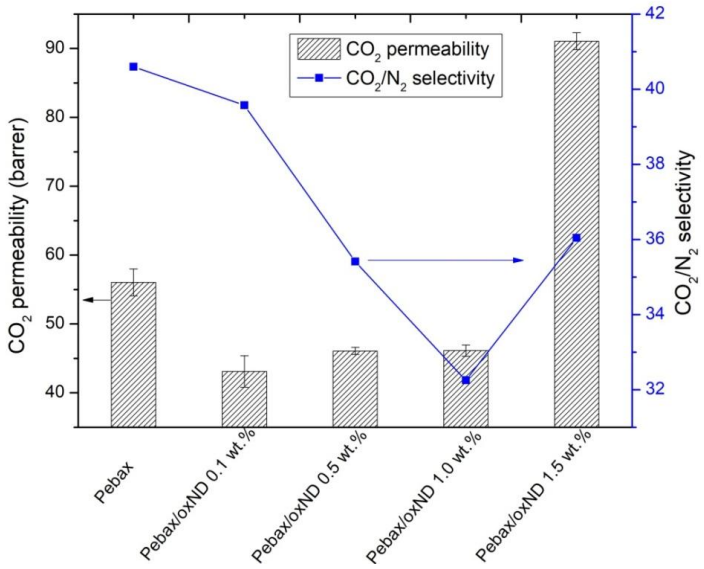

Figure 3.9. Gas separation performance of Pebax/oxND MMMs

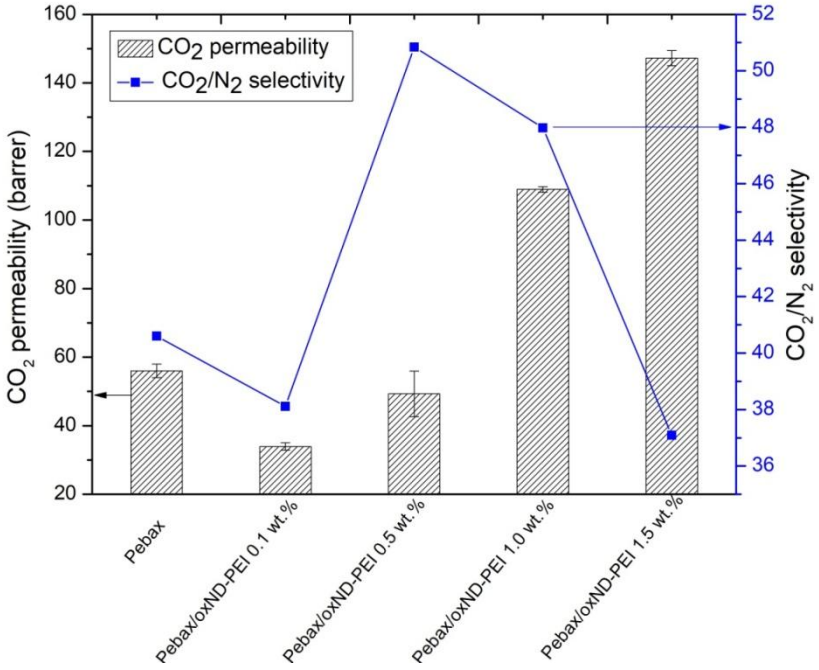

Figure 3.10. Gas separation performance of Pebax/oxND-PEI MMMs

Table 3.3. Gas permeability and selectivity of pure Pebax membrane, PZ MMM and PZ/IL MMM

Sample	Permeability (barrer)		Selectivity
	CO_2	N_2	CO_2/N_2
Pebax	56.03±1.96	1.38±0.50	40.60
Pebax/oxND 0.1 wt.%	43.12±2.29	1.09±0.14	39.57
Pebax/oxND 0.5 wt.%	46.08±0.53	1.30±0.19	35.41
Pebax/oxND 1.0 wt.%	46.12±0.84	1.43±0.29	32.25
Pebax/oxND 1.5 wt.%	91.06±1.23	2.53±0.21	36.04
Pebax/oxND-PEI 0.1 wt.%	33.92±1.11	0.89±0.21	38.11
Pebax/oxND-PEI 0.5 wt.%	49.31±6.63	0.97±0.24	50.84
Pebax/oxND-PEI 1.0 wt.%	108.92±0.84	2.27±0.89	47.98
Pebax/oxND-PEI 1.5 wt.%	147.23±2.21	3.97±0.31	37.09

3.5. Conclusion

In this chapter, mixed matrix membranes formed using ND nanoparticles as the filler and Pebax as the polymer matrix were investigated for CO_2/N_2 separation. Surface modification of ND by

grafting with PEI has been conducted and confirmed by the elemental analysis. The presence of PEI layer on ND surface, while reducing the BET surface area and gas adsorption capacity of ND, still effectively improved the interfacial adhesion and dispersion of ND in the Pebax matrix, as clearly indicated by conventional SEM and FIB-SEM observations. The ideal selectivity of CO_2/N_2 was also significantly improved with the incorporation of PEI up to 1 wt.% of oxND-PEI filler in the MMMs, due to the "CO_2 carrier" role of PEI and the reduction in polymer free volume, increasing the relative resistance of diffusion for N_2. These results show that polymeric grafting with a compatible polymer is an effective modification approach for applying the potential non-porous ND into gas separation membrane applications.

Reference

[1] P. Luis, T. Van Gerven, B. Van Der Bruggen, Recent developments in membrane-based technologies for CO_2 capture, Prog. Energy Combust. Sci. 38 (2012) 419–448.

[2] A. Jomekian, R.M. Behbahani, T. Mohammadi, A. Kargari, CO_2/CH_4 separation by high performance co-casted ZIF-8/Pebax 1657/PES mixed matrix membrane, J. Nat. Gas Sci. Eng. 31 (2016) 562–574.

[3] E. Ahmadpour, A.A. Shamsabadi, R.M. Behbahani, M. Aghajani, A. Kargari, Study of CO_2 separation with PVC/Pebax composite membrane, J. Nat. Gas Sci. Eng. 21 (2014) 518–523.

[4] N. Azizi, T. Mohammadi, R.M. Behbahani, Synthesis of a new nanocomposite membrane (PEBAX-1074/PEG-400/TiO_2) in order to separate CO_2 from CH_4, J. Nat. Gas Sci. Eng. 37 (2017) 39–51.

[5] P.D. Sutrisna, J. Hou, H. Li, Y. Zhang, V. Chen, Improved operational stability of Pebax-based gas separation membranes with ZIF-8: A comparative study of flat sheet and composite hollow fibre membranes, J. Membr. Sci. 524 (2017) 266–279.

[6] N. Azizi, T. Mohammadi, R. Mosayebi Behbahani, Comparison of permeability performance of PEBAX-1074/TiO_2, PEBAX-1074/SiO_2 and PEBAX-1074/Al_2O_3 nanocomposite membranes for CO_2/CH_4 separation, Chem. Eng. Res. Des. 117 (2017) 177–189.

[7] W.J. Koros, Evolving beyond the thermal age of separation processes: Membranes can lead the way, AIChE J. 50 (2004) 2326–2334.

[8] L.M. Robeson, The upper bound revisited, J. Membr. Sci. 320 (2008) 390–400.

[9] G. Dong, H. Li, V. Chen, Challenges and opportunities for mixed-matrix membranes for gas separation, J. Mater. Chem. A. 1 (2013) 4610–4630.

[10] T.S. Chung, L.Y. Jiang, Y. Li, S. Kulprathipanja, Mixed matrix membranes (MMMs) comprising organic polymers with dispersed inorganic fillers for gas separation, Prog. Polym.

Sci. 32 (2007) 483–507.

[11] M. Vinoba, M. Bhagiyalakshmi, Y. Alqaheem, A.A. Alomair, A. Pérez, M.S. Rana, Recent progress of fillers in mixed matrix membranes for CO_2 separation: A review, Sep. Purif. Technol. 188 (2017) 431–450.

[12] J. Xia, S. Liu, C.H. Lau, T.S. Chung, Liquidlike poly(ethylene glycol) supported in the organic-inorganic matrix for CO2 removal, Macromolecules. 44 (2011) 5268–5280.

[13] M. Galizia, W.S. Chi, Z.P. Smith, T.C. Merkel, R.W. Baker, B.D. Freeman, 50th Anniversary Perspective: Polymers and Mixed Matrix Membranes for Gas and Vapor Separation: A Review and Prospective Opportunities, Macromolecules. 50 (2017) 7809–7843.

[14] S. Feng, J. Ren, Z. Li, H. Li, K. Hua, X. Li, M. Deng, Poly (amide-12-b-ethylene oxide)/glycerol triacetate blend membranes for CO_2 separation, Int. J. Greenh. Gas Control. 19 (2013) 41–48.

[15] J. Potreck, K. Nijmeijer, T. Kosinski, M. Wessling, Mixed water vapor/gas transport through the rubbery polymer PEBAX®1074, J. Membr. Sci. 338 (2009) 11–16.

[16] V.I. Bondar, B.D. Freeman, I. Pinnau, Gas transport properties of poly(ether-b-amide) segmented block copolymers, J. Polym. Sci. Part B Polym. Phys. (2000).

[17] P. Bernardo, J.C. Jansen, F. Bazzarelli, F. Tasselli, A. Fuoco, K. Friess, P. Izák, V. Jarmarová, M. Kačírková, G. Clarizia, Gas transport properties of Pebax®/room temperature ionic liquid gel membranes, Sep. Purif. Technol. 97 (2012) 73–82.

[18] C. Zhang, L. Dong, Y. Zhang, Y. Bai, J. Gu, Y. Sun, M. Chen, Poly(ether-b-amide)/Tween20 Gel Membranes for CO2/N2Separation, Sep. Sci. Technol. 50 (2015) 2375–2383.

[19] S. Rabiei, A. Shojaei, Vulcanization kinetics and reversion behavior of natural rubber/styrene-butadiene rubber blend filled with nanodiamond - The role of sulfur curing system, Eur. Polym. J. 81 (2016) 98–113.

[20] Z. Delavar, A. Shojaei, Enhanced mechanical properties of chitosan/nanodiamond composites by improving interphase using thermal oxidation of nanodiamond, Carbohydr. Polym. 167 (2017) 219–228.

[21] V.Y. Dolmatov, Detonation-synthesis nanodiamonds: synthesis, structure, properties and applications, Russ. Chem. Rev. 76 (2007) 339–360.

[22] S. Osswald, G. Yushin, V. Mochalin, S.O. Kucheyev, Y. Gogotsi, Control of sp2 / sp3 Carbon Ratio and Surface Chemistry of Nanodiamond Powders by Selective Oxidation in Air, J. Am. Chem. Soc. 128 (2006) 11635–11642.

[23] F. Hajiali, A. Shojaei, Silane functionalization of nanodiamond for polymer nanocomposites-effect of degree of silanization, Colloids Surfaces A Physicochem. Eng. Asp. 506 (2016)

254–263.

[24] V.N. Mochalin, O. Shenderova, D. Ho, Y. Gogotsi, The properties and applications of nanodiamonds, Nat. Nanotechnol. 7 (2012) 11–23.

[25] O. Faklaris, V. Joshi, T. Irinopoulou, P. Tauc, M. Sennour, H. Girard, C. Gesset, J. Arnault, A. Thorel, J.-P. Boudou, P.A. Curmi, F. Treussart, P.D. Nanoparticles, C. Labeling, U. Mechanism, M. Cells, Ḱ.H. Girard, Ḱ.J. Boudou, Photoluminescent diamond nanoparticles for cell labeling : Study of the uptake mechanism in mammalian cells, ACS Nano. 3 (2009) 3955–3962.

[26] A. Krueger, Diamond nanoparticles: Jewels for chemistry and physics, Adv. Mater. 20 (2008) 2445–2449.

[27] H.A. Girard, J.C. Arnault, S. Perruchas, S. Saada, T. Gacoin, J.P. Boilot, P. Bergonzo, Hydrogenation of nanodiamonds using MPCVD: A new route toward organic functionalization, Diam. Relat. Mater. 19 (2010) 1117–1123.

[28] M. Bhadra, S. Roy, S. Mitra, Nanodiamond immobilized membranes for enhanced desalination via membrane distillation, DES. 341 (2014) 115–119.

[29] G.A. Polotskaya, N. V Avagimova, A.M. Toikka, N. V Tsvetkov, A.A. Lezov, I.A. Strelina, I. V Gofman, Z. Pientka, Optical , Mechanical , and Transport Studies of Nanodiamonds / Poly (Phenylene Oxide) Composites, Polym. Comp. 39 (2018) 3952–3961.

[30] N. Avagimova, G. Polotskaya, A. Toikka, A. Pulyalina, Z. Morávková, M. Trchová, Z. Pientka, Effect of nanodiamond additives on the structure and gas-transport properties of a poly(phenylene–isophtalamide) matrix, J. Appl. Polym. Sci. 135 (2018) 1–8.

[31] Y. Liu, Z. Gu, J.L. Margrave, V.N. Khabashesku, Functionalization of nanoscale diamond powder: Fluoro-, alkyl-, amino-, and amino acid-nanodiamond derivatives, Chem. Mater. 16 (2004) 3924–3930.

[32] V.F. Loktev, V.I. Makal'skii, I. V. Stoyanova, A. V. Kalinkin, V.A. Likholobov, V.N. Mit'kin, Surface modification of ultradispersed diamonds, Carbon N. Y. 29 (1991) 817–819.

[33] M. Alishiri, A. Shojaei, M.J. Abdekhodaie, Biodegradable polyurethane acrylate/HEMA-grafted nanodiamond composites with bone regenerative potential applications: Structure, mechanical properties and biocompatibility, RSC Adv. 6 (2016) 8743–8755.

[34] F. Hajiali, A. Shojaei, Network structure and mechanical properties of polydimethylsiloxane filled with nanodiamond – Effect of degree of silanization of nanodiamond, Compos. Sci. Technol. 142 (2017) 227–234.

[35] https://scmb.uq.edu.au/research/facilities-and-services/scientific-facilities-and-techniques/elemental-microanalysis-c-h-n-s-and-o

CHAPTER 4. EFFECTS OF DIFFERENT FILLER MORPHOLOGIES ON THE INTERFACIAL ENHANCEMENT AND GAS SEPARATION EFFICIENCY IN MIXED MATRIX MEMBRANES

Contribution to the field

This chapter investigated three different shapes and morphologies of cobalt-based zeolitic imidazole framework (ZIF) including conventional polyhedral shape (P-ZIF), nanorod shape (R-ZIF) and leaf-shaped nanosheet (L-ZIF) and their effects on gas separation of 6FDA-durene based MMMs. Compared to Pebax used in Chapter 3, 6FDA-durene is more versatile and offer higher gas permeability. Moreover, 6FDA-durene is more suitable for adding ZIF, which is not stable in water, as Pebax needs to be dissolved in the ethanol/water solution. Differing from nanodiamond in Chapter 3, ZIF possesses a porous network which potentially increases the gas permeability as well as gas selectivity by size-exclusion. Additionally, the shape and morphology of ZIF are tailorable. Previous literature has shown that different morphologies of filler have a significant effect on the gas separation performance, however relatively little is known about the impact of morphology on MMM performance for porous fillers. The aspect ratios as well as the shape of the fillers was varied in this study and these morphology differences may affect not only the orientation, dispersion of fillers in polymer matrix but also the travelling pathways of gas molecules through the MMMs. This characteristic was expected to vary the gas separation performance of the ZIF-contained MMMs. In this chapter, improved interfacial adhesion was observed in the R-ZIF MMMs and L-ZIF MMMs compared to the conventional P-ZIF MMMs, which was evidenced by the traditional scanning electron microscopy (SEM) and the focus ion beam scanning electron microscopy (FIB-SEM) as well. This interfacial improvement consequently led to the enhancement in gas selectivity for CO_2/N_2, CO_2/CH_4 and C_3H_6/C_3H_8. This chapter gave contribution of understanding the effects of different filler shapes on the gas separation efficiency of MMMs, which can guide the morphology selection and tailoring to achieve the optimal performance.

4.1. Introduction

Membranes have been considered key components in various systems such as batteries, fuel cells, barrier packages, controlled delivery devices, solar cells and energy/gas purification systems for a long time [1]. In term of gas separation, membrane-based technology possesses several advantages

in comparison with other traditional technologies such as distillation or adsorption. These advantages include: avoidance of harmful chemicals, small footprint with simple process design and scalability as well as low energy consumption [2]. Hundreds of polymers have been studied for gas separation, but only a few of them have made it to commercial deployment [3]. Polymeric membranes suffer from a trade-off between gas permeability and selectivity referred by the Robeson upper bound, which limited their applications [4]. In recent years, new type of membranes has been proposed as mixed matrix membranes (MMMs), which combining the processability of polymers with the outstanding separation ability of inorganic molecular sieve materials. Early work on MMMs focusing on zeolites gained no success primarily due to the incompatibility between phases, the discovery of promising new sieve materials including metal-organic frameworks (MOFs) has brought back new hope for this type of membranes.

MOFs are considered an emerging class of porous materials, which show great potential in various applications such as membrane separation, chemical sensing, catalysis, drug delivery, gas capture and storage [5]. Recently, MOFs have attracted increasing research interest thanks to their ultra high porosity, large surface area as well as tailorable function. Much effort has been devoted in designing new MOFs with different structure and function, nevertheless, tailoring the size, shape and morphology is also essential in order to achieve certain unique features as well as adapt to specific requirements for many different applications - the principles of "structure dictates function" in inorganic nanomaterials [6,7]. Several attempts have been made to architecturally control of MOFs shapes in the literature, including 1D, 2D and 3D structures. Nanosheets of MOFs have been prepared and studied for gas separation membranes by Peng et.al and Rodenas et.al, which achieved much higher gas selectivity than MOFs in other morphologies [8,9]. Guo and coworkers developed different morphologies of MIL-53 (Fe-based MOFs) from octahedron to nanorod as a template for anode materials in batteries [10]. More recently, Zhan et.al successfully fabricated copper-based MOFs with various morphologies including nanosheets, nanorods and nanofibers and studied their potential as 2D catalysts [5].

Zeolitic imidazolate frameworks (ZIFs) are a sub-class of MOFs, which consisting of tetrahedral metal ions linked with imidazole ligands. While being considered attractive materials for gas separation membranes due to their excellent stability and molecular sieving features [11], successful attempts at tailoring the shape and morphology of ZIFs have seldom been reported in the literature. Recently, Yang’s research group successfully fabricated ZIF-8 with various shapes such as nanocube, nanorod, rhombic-dodecahedron and octagonal plates using cetyltrimethylammonium

bromide as surfactant, and applied in mixed matrix membranes (MMMs) for gas separation, among which the nanorod crystals exhibited the highest improvement in C_3H_6/C_3H_8 separation for the ZIF-8 MMMs [6]. Lately, a new type of 2D ZIF, named as ZIF-L, with thin leaf shape morphology fabricated based on zinc metal source and 2-methylimidazole ligands, has been applied in MMMs for gas separation and reported by Kim and coworker [11], which show significant improvement in H_2/CO_2 selectivity.

In this chapter, different shapes and morphologies of cobalt-based ZIF including conventional polyhedral shape (P-ZIF), rod shape (R-ZIF) and leaf-sheet shape (L-ZIF) have been fabricated and introduced in 6FDA-durene matrix to prepare MMMs for gas separation. Compared to Pebax polymer used in Chapter 3, 6FDA-durene is more versatile which provide much higher gas permeability for different types of gas. Additionally, 6FDA-durene is more suitable for incorporating ZIF, a water-susceptible filler, than Pebax, which need to be dissolve in ethanol/water solution. Based on previous studies in the literature, both nanorod and nanosheet morphology may provide better interaction with the polymer matrix due to higher surface area as well as improving gas permeability with additional diffusion pathways. The nanosheet morphology is further expected to enhance the gas selectivity of the membranes by forcing the undesired gas to adopt a tortuous path around the nanosheet, which results in the increase of diffusion path through the membranes, leading to the enhancement of gas selectivity [12]. The size, shapes and the effects of different morphologies of ZIF fillers on the dispersion and interfacial adhesion with the polymer matrix was investigated via scanning electron microscopy along with the focused ion beam analysis. The gas separation performance of MMMs based on each morphologies were characterized by single gas permeability tests for CO_2, N_2, CH_4, C_3H_6 and C_3H_8.

4.2. Experimental

4.2.1. Materials

6FDA-durene polyimide was supplied by Arkon (USA) and chloroform were supplied by Sigma–Aldrich. Cobalt nitrate hexahydrate ($Co(NO_3)_2.6H_2O$, 98%, Sigma-Aldrich), cobalt acetate dihydrate $Co(CH_3COO)_2{\cdot}2H_2O$ 98%, Sigma-Aldrich), 2-methylimidazole ($C_4H_6N_2$, 99%, Sigma-Aldrich), cetyltrimethylammonium bromide (CTAB) (Sigma Aldrich) and methanol (Merck) were used for the synthesis of ZIF nanoparticles without further purification.

4.2.2. Preparation of P-ZIF particles

Polyhedral ZIF particles (P-ZIF) were synthesized at room temperature according to a literature procedure [13]. The first solution of cobalt metal source was made of 8.15g of $Co(NO_3)_2.6H_2O$ in 700 mL methanol while the second solution of ligand source included 9.19g of 2-methylimidazole (HmIm) in 700 mL methanol. The first solution was then added dropwise into the second one and the mixed solution was gently stirred at 150 rpm for 18h. The obtained purple mixture was centrifuged at 8000 rpm for 30 min and the purple particles were collected. In order to remove all the residual solvent and unreacted species, the prepared particles were washed in methanol for at least three times and then dried at 100 ^oC under vacuum for 24 h before use.

The rod shape ZIF (R-ZIF) was synthesized as follow [6]: Cetyltrimethylammonium bromide (CTAB, 99%) was served as surfactants with the amount of 0.33 mmol was dissolve in 16 mL of deionized (DI) water, then 2-methylimidazole (Hmim, 29.577 mmol) was added. $Co(CH_3COO)_2 \cdot 2H_2O$ (0.986 mmol) was dissolved separately in 16 mL of deionized (DI) water before mixing with the previous solution, and the molar ratio of Zn^{2+}/Hmim/H_2O was 1: 30: 1800. The resulting solution was stirred at room temperature (~25 ^oC) for ~5 min, and was then transferred to a Teflon-lined stainless steel autoclave for hydrothermal synthesis at 120 ^oC with synthesis time of 24 h. After synthesis, the reaction was stopped by cooling down to room temperature and the resultant product was washed three times with methanol and collected by centrifuging at 8000 rpm for 20 min, followed by drying in an vacuum oven at 60 ^oC overnight.

Nanosheet leaf shaped L-ZIF was prepared in DI water [14]. 0.3 g of cobalt nitrate hexahydrate and 0.65 g of HMIM were separately dissolved in 20 mL of DI water. The two solutions were mixed and stirred for 3 h at room temperature. The obtained solution was washed two times with ethanol and centrifuged (5000 rpm for 20 min). Then, the obtained L-ZIF was dried in vaccuum at 60 °C for 24 h .

4.2.3. Fabrication of MMMs

For the pure 6FDA-durene membrane, 0.45 g 6FDA-durene was dissolved into 3 mL chloroform and then cast onto a clean glass plate and covered to slowly dry at room temperature for 24 h. After that, the membrane was dried at 100 ^oC for 24 h under vacuum.

For the MMMs, a calculated amount of as-synthesized P-ZIF was dispersed in chloroform under sonication. 0.45 g 6FDA-durene was dissolved into this suspension further stirred for 12 h. The

resulting mixture was cast on glass plate and dried at room temperature for 24 h, followed by drying at 100 ^{o}C for another 24 h under vacuum. The selected thickness for casting was 40 μm. The loading of P-ZIF in MMMs were 10 wt.% and 20 wt.% calculated based on equation below:

$$\Phi = \frac{m_{filler}}{m_{filler} + m_{6FDA-durene}} \times 100\ (\%)$$

where Φ is the filler loading (%), m_{filler} and $m_{6FDA\text{-}durene}$ are the mass of P-ZIF and mass of polymer in the MMMs, respectively. Samples used in this study were named as in Table 4.1:

Table 4.1. Sample names and nomenclature in this study

Sample	**Pure 6FDA-durene membrane**	**6FDA-durene/P-ZIF membrane**	**6FDA-durene/R-ZIF membrane**	**6FDA-durene/L-ZIF membrane**
Nomenclature	PI	PZ (x)	PR(x)	PL(x)
			x: P-ZIF weight percent	

4.2.4. Characterization

The X-ray diffraction (XRD) data were obtained from a Brucker Advanced X-ray Diffractometer (40 kV, 30 mA) with Cu Kα (λ= 0.15406 nm) radiation at a scanning rate of 1^{o} min^{-1} from 5^{o} to 50^{o}.

The N_2 adsorption isotherms were obtained from a Micromeritics ASAP 2020 at 77 K. Samples were firstly degassed at 180 ^{o}C for 24 h. BET surface area was calculated over the range of relative pressures between 0.005 and 0.05. The CO_2, N_2, CH_4, C_3H_8 and C_3H_6 adsorption isotherms at 303K were also carried out.

The cross-surface morphologies of the samples were obtained with a JEOL JSM7100 scanning electron microscope (SEM) at 10 kV.

Focused ion beam scanning electron microscopy (FIB-SEM) observation was carried out in a FEI SCIOS FIB/SEM dual beam system to determine the contact of the inorganic phase and polymeric matrix. A trench was firstly milled on the surface of the membrane with a Ga+ focused ion beam (FIB) (Fig 4.1). Numbers of slices with fixed thickness were cut from the specimen by the Ga+ FIB at 30kV and 3nA, while a series of exposed cross-section SEM images were collected in back-

scattered electron (BSE) mode at 2kV. The segmentation of the individual phases (e.g. polymer, filler, voids) was conducted by image thresholding based on their different grayscale [29,30]. The whole stack of these SEM images was aligned and reconstructed in three-dimensions using Avizo software (FEI Visualization Sciences Group).

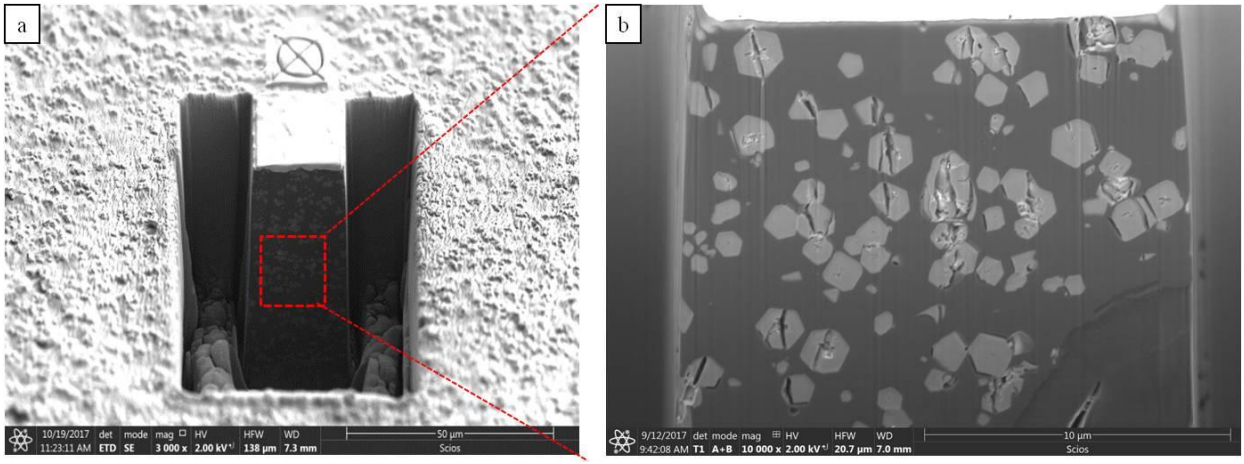

Figure 4.1. Typical FIB-SEM images of PZ20 MMMs: (a) FIB milling trend and (b) cross-sectional image in BSE mode

4.2.5. Gas permeation test

The single gas permeation test was conducted with the same conditions as described in section 3.3.1 as well as showed in the Appendix.

4.3. Results and Discussion

4.3.1. Preparation and characterization of ZIFs

The crystal structure of ZIFs was demonstrated by the XRD patterns displayed in Fig. 4.2. The diffraction patterns of P-ZIF and R-ZIF are similar, demonstrating the typical SOD zeolite-type structure and are well-matched with other previous reports in the literature [6,16,17]. The position of characteristic peaks in the XRD pattern of L-ZIF was also consistent with the literature, expressing the semi-SOD structure [18,19]. The changes in position and intensity of diffraction peaks, especially at 2θ of 15-20° in the XRD pattern of L-ZIF indicated the increase of a specific crystal face originating from the 2D network of L-ZIF crystal [18]. The L-ZIF exhibited similar crystal structure to P-ZIF and R-ZIF with same apertures perpendicular to the 2D crystal layer, which was expected to provide comparable sieving properties with P-ZIF and R-ZIF [20]. Fig. 4.3

shows the SEM images of the ZIFs with different morphologies. The P-ZIF particles showed polyhedral shapes with size range from 0.6 to 1.3 µm, while the R-ZIF exhibited rod-like crystals with the length and width around 1.2 µm and 150 nm, respectively. The L-ZIF crystal showed leaf-like morphology with an average dimension of 2 µm x 5 µm and thickness of 100 nm. The XRD patterns and SEM images confirmed the successful fabrication of ZIFs with different morphologies.

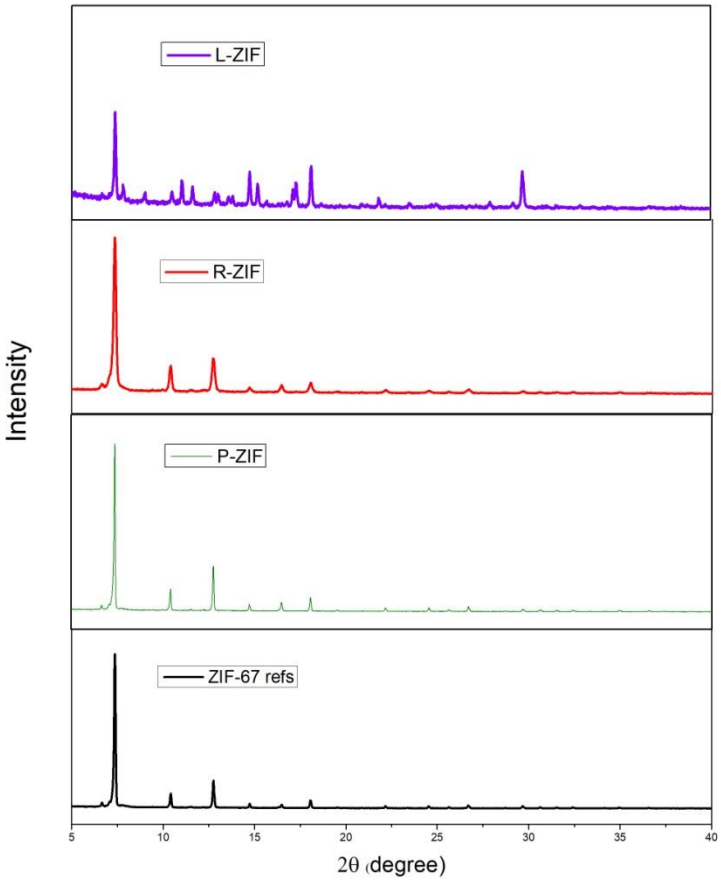

Figure 4.2. XRD patterns of P-ZIF, R-ZIF, L-ZIF and polyhedral ZIF-67 in literature

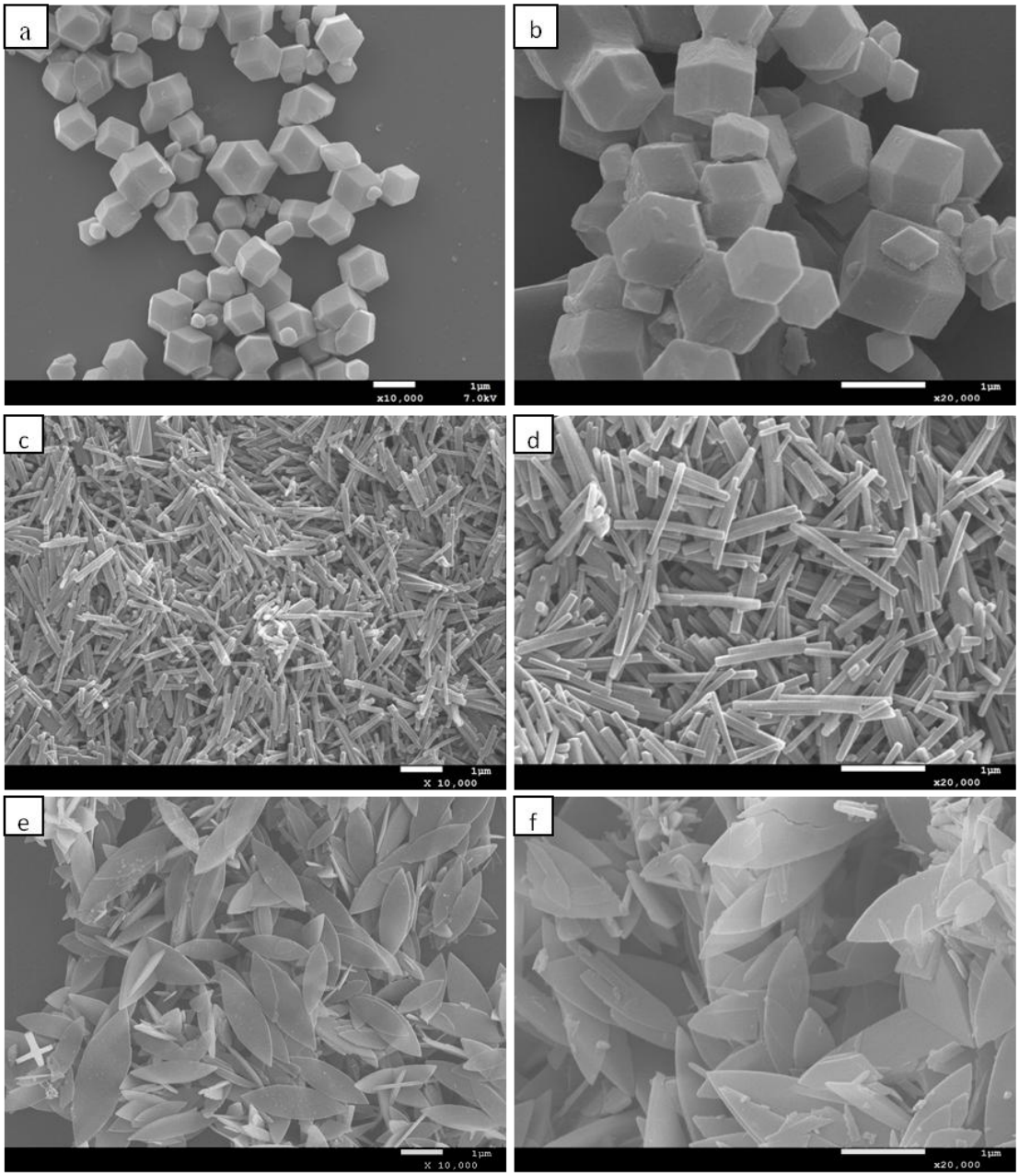

Figure 4.3. SEM images of P-ZIF: (a, b), R-ZIF: (c, d) and L-ZIF (e,f)

N_2 adsorption at 77K of P-ZIF, R-ZIF and L-ZIF all exhibited type I isotherms which show a sharp increase adsorption at low relative pressures (Fig. 4.4). The BET surface area of P-ZIF, R-ZIF and L-ZIF are 1402 ± 30 m^2g^{-1}, are 990 ± 26 m^2g^{-1} and 210 ± 36 m^2g^{-1}, respectively. The lower surface area of L-ZIF may be due to the smaller pore size structure and higher density (density of metal atoms per unit volume) which have been discussed in the previous literature [21]. The reduction in porosity of R-ZIF compared to P-ZIF is speculated to be attributed to the occupation of residue CTAB molecules inside the R-ZIF framework as well as on the crystal surface. During the synthesis

process, CTAB molecules may first be anchored on the surface of nuclei, then embedded inside the ZIF structure along with the growth of crystals [22].

The adsorption of CO_2, N_2, CH_4, C_3H_6 and C_3H_8 at 303K for P-ZIF, R-ZIF and L-ZIF was also conducted and isotherms are displayed in Fig 4.5. Similar trends were observed as P-ZIF showed higher gas adsorption capacity than R-ZIF. Interestingly, L-ZIF exhibited superior CO_2 adsorption capacity as well as CO_2/N_2 and CO_2/CH_4 selectivity compared to both P-ZIF and R-ZIF though possessed lower surface area (Fig. 4.5a, 4.5b). This result may be attributed to the unique cushion-shape cavities and strong interaction between CO_2 molecules with the Hmim molecules in L-ZIF as discussed in a previous study [21]. The propane adsorption capacity of all ZIF samples were higher than the propylene adsorption amount at pressures below 400 mmHg while the reverse was observed at pressures higher than 400 mmHg (Fig. 4.5(c)), which suggested that the C_3H_6/C_3H_8 adsorption selectivity of P-ZIF, R-ZIF and L-ZIF may become more significant at higher pressures than 400 mmHg. Similar results have also been reported in previous studies [15,36]. Based on the isotherms, the ideal gas selectivities of P-ZIF, R-ZIF and L-ZIF at 1 bar were calculated and are shown in Table 4.2.

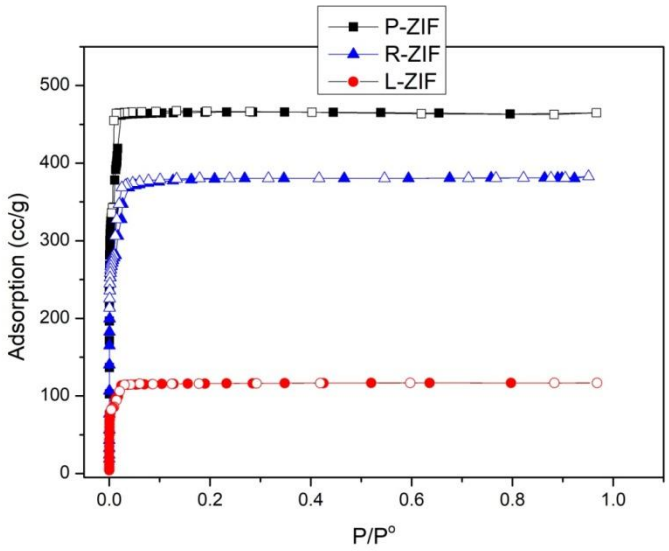

Figure 4.4. N_2 adsorption isotherm at 77K of P-ZIF, R-ZIF and L-ZIF

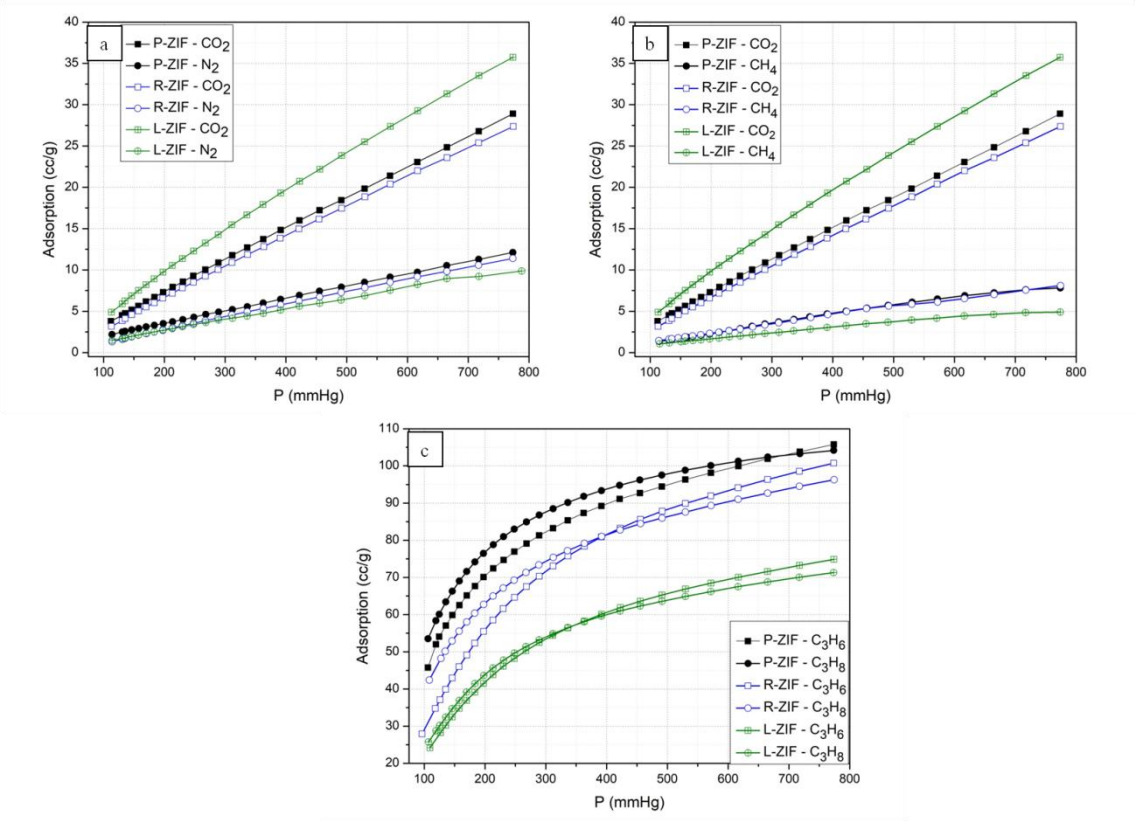

Figure 4.5. Gas adsorption isotherm of P-ZIF, R-ZIF and L-ZIF at 303K: (a): CO_2/N_2, (b) CO_2/CH_4 and (c) C_3H_6/C_3H_8

Table 4.2. Ideal selectivity of ZIFs with different shapes at 1 bar

Samples	Gas adsorption at 1 bar (cc/g)					Ideal selectivity at 1 bar		
	CO_2	N_2	CH_4	C_3H_6	C_3H_8	CO_2/N_2	CO_2/CH_4	C_3H_6/C_3H_8
P-ZIF	28	12	8	105	104	2.33	3.50	1.009
R-ZIF	26.5	11	8	100	95	2.41	3.31	1.053
L-ZIF	35	9	5	74.5	71	3.89	7	1.05

4.3.2. Characterization of mixed matrix membranes

FESEM observation was conducted to investigate the interfacial morphology of PZ, PR and PL MMMs which critically affect the gas separation performance of MMMs and the images are displayed in Fig. 4.6. In Fig. 4.6 (a,b) poor adhesion between P-ZIF and polymer matrix is clearly observed, as there are interfacial voids between the filler and polymer phases and the polymer barely covers the P-ZIF particles. This "sieve in cage" morphology is in agreement with other previous studies using large size MOF particles as fillers, which is often associated with the poor gas separation efficiency of the MMMs [23–25]. At higher loading of P-ZIF (20 wt.%) (Fig. 4.6(b)), more interfacial voids appeared due to the fact that the van der Waals interaction between P-ZIF particles are stronger than the P-ZIF interaction with polymer [26,27]. These interfacial defects will likely deteriorate the gas separation performance of the PZ MMMs.

For the PR MMMs (Fig. 4.6 (c, d)), a significantly improved interface between filler and polymer matrix is observed. The dispersion of R-ZIF in the polymer matrix was more uniform and less interfacial voids were observed. However, at higher loading of R-ZIF (20 wt.%), some filler agglomeration and interfacial voids can be observed. Similar trends were also observed with the PL MMMs, as at 10 wt.% of L-ZIF, uniform dispersion and strong integration of L-ZIF in the polymer matrix was obtained. This was in contrast with the images obtained at 20 wt.% loading of L-ZIF. Compared to PZ MMMs, the improvement of filler/polymer interface in PR MMMs and PL MMMs can be attributed to the high aspect ratio and distortion of R-ZIF and L-ZIF fillers in the membranes, which facilitates the good interfacial structure between polymer and filler due to the easy covering of the filler by the polymer [6]. In contrast, the rigid structure of P-ZIF plus the relative large surface area make it difficult for the polymer to effectively cover the particle, leading to the poor interfacial interaction and non-selective voids in PZ MMMs. As more R-ZIF and L-ZIF were introduced into the membranes, the filler/filler interaction becomes dominant compared to the polymer/filler interaction, leading to the formation of aggregates in the MMMs. This result indicates that rod shaped and leaf shaped ZIF particles are better morphologies for achieving uniform filler dispersion and reducing filler/matrix interfacial voids in the MMMs.

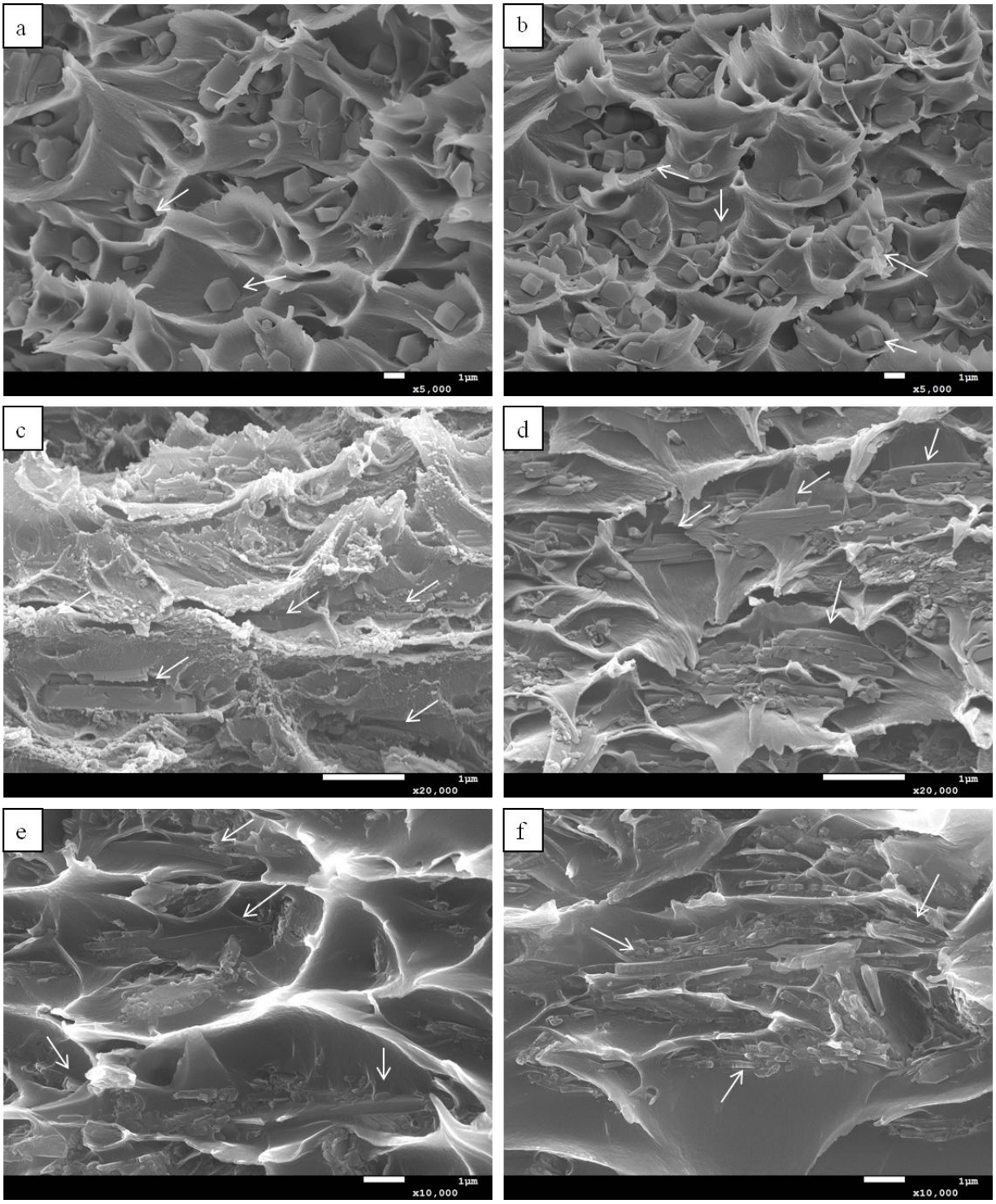

Figure 4.6. SEM images of PZ MMMs, PR MMMs and PL MMMs: (a) PZ10, (b) PZ20, (c) PR10, (d) PR20, (e) PL10, (f) PL20 (Arrows point to the ZIF particles embedded in polymer matrix)

To further study the internal structure of MMMs, FIB-SEM was used to investigate the distribution of fillers and interfacial voids. The volume fractions of filler, polymer and voids in MMMs were

also quantified. Fig 4.7, Fig 4.8 and Fig 4.9 show the 3D representation of the distribution of the fillers and voids in PZ MMM, PR MMM and PL MMM samples. The volume fractions of the filler, polymer phase and voids were calculated based on 3D image analysis and shown in Table 4.3. The volume fraction of the voids in MMMs are 0.835% with P-ZIF and reduced to 0.026 % and 0.010% when incorporating 20 wt.% of L-ZIF and R-ZIF, respectively. Fewer voids were formed with R-ZIF and L-ZIF as fillers in the MMMs compared to the P-ZIF, which indicated that the shape of fillers play a significant role in managing filler/polymer adhesion in the MMMs. The rod and flat sheet structure with higher aspect ratio can be more effectively covered by the polymer matrix, which result in better interfacial interaction and less void formation in the PR MMMs and PL MMMs compared to the PZ MMMs. As showed in Fig 4.9a, the large portion of L-ZIF sheets are facing the gas permeation pathway, which potentially enhance the gas selectivity of the PL MMMs. These results are also in agreement with the SEM observation discussed above. It is important to note that there is a possibility that a small number of additional voids were created during the FIB-SEM sample preparation (due to the ultra high vacuum and high ion energy applied in the milling process), however it can not be quantified.

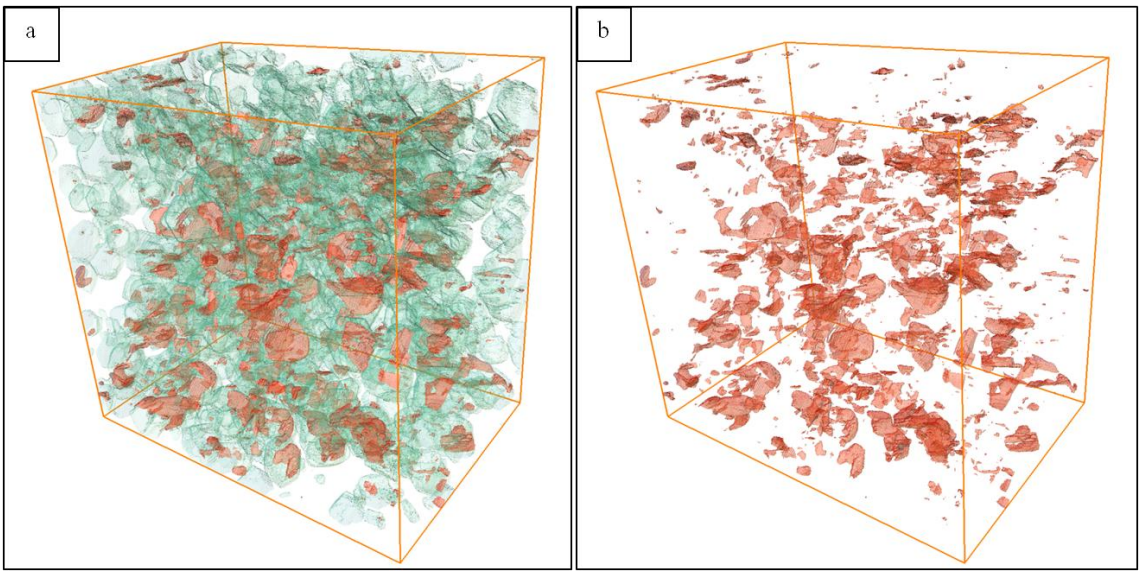

Figure 4.7. FIB surface rendered view of PZ20 MMM: (a) Fillers and voids, (b) Voids. Filler appear in blue and voids are in red. Box size: (7.5x7.3x6.8 µm)

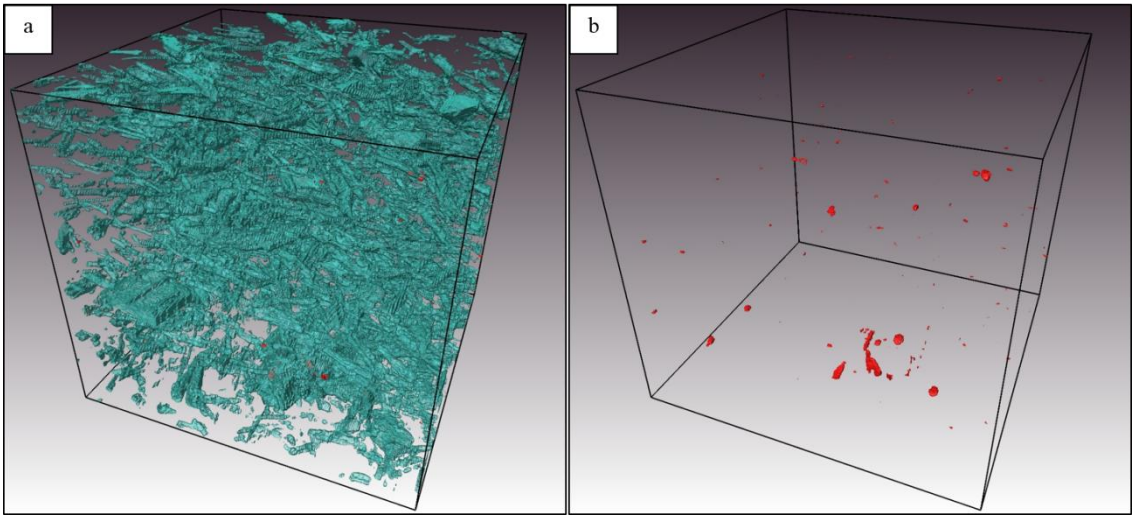

Figure 4.8. FIB surface rendered view of PR20 MMM: (a) Fillers and voids, (b) Voids. Filler appear in blue and voids are in red. Box size: (7.5x7.3x6.8 µm)

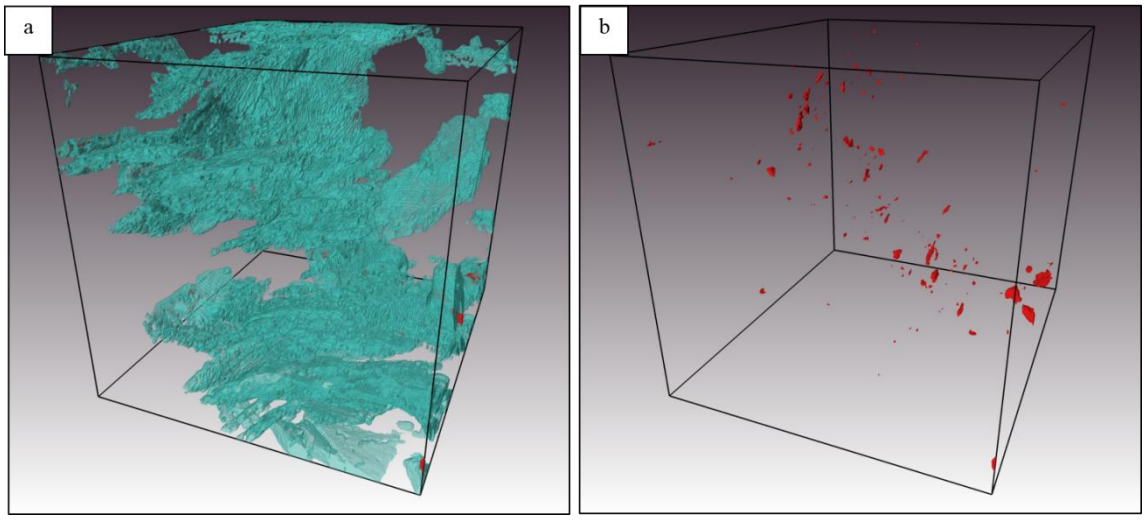

Figure 4.9. FIB surface rendered view of PL20 MMM: (a) Fillers and voids, (b) Voids. Filler appear in blue and voids are in red. Box size: (7.5x7.3x6.8 µm)

Table 4.3. Calculated - phase volume in PZ20 MMM and PZ20/IL MMMs based on FIB analysis

Sample	PZ20		PR20		PL20	
	Vol (nm^3)	%	Vol (nm^3)	%	Vol (nm^3)	%
Void	2.53×10^{9}	0.835	2.84×10^{7}	0.010	7.81×10^{7}	0.026
Filler	9.86×10^{10}	32.494	1.78×10^{10}	5.870	3.36×10^{10}	11.058
Polymer	2.02×10^{11}	66.671	2.86×10^{11}	94.120	2.70×10^{11}	88.916

4.3.3. Gas separation performance

The ideal gas separation performance of the PZ MMMs and PZ/IL MMMs was investigated through single gas permeability measurements. Fig. 4.10 (a, b, c) and Table 4.4 show the CO_2 and C_3H_6 permeability and the gas selectivity for CO_2/N_2, CO_2/CH_4 and C_3H_6/C_3H_8 gas pairs of neat PI membrane, PZ MMMs, PR MMMs and PL MMMs. By incorporating P-ZIF into the 6FDA-durene matrix, the CO_2 and C_3H_6 permeability of MMM increased from 630.25 barrer and 66.18 barrer to 750.34 barrer and 75.89 barrer with a 10% filler loading, and reached 976.32 barrer and 97.56 barrer with a 20 wt.% loading, respectively. However, the improvement in gas permeability is accompanied by lower CO_2/N_2, CO_2/CH_4 and C_3H_6/C_3H_8 selectivity compared to the pure polymeric membrane. The addition of highly porous fillers into the polymer matrix may result in more free space for gas diffusion through the membrane, leading to the increase in gas permeability [28]. If the porous filler has limited kinetic selectivity, as it does in this case, where selectivity is based on adsorption rather than pore size, then the selectivity of the MMM will also correspondingly decrease. The increase in permeability and decrease in selectivity for the PZ MMMs also originated from interfacial voids which results from the poor filler/polymer adhesion as indicated by the SEM and FIB-SEM investigation.

In the case of PR MMMs, the introduction of rod shape ZIF showed enhancement in both the CO_2 and C_3H_6 permeability, which were comparable with the polyhedral ZIF MMMs. Moreover, gas selectivity for CO_2/N_2, CO_2/CH_4 and C_3H_6/C_3H_8 gas pairs exhibited slight improvement compared

to the pure polymer and the PZ MMMs. When the loading of R-ZIF increased to 20 wt.%, the PR MMM showed higher CO_2 and C_3H_6 permeability but a slight decline in gas selectivity for CO_2/N_2, CO_2/CH_4 and C_3H_6/C_3H_8. As discussed above, rod shape ZIF with higher aspect ratio results in better cover and interfacial interaction with polymer matrix, which minimized the formation of non-selective voids and lead to the improvement in both gas permeability and selectivity of the PR MMMs. Nevertheless, for MMM with 20 wt.% loading of R-ZIF, some minor aggregates can be observed, which explains the increase in gas permeability accompanied with slight lower gas selectivity of PR20 MMMs compared to the PR10 MMMs [6].

For PL MMMs, a different trend was observed as more significant enhancement of gas selectivity was achieved for CO_2/N_2 and CO_2/CH_4 but this was a trade-off, with a substantial reduction in CO_2 permeability. Properly orientation of flat sheet fillers in the polymer matrix (forming an angle of 90 degree with the gas diffusion pathway) can increase the diffusion pathway of un-wanted gas compared to the desired one, leading to the decrease in permeability of non-desire gas and improving the gas selectivity of the MMM [11,20]. From the SEM and FIB-SEM analysis, not all the L-ZIF sheets were perfectly oriented perpendicular with the gas diffusion path, however, a substantial portion of the L-ZIF sheets were still facing the gas diffusion direction, resulting in the improvement in CO_2/N_2 and CO_2/CH_4 selectivity of the PL MMMs. This result is also in agreement with the ideal adsorption selectivity previously mentioned, in which L-ZIF exhibited the superior CO_2/N_2 and CO_2/CH_4 selectivity compared to P-ZIF and R-ZIF. On the other hand, L-ZIF possessed lower porosity and surface area compared to the R-ZIF and P-ZIF as discussed above, which explained the considerable reduction in gas permeability of PL MMMs compared to the neat polymer membrane as well as both PZ MMMs and PR MMMs.

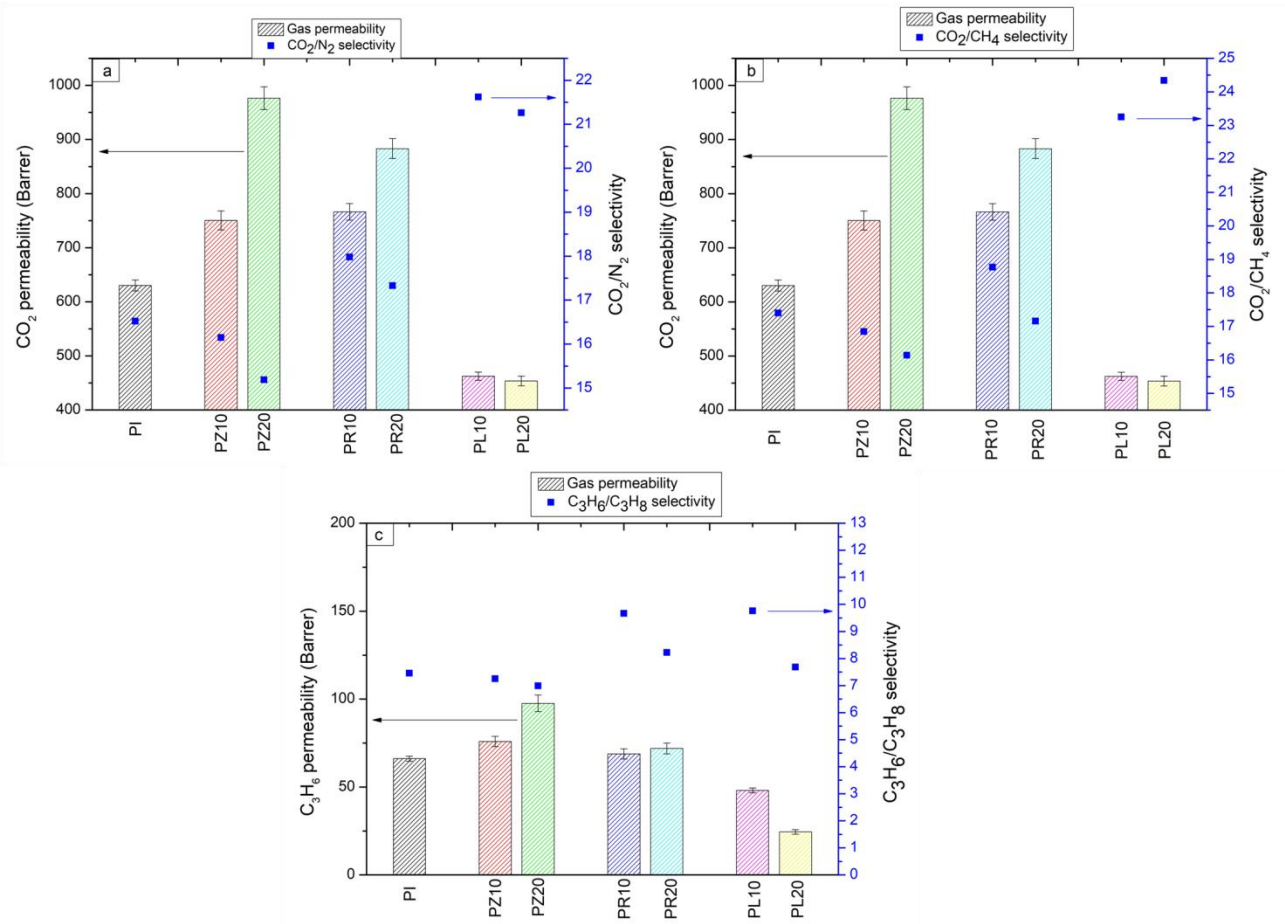

Figure 4.10. Gas permeability and selectivity of PZ MMM and PZ/IL MMMs: (a) CO_2/N_2, (b) CO_2/CH_4 and (c) C_3H_6/C_3H_8

Table 4.4. Gas permeability and selectivity of pure PI membrane, PZ MMM and PZ/IL MMM

Sample	Permeability (barrer)					Selectivity		
	CO_2	N_2	CH_4	C_3H_6	C_3H_8	CO_2/N_2	CO_2/CH_4	C_3H_6/C_3H_8
PI	630.25±10.33	38.15±0.87	36.08±0.73	66.18±1.45	8.87±0.17	16.52	17.4	7.46
PZ10	750.34±17.69	40.546±2.45	38.343±1.15	75.89±2.89	10.46±0.23	16.15	16.845	7.25
PZ20	976.32±21.12	64.25±3.15	60.48±5.89	97.56±4.76	13.95±0.45	15.19	16.14	6.99
PR10	766.390±15.22	42.630±1.79	40.82±1.12	68.826±2.91	7.048±0.15	17.98	18.77	9.67
PR20	883.203±18.46	50.95±2.21	51.47±2.56	71.914±3.06	8.75±0.21	17.33	17.16	8.22
PL10	462.373±7.64	21.380±0.45	19.886±0.83	48.084±1.34	4.923±0.11	21.62	23.25	9.76
PL20	453.757±9.15	21.342±0.76	18.64±0.91	24.445±1.26	3.180±0.10	21.26	24.34	7.68

4.4. Conclusion

In this study, ZIF particles with different morphologies has been synthesized and incorporating in mixed matrix membranes for gas separation. The effect of filler morphologies and dimension on the interfacial adhesion and interaction between polymer/filler as well as the gas separation efficiency of the MMMs were explored. The PR MMMs and PL MMMs showed better interfacial adhesion and fewer non-selective voids compared to the PZ MMMs, leading to the improvement in gas separation performance, particularly the enhancement in gas selectivity for PL MMMs and the increase in both gas permeability and gas selectivity for the PR MMMs. At high loading of filler (20 wt.%), the PR MMMs and PL MMMs still maintained the gas selectivity higher than that of the pure polymer membrane and the PZ MMMs. With these results, the 1D rod shape and the 2D leaf-sheet can be considered the more effective morphologies of fillers, especially at micron size, to improve the filler/polymer interfacial adhesion in order to achieve better gas-separation performance in mixed matrix membranes.

References

[1] W.J. Koros, C. Zhang, Materials for next-generation molecularly selective synthetic membranes, Nat. Mater. 16 (2017) 289–297.

[2] M. Ahmadi, S. Janakiram, Z. Dai, L. Ansaloni, L. Deng, Performance of Mixed Matrix Membranes Containing Porous Two-Dimensional (2D) and Three-Dimensional (3D) Fillers for CO2 Separation: A Review, Membranes (Basel). 8 (2018) 50.

[3] Z. Low, P.M. Budd, N.B. Mckeown, D.A. Patterson, Gas Permeation Properties , Physical Aging , and Its Mitigation in High Free Volume Glassy Polymers, Chem. Rev. 118 (2018) 5871–5911.

[4] L.M. Robeson, The upper bound revisited, J. Membr. Sci. 320 (2008) 390–400.

[5] G. Zhan, H.C. Zeng, Synthesis and Functionalization of Oriented Metal – Organic-Framework Nanosheets : Toward a Series of 2D Catalysts, (2016) 3268–3281.

[6] F. Yang, H. Mu, C. Wang, L. Xiang, K.X. Yao, L. Liu, Y. Yang, Y. Han, Y. Li, Y. Pan, Morphological Map of ZIF-8 Crystals with Five Distinctive Shapes: Feature of Filler in Mixed-Matrix Membranes on C_3H_6 /C_3H_8 Separation, Chem. Mater. 30 (2018) 3467–3473.

[7] M. Zhao, Q. Lu, Q. Ma, H. Zhang, Two-Dimensional Metal – Organic Framework Nanosheets, (2017) 1–8.

[8] Y. Peng, Y. Li, Y. Ban, H. Jin, W. Jiao, X. Liu, W. Yang, Metal-organic framework nanosheets as building blocks for molecular sieving membranes, Science 346 (2014) 1356–1359.

[9] T. Rodenas, I. Luz, G. Prieto, B. Seoane, H. Miro, A. Corma, F. Kapteijn, F.X. Llabrés I Xamena, J. Gascon, Metal-organic framework nanosheets in polymer composite materials for gas separation, Nat. Mater. 14 (2015) 48–55.

[10] W. Guo, W. Sun, L.P. Lv, S. Kong, Y. Wang, Microwave-Assisted Morphology Evolution of Fe-Based Metal-Organic Frameworks and Their Derived Fe_2O_3 Nanostructures for Li-Ion Storage, ACS Nano. 11 (2017) 4198–4205.

[11] S. Kim, E. Shamsaei, X. Lin, Y. Hu, G.P. Simon, J. Geun, J. Sung, W. Hee, Y. Moo, H. Wang, The enhanced hydrogen separation performance of mixed matrix membranes by incorporation of two-dimensional ZIF-L into polyimide containing hydroxyl group, J. Membr. Sci. 549 (2018) 260–266.

[12] S.A.S.C. Samarasinghe, C.Y. Chuah, Y. Yang, T.H. Bae, Tailoring CO_2/CH_4 separation properties of mixed-matrix membranes via combined use of two- and three-dimensional metal-organic frameworks, J. Membr. Sci. 557 (2018) 30–37.

[13] K.Y.A. Lin, H.A. Chang, Zeolitic Imidazole Framework-67 (ZIF-67) as a heterogeneous catalyst to activate peroxymonosulfate for degradation of Rhodamine B in water, J. Taiwan Inst. Chem. Eng. 53 (2015) 40–45.

[14] J.S. Jang, W.T. Koo, D.H. Kim, I.D. Kim, In Situ Coupling of Multidimensional MOFs for Heterogeneous Metal-Oxide Architectures: Toward Sensitive Chemiresistors, ACS Cent. Sci. 4 (2018) 929–937.

[15] L. Ge, Z. Zhu, F. Li, S. Liu, L. Wang, X. Tang, V. Rudolph, Investigation of gas permeability in carbon nanotube (CNT)-polymer matrix membranes via modifying CNTs with functional groups/metals and controlling modification location, J. Phys. Chem. C. 115 (2011) 6661–6670.

[16] J. Shao, Z. Wan, H. Liu, H. Zheng, T. Gao, M. Shen, Q. Qu, H. Zheng, Metal organic frameworks-derived Co_3O_4 hollow dodecahedrons with controllable interiors as outstanding anodes for Li storage, J. Mater. Chem. A. 2 (2014) 12194–12200.

[17] X. Guo, T. Xing, Y. Lou, J. Chen, Controlling ZIF-67 crystals formation through various cobalt sources in aqueous solution, J. Solid State Chem. 235 (2016) 107–112.

[18] G. Liu, Z. Jiang, K. Cao, S. Nair, X. Cheng, J. Zhao, Pervaporation performance comparison of hybrid membranes filled with two-dimensional ZIF-L nanosheets and zero-dimensional ZIF-8 nanoparticles, J. Membr. Sci. 523 (2017) 185–196.

[19] F. Zhang, J. Dou, H. Zhang, Mixed membranes comprising carboxymethyl cellulose (as capping agent and gas barrier matrix) and nanoporous ZIF-L nanosheets for gas separation applications, Polymers (Basel). 10 (2018) 1340–1355.

[20] H.W. Z. Zhong, J. Yao, R. Chen, Z. Low, M. He, J.Z. Liu, Oriented two-dimensional zeolitic imidazolate framework-L membranes and their gas permeation properties, J. Mater. Chem. A. 3 (2015) 15715–15722.

[21] H.W. R.Chen, J. Yao, Q.Gu, S. Smeets, C. Baerlocher, H. Gu, D. Zhu, W. Morris, O.M. Yaghi, A two-dimensional zeolitic imidazolate framework with a cushion-shaped cavity for CO 2 adsorption, Chem. Comm. 7398 (2013) 9500–9502.

[22] L. Huang, X. Zhang, Y. Han, Q. Wang, Y. Fang, S. Dong, In situ synthesis of ultrathin metal – organic framework nanosheets : a new method for 2D, J. Mater. Chem. A Mater. Energy Sustain. 5 (2017) 18610–18617.

[23] R. Lin, L. Ge, H. Diao, V. Rudolph, Z. Zhu, Ionic Liquids as the MOFs/Polymer Interfacial Binder for Efficient Membrane Separation, ACS Appl Mater Interfaces. 8 (2016) 32041–32049.

[24] O.G. Nik, X.Y. Chen, S. Kaliaguine, Functionalized metal organic framework-polyimide mixed matrix membranes for CO_2/CH_4 separation, J. Membr. Sci. 413–414 (2012) 48–61.

[25] L. Ge, W. Zhou, V. Rudolph, Z. Zhu, Mixed matrix membranes incorporated with size-reduced Cu-BTC for improved gas separation, J. Mater. Chem. A. 1 (2013) 6350–6358.

[26] G. Dong, H. Li, V. Chen, Challenges and opportunities for mixed-matrix membranes for gas separation, J. Mater. Chem. A. 1 (2013) 4610–4630.

[27] R. Mahajan, W.J. Koros, Factors controlling successful formation of mixed-matrix gas separation materials, Ind. Eng. Chem. Res. 39 (2000) 2692–2696.

[28] M.A. Aroon, A.F. Ismail, T. Matsuura, M.M. Montazer-Rahmati, Performance studies of mixed matrix membranes for gas separation: A review, Sep. Purif. Technol. 75 (2010) 229–242.

CHAPTER 5. IONIC LIQUIDS AS THE BINDING COMPONENT FOR INTERFACIAL ENHANCEMENT AND GAS SEPARATION EFFICIENCY IN ZIF-NANOROD/6FDA-DURENE MIXED MATRIX MEMBRANES

Contribution to the field

The presence of ZIF nanorod (R-ZIF) in MMM has showed good interfacial adhesion with the polymer matrix, which consequently improved the gas separation efficiency of the R-ZIF MMMs as investigated in Chapter 4. Nevertheless, as the filler loading increased, some aggregates were formed which decreased the gas selectivity of the membranes. In this chapter, ionic liquids as a third component were incorporated onto the surface of R-ZIF, which is expected to improve polymer/filler interaction, minimize the agglomeration and enhancing gas separation efficiency of the MMMs. With ILs as a interfacial compatibilizer, R-ZIF/IL MMMs showed improvement in polymer/ZIF adhesion as well as filler dispersion that were evidenced by the scanning electron microscopy (SEM). Additionally, the ILs also took part in the role of "gas carrier agent" which further enhanced the gas selectivity for CO_2/N_2, CO_2/CH_4 and C_3H_6/C_3H_8, particularly at high loading of R-ZIF (20 wt.%), compared to the non-IL MMMs and neat polymer. This chapter has suggested that the incorporation of ILs with ZIF nanorod is a simple but effective technique to enhance the interfacial interaction in MMMs, especially with high loading of fillers, in order to achieve improved gas separation performance.

5.1. Introduction

In the previous chapter, different shapes and morphologies of cobalt-based ZIF including conventional polyhedral shape (P-ZIF), rod shape (R-ZIF) and leaf-sheet shape (L-ZIF) have been fabricated and introduced into MMMs for gas separation. The results showed that both rod and sheet morphology provided better interaction with the polymer matrix due to higher aspect ratio as well as improving gas separation efficiency of the MMMs for CO_2/N_2, CO_2/CH_4 and C_3H_6/C_3H_8. However, at high loading of ZIFs, (20 wt.%), deterioration of gas selectivity of the MMMs due to the formation of non-selective interfacial voids can be observed. These issues raise questions of improving the interfacial adhesion and interaction between polymer/filler in the MMMs in order to further enhance the gas separation efficiency even at higher loading of fillers.

The non-ideal interfacial adhesion and morphology between the polymer matrix and filler still pose a great challenge on the applicability of MMMs despite the many advantages brought by ZIFs in MMMs and attempts at improving the ideal selectivity of various gas pairs. One of the most commonly occurred issues are filler agglomeration and interfacial voids caused by poor filler/polymer matrix interaction during fabrication [1,2], which have been attempted to solve by researchers with several techniques including: grafting functional groups onto the filler surface as was done in Chapter 3 of this thesis (more examples can be found in [3,4], modification of the polymeric matrix [5,6], in situ synthesis of the filler in the polymer solution before casting [7], coating the surface of the filler with a compatibilising compound and using composite fillers which are combination of different types of fillers [8,9]. Using ionic liquids (ILs) as a third component to improve the gas separation performance of MMMs shows great potential since ILs might increase the permeability of targeted gas species through the membranes whilst also offering improved interfacial wetting between the polymer matrix and filler particles [10]. For example, SAPO-34 particles were coated with IL on the surface and used as filler for MMMs fabrication by Hudiono's research group [11]. The presence of ILs not only enhanced the compatibility of polymer matrix and the zeolite particles, but also created a selective layer around the SAPO-34 particles, which consequently improves the CO_2 permeability and selectivity over CH_4 and N_2. In another study, MMMs comprised of titanosilicate ETS-10/chitosan and acetate based ILs were fabricated and showed a sharp increment in both permeability and selectivity for CO_2/N_2 separation. Additionally, the processability of the membranes were enhanced due to the increased flexibility of polymer segments with the incorporation of ILs [12]. Hao et.al. [13] coated the surface of ZIF-8 particles with ILs before incorporation into a Pebax matrix. This resulted in both an enhancement of

polymer/filler compatibility as well as CO_2/N_2 and CO_2/CH_4 gas separation performance. In recent work by Lin et.al [1], ILs were applied onto the surface of HKUST-1 and effectively reducing the interfacial void between the HKUST-1 and polymer matrix. The presence of IL also improved the selectivity for CO_2/N_2 and CO_2/CH_4 gas pairs compared to the non-IL MMMs.

The majority of work with ILs has focused on MOFs with conventional shapes being incorporated into MMMs. However, study the effects of ILs on specific shaped MOFs is still scarce due to the difficulties in fabricating those MOFs. In this study, ZIF nanorod (R-ZIF) was chosen as the filler and two types of ILs: 1-ethyl-3-methylimidazolium bis(trifluoromethanesulfonyl)imide ([Emim][Tf_2N]) and 1-Butyl-3-methylimidazolium bis(trifluoromethanesulfonyl)imide ([Bmim][Tf_2N]) were used as the interfacial binder for the 6FDA-durene/R-ZIF MMMs. R-ZIF presence as filler showed compatibility with the 6FDA-durene matrix and can improve the gas separation performance of the MMMs as mentioned in the previous chapter. Based on studies in the literature, both the [Emim][Tf_2N] and [Bmim][Tf_2N] are able to provide excellent intrinsic CO_2 solubility [25, 26]. Beside the dominant effect of the anions, the difference in alkyl chain length of the cations and IL molecular size may also affect the performance of each ILs in the MMMs. R-ZIF and R/IL were investigated by XRD and FTIR to confirm the structure and success of the coating process. The enhancement of interfacial adhesion of R-ZIF with the 6FDA-durene matrix in the presence of ILs was investigated using scanning electron microscopy. The effects of ILs on membrane separation efficiency was characterized via gas permeability and permselectivity measurements for CO_2, N_2, CH_4, C_3H_6 and C_3H_8 as well as a 50:50 CO_2:CH_4 gas mixture so as to compare the ideal and real selectivities.

5.2. Experimental

5.2.1. Materials

6FDA-durene polyimide was supplied by Arkon (USA) and chloroform were supplied by Sigma–Aldrich.

Cobalt acetate dihydrate ($Co(CH_3COO)_2{\cdot}2H_2O$, 98%, Sigma-Aldrich), 2-methylimidazole ($C_4H_6N_2$, 99%, Sigma-Aldrich), cetyltrimethylammonium bromide (CTAB) (Sigma Aldrich) and methanol (Merck) were used for the synthesis of ZIF nanorod without further purification.

5.2.2. Preparation of ZIF nanorod (R-ZIF) and ZIF nanorod/IL (R/IL)

The rod shape ZIF (R-ZIF) was synthesized as described in Chapter 4: Cetyltrimethylammonium bromide (CTAB, 99%) was served as surfactants with the amount of 0.33 mmol was dissolve in 16

mL of deionized (DI) water, then 2-methylimidazole (Hmim, 29.577 mmol) was added. $Co(CH_3COO)_2 \cdot 2H_2O$ (0.986 mmol) was dissolved separately in 16 mL of deionized (DI) water before mixing with the previous solution, and the molar ratio of Zn^{2+}/Hmim/H_2O was 1: 30: 1800. The resulting solution was stirred at room temperature (~25 ^oC) for ~5 min, and was then transferred to a Teflon-lined stainless steel autoclave for hydrothermal synthesis at 120 ^oC with synthesis time of 24 h. After synthesis, the reaction was stopped by cooling down to room temperature and the resultant product was washed three times with methanol and collected by centrifuging at 8000 rpm for 20 min, followed by drying in an vacuum oven at 60 ^oC overnight.

IL-incorporated R-ZIF samples were prepared in the open atmosphere. Firstly, a preset amount of IL was put in an empty vial and weigh with the balance. Based on the amount of IL in the vial, the quantity of R-ZIF was calculated to make the ratio of R-ZIF/IL = 95/5. 15 mL of chloroform was poured in the vial and stir to dissolve the IL then the R-ZIF was added into the solution and the resulting mixture was stirred continuously at 25 °C while leaving expose to air until most of the solvent evaporated. The resulting sample was consequently dried in a vacuum oven at 100 ^oC for 24 h. The ratios of R-ZIF/IL were made at 95/5 wt.%. The obtained samples were labeled as R/IL1, R/IL2 considering the ILs ([Emim][Tf_2N]) and ([Bmim][Tf_2N]), respectively.

5.2.3. Fabrication of MMMs

For the pure 6FDA-durene membrane, 0.45 g 6FDA-durene was dissolved into 3 mL chloroform and then cast onto a clean glass plate and covered to slowly dry at room temperature for 24 h. After that, the membrane was dried at 100 ^oC for 24 h under vacuum.

For the MMMs, a calculated amount of as-synthesized P-ZIF was dispersed in chloroform under sonication. 0.45 g 6FDA-durene was dissolved into this suspension further stirred for 12 h. The resulting mixture was cast on glass plate and dried at room temperature for 24 h, followed by drying at 100 ^oC for 24 h under vacuum. The loading of P-ZIF in MMMs were 10 wt.% and 20 wt.% calculated based on equation below:

$$\Phi = \frac{m_{filler}}{m_{filler} + m_{6FDA-durene}} \times 100\ (\%)$$

where Φ is the filler loading (%), m_{filler} and $m_{6FDA\text{-}durene}$ are the mass of R-ZIF and mass of polymer in the MMMs, respectively. Samples used in this study were named as in Table 5.1:

Table 5.1. Sample names and nomenclature in this study

Sample	Pure 6FDA-durene membrane	6FDA-durene/R-ZIF membrane	6FDA-durene/R-ZIF/IL membrane	R-ZIF/IL particles
Nomenclature	PI	PR (x) x: R-ZIF weight percent	PR(x)/IL(y) x: R-ZIF weight percent y: type of IL	R/IL(y) y: type of IL

5.2.4. Characterization

The XRD, FTIR, N_2 adsorption isotherm analyses as well as the cross-sectional morphologies of the samples were carried out at the same conditions as mentioned in section 4.2.4 in chapter 4.

5.2.5. Gas permeation test

5.2.5.1. Single gas permeation test

The single gas permeation test was conducted with the same conditions as described in section 3.3.1, chapter 3 as well as showed in the Appendix.

5.2.5.2. Mixed gas permeation test

The mix-gas permeation test was carried out with a CO_2/CH_4 (50/50) mixture gas provided by Coregas Pty Ltd and the test procedure was described in detail in the Appendix. The membrane sample was firstly fixed onto the membrane cell and the whole system was vacuumed to remove residual gases. The feed gas was inserted to the upstream chamber at 3 bar, and the gas at the permeate side was swept by Argon (1 bar). The composition of gas in the permeate chamber was collected and analyzed by gas chromatography (Shimazu) to calculate the permeability of each components. The temperature of the permeation system was kept at 30°C. The measurements was repeated no less than 3 times to confirm the reproducibility of the results [15].

5.3. Results and Discussion

5.3.1. R-ZIF preparation and characterization

The crystal structure of R-ZIF and R/IL was demonstrated by the XRD patterns displayed in Fig. 5.1. The diffraction patterns of R/IL and original R-ZIF are similar which demonstrated the typical SOD zeolite-type structure and no change on the crystallinity of the R-ZIF occurred with the ILs incorporation [16]. Fig. 5.2 shows the SEM images of the pure R-ZIF and the IL-coated R-ZIF. The R-ZIF particles showed rectangular rod-like crystals with a length of around 1.2μm and and width of about 150 nm respectively. As showed in Fig. 5.2 (c,d), the morphology of R-ZIF remains intact after the IL coating has been applied, indicating that the IL had no effect on the structure of R-ZIF. It also demonstrates that the coated IL layer is extremely thin (<10nm) as the average size remains unchanged.

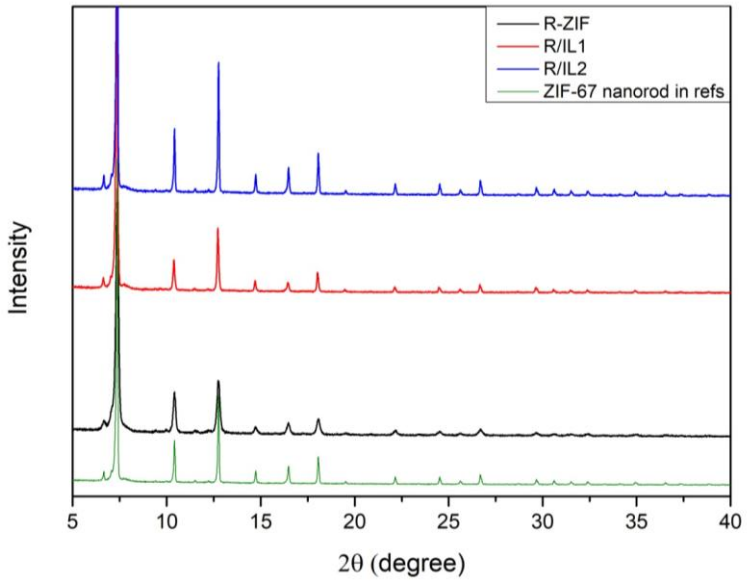

Figure 5.1. XRD patterns of R-ZIF, R/IL1 and R/IL2

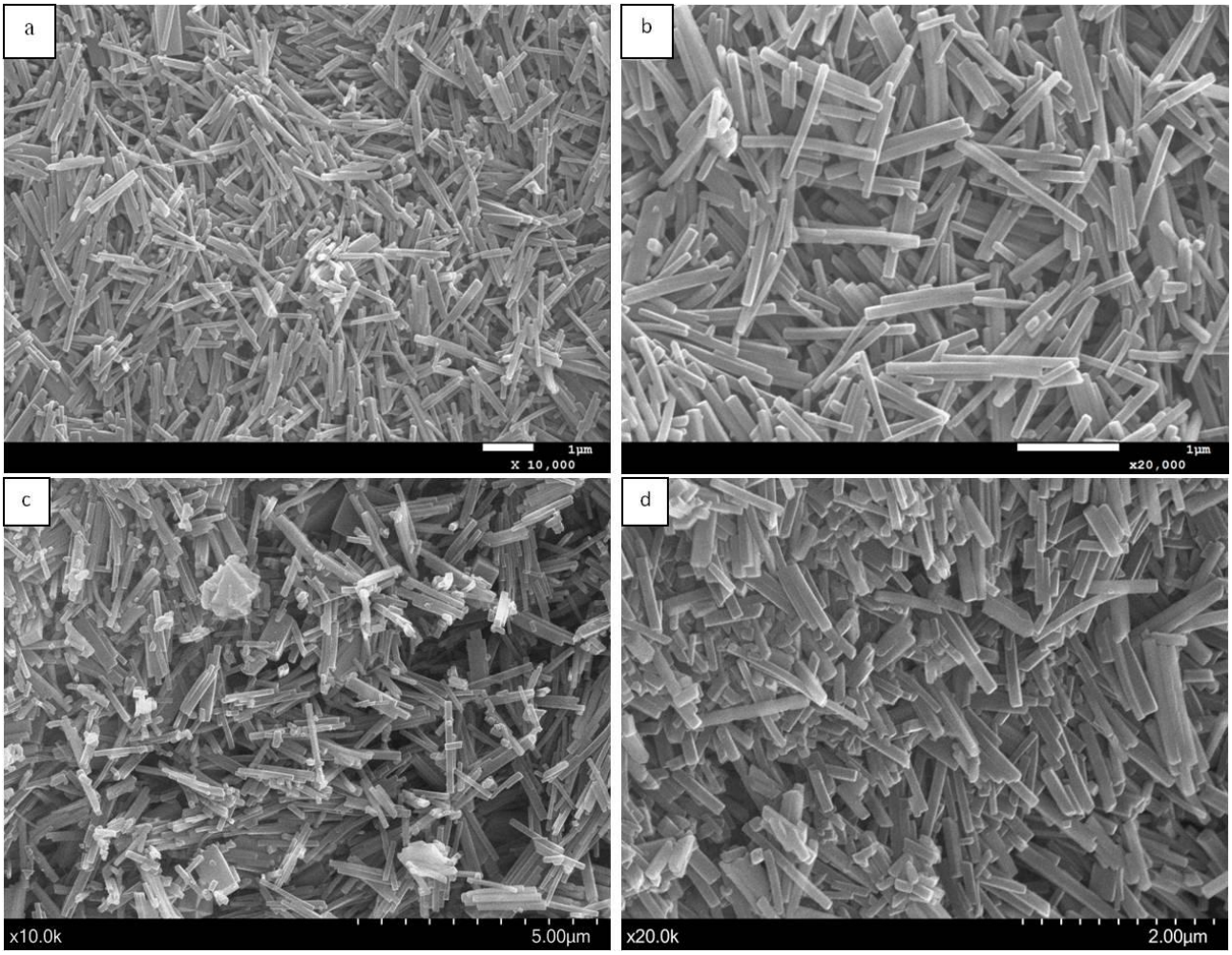

Figure 5.2. SEM images of R-ZIF (a, b) and R/IL1 (c, d)

The FTIR spectra of as-synthesized R-ZIF and R/IL are shown in Fig. 5.3. The bands at 680-760 cm^{-1} and between 900-1350 cm^{-1} correspond to the out of plane and in-plane bending of the imidazole ring of R-ZIF. The peaks at ~1650 cm^{-1} are assigned to the stretching and bending vibration of the N-H group in the imidazole ring while the bands at 1350-1500 cm^{-1} are associated with the entire ring stretching. The IL spectra showed signal of C=C double bond of the imidazole ring at around 1572 cm^{-1}, while the bands in the range of 1150-1250 cm^{-1} are assigned to the CF_3 groups of the IL [17,18]. For the spectra of R/ILs, new peaks are observed at 1065 cm^{-1} which correspond to the stretching vibration of the $[Tf_2N]^-$. Other new peaks also appeared at 836 cm^{-1} (ring C-H in ILs) and 1197 cm^{-1} (C-F) for IL1 and IL2 spectra compared to the original R-ZIF spectra. This result indicated the successful incorporation of the ionic liquid onto the R-ZIF framework [1,13,17–19].

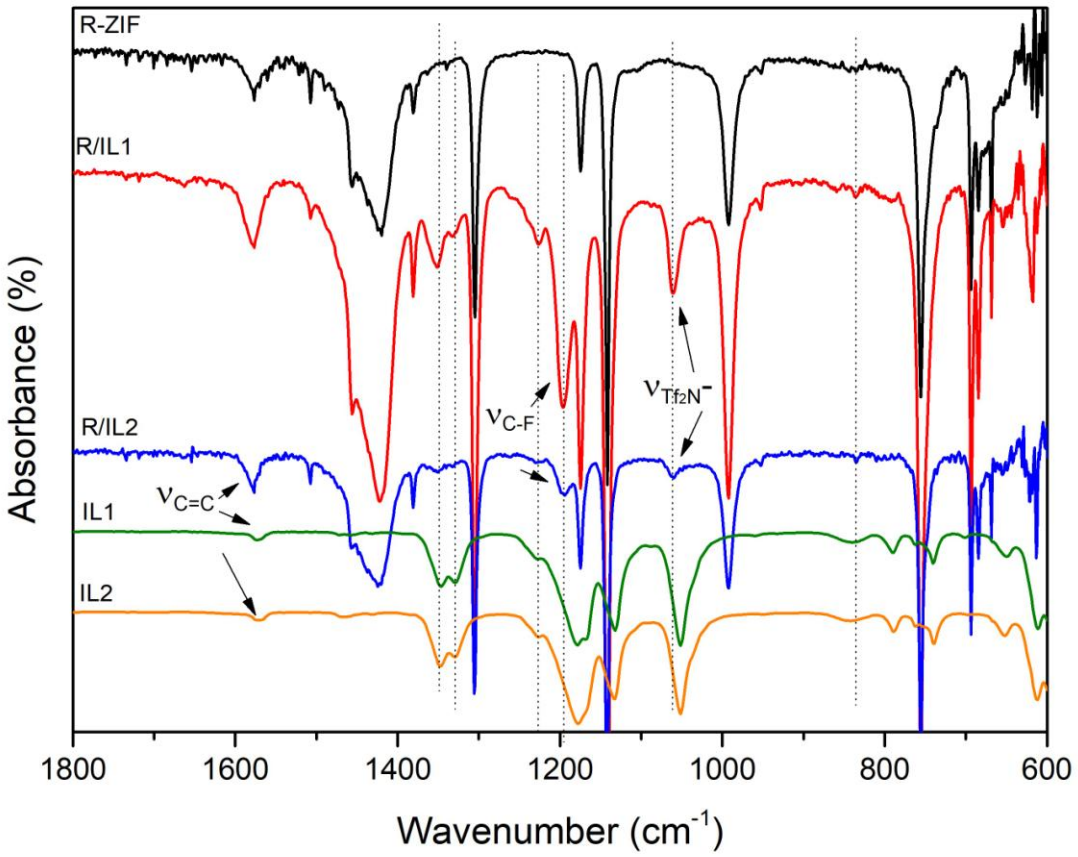

Figure 5.3. FTIR spectra of R-ZIF, IL1, IL2, R/IL1 and R/IL2

N_2 adsorption at 77K of both the R-ZIF and R/ILs exhibited type I isotherms which show sharp increasing adsorption at low relative pressures (Fig. 5.4) consistent with type I isotherm indicating microporous materials. Compared to the conventional R-ZIF which possessed a BET surface area of 995 ± 14 m^2g^{-1}, the N_2 adsorption capacity of R/ILs was lower, with a BET surface area of 880 ± 17 m^2g^{-1} for R/IL1 and 715 ± 14 m^2g^{-1} for R/IL2, respectively. The lower surface area of R/ILs samples is likely due to the occupation of surface and pore volume in the R-ZIF, causing a decrease of BET surface area as well as the N_2 adsorption capacity. These results agree with previous literature [13].

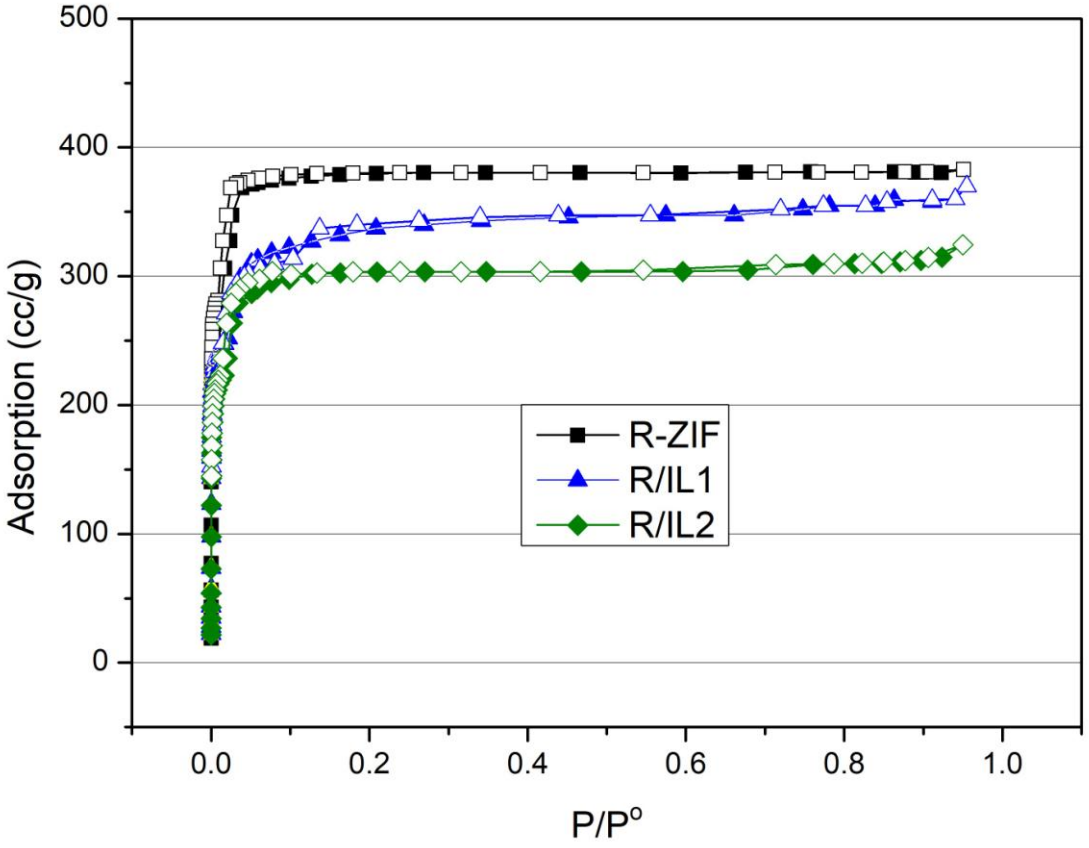

Figure 5.4. N_2 adsorption isotherm at 77K of R-ZIF, R/IL1 and R/IL2

The adsorption capacity for the gases of interest, namely CO_2, N_2, CH_4, C_3H_6 and C_3H_8, at 303K was also investigated for R-ZIF, R/IL1 and R/IL2. The isotherms are displayed in Fig. 5.5. Correlative trends were observed with the presence of ILs lowering the gas adsorption capacity of R-ZIF. Surprisingly, all samples showed lower propylene adsorption capacity compared to the propane adsorption amount at pressures below 400 mmHg but the adsorption capacity was reversed at pressures above 400 mmHg (Fig. 5.5c). It is possible that the C_3H_6/C_3H_8 adsorption selectivity of R-ZIF and R/ILs is more significant at higher pressures than 400 mmHg. Similar results have also been reported in previous studies in the literature [20,21]. Based on the isotherms, the ideal gas selectivity of IL-incorporated R-ZIF at 1 bar was calculated and is shown in Table 5.2. Importantly for MMM performance, whilst the gas adsorption capacity was reduced, the ideal gas selectivity for CO_2/N_2, CO_2/CH_4 and C_3H_6/C_3H_8 of R-ZIF with the ILs was improved. The higher sorption affinity of ILs for CO_2 and C_3H_6 over N_2, CH_4 and C_3H_8 respectively, can contribute to the enhancement in CO_2/N_2, CO_2/CH_4 and C_3H_6/C_3H_8 selectivity in the MMM. Additionally, the IL with fluoroalkyl and S=O group in the $[Tf_2N]^-$ anion has high CO_2 solubility, which also leads to the improvement in ideal selectivity of CO_2/N_2 and CO_2/CH_4 [22,23].

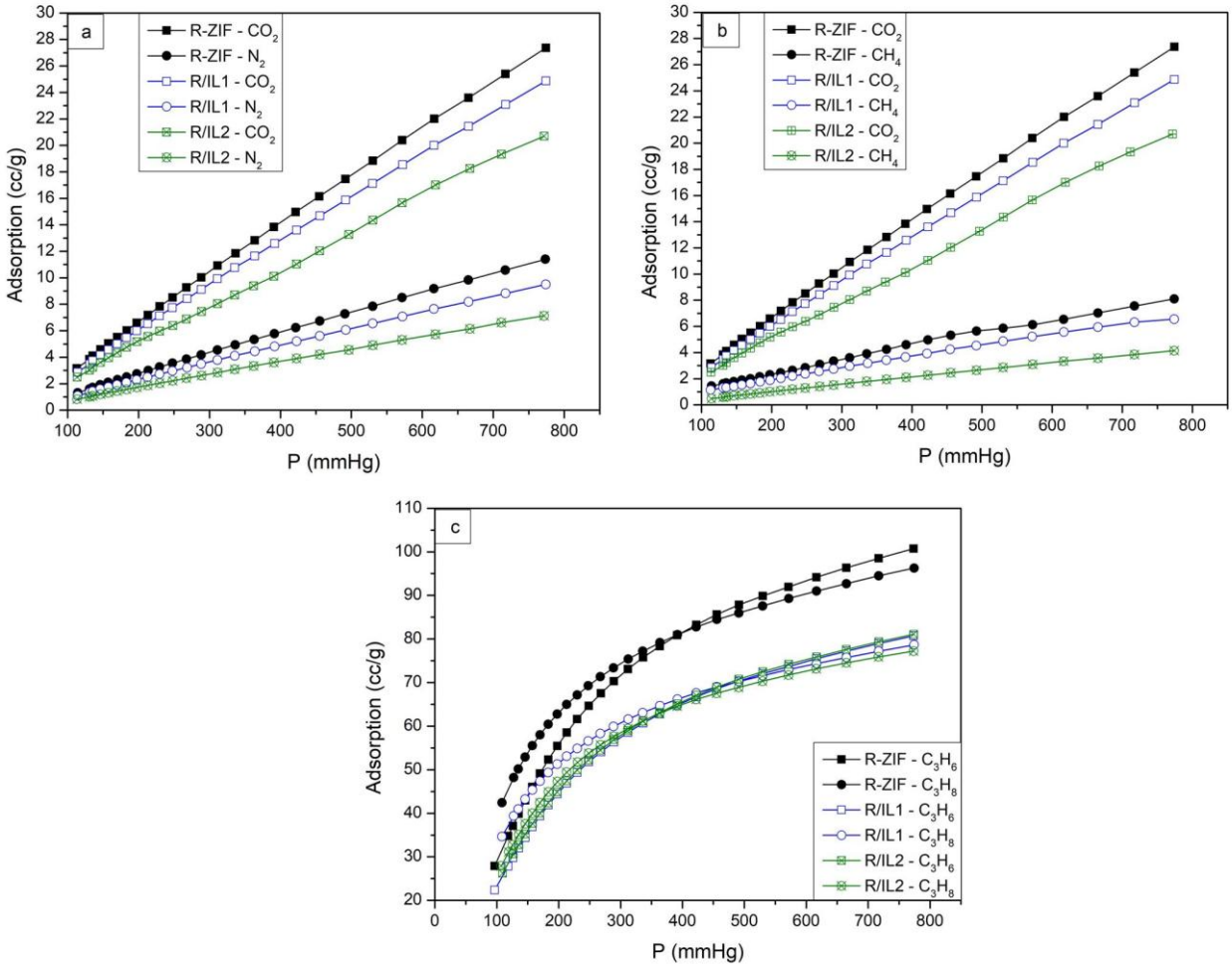

Figure 5.5. Gas adsorption isotherm of R-ZIF, R/IL1 and R/IL2 at 303K: (a): CO_2/N_2, (b) CO_2/CH_4 and (c) C_3H_6/C_3H_8

Table 5.2. Ideal selectivity of ZIFs with different shapes at 1 bar

Samples	Gas adsorption at 1 bar (cc/g)					Ideal selectivity at 1 bar		
	CO_2	N_2	CH_4	C_3H_6	C_3H_8	CO_2/N_2	CO_2/CH_4	C_3H_6/C_3H_8
R-ZIF	26.5	11	8	100	95	2.41	3.31	1.053
R/IL1	24	9.2	6.5	80.2	75	2.61	3.69	1.069
R/IL2	20.2	7	4.1	80	74	2.89	4.93	1.081

5.3.2. Mixed matrix membrane characterization

Conventional FESEM was conducted to investigate the filler dispersion and polymer/filler interfacial adhesion which are critical aspects affecting the gas separation performance of the MMMs. The FESEM images of the PR MMMs and PR/IL MMMs are displayed in Fig. 5.6. The dispersion of R-ZIF in 10 wt.% loading PR MMM (Fig. 5.6a) is uniform and interfacial voids were hardly observed with the R-ZIF particles well covered by the polymer matrix, as was previously shown in Chapter 4. Likewise, for PR MMM with higher loading of R-ZIF (20 wt.%), filler agglomeration and interfacial voids were observed in Fig. 5.6b.

For the PR/IL MMMs (Fig. 5.6c-5.6f), improved polymer/fillers adhesion in the MMMs is observed. R-ZIF particles dispersed uniformly in the polymer matrix with fewer interfacial voids. The improved polymer/filler interface is attributed to the excellent interaction between R/IL particles and the polymer with the presence of ILs. Being immobilized on the R-ZIF surface, the ILs play the role as the binding component which enhances the compatibility and adhesion between R-ZIF and the polymer matrix, leading to an improved interface and reduced interfacial voids. Even at higher loading of R-ZIF/IL (20 wt.%), less interfacial voids were observed compared to the R-ZIF MMM without IL incorporation, which further indicated the better interaction between R-ZIF and polymer matrix with the presence of ILs. The better interfacial adhesion in PR/IL MMMs may lead to the improvement in gas separation efficiency of the membranes. These results indicate that the incorporation of ILs can be an effective way to enhance the polymer/filler interfacial interaction and reduce the filler aggregation in the MMMs.

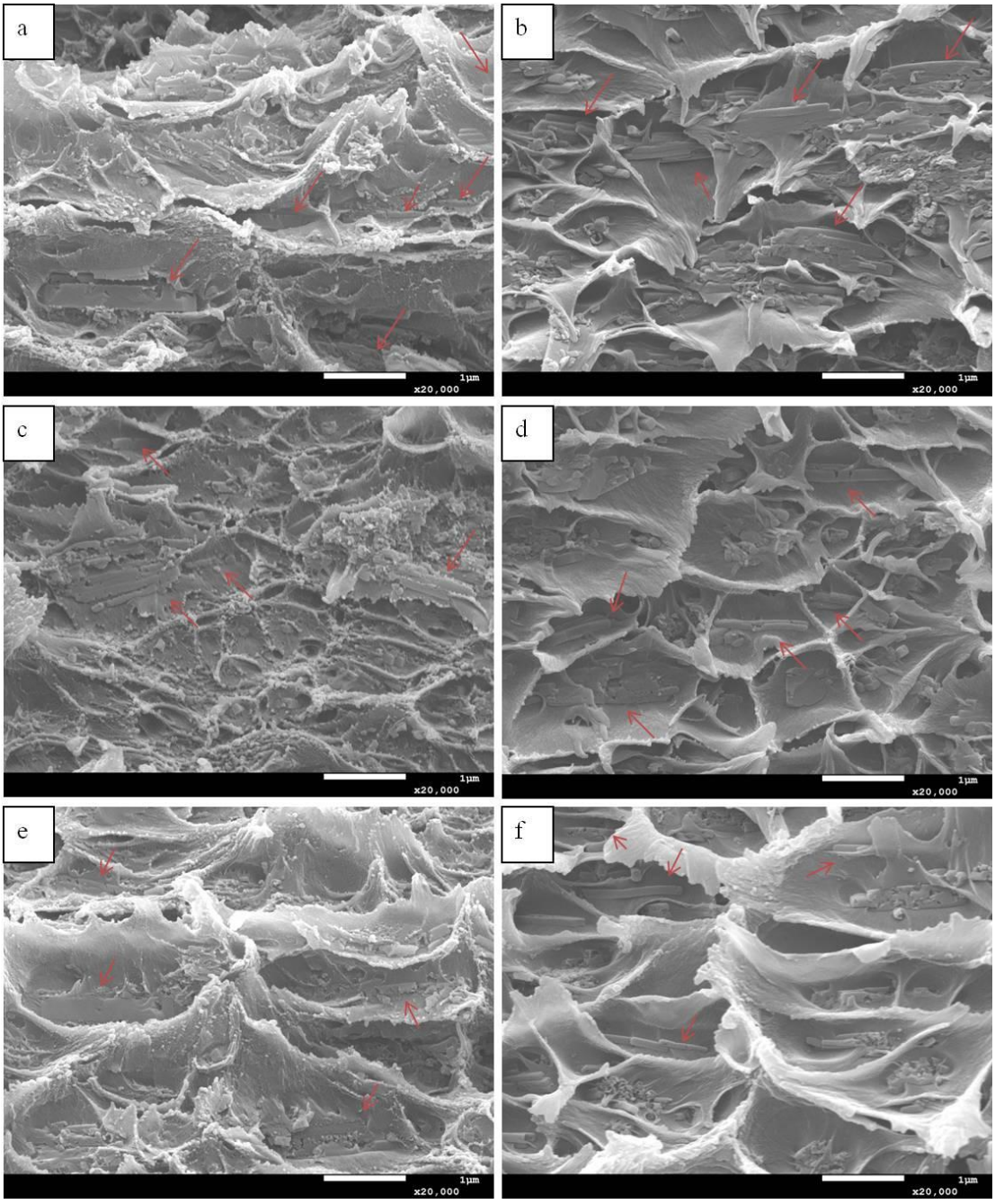

Figure 5.6. SEM images of PZ MMMs, PR MMMs and PL MMMs: (a) PR10, (b) PR20, (c) PR10/IL1, (d) PR20/IL1, (e) PR10/IL2, (f) PR20/IL2 (Arrows point to the ZIF nanorod embedded in polymer matrix)

5.3.3. Gas separation performance

The single gas permeability measurements has been conducted to investigate the ideal gas separation performance of the PR MMMs and PR/IL MMMs. Fig. 5.7 shows the CO_2 and C_3H_6 permeability and the gas selectivity for CO_2/N_2, CO_2/CH_4 and C_3H_6/C_3H_8 gas pairs of neat 6FDA-

durene membrane, PR MMMs and PR/IL MMMs. As discussed in Chapter 4, incorporating R-ZIF into 6FDA-durene matrix increased the permeability of CO_2 and C_3H_6 of the MMM accompanied by slight improvement in CO_2/N_2, CO_2/CH_4 and C_3H_6/C_3H_8 selectivity in comparison with the neat 6FDA-durene membrane. When the R-ZIF loading increase up to 20 wt.%, the PR20 MMM exhibited a higher gas permeability with a slight decline in gas selectivity compared to the PR10 MMM.

In the case of PR/IL MMMs, improvement in both the CO_2 and C_3H_6 permeability and selectivity was achieved with the incorporation of ILs. The introduction of ILs significantly improved the interfacial interaction between the R-ZIF particles and polymer matrix, leading to the better gas separation performance of the MMM, which is in agreement with the SEM observations above. Besides, the IL layer on R-ZIF surface may further increases the sorption affinity of the filler toward CO_2 and C_3H_6 gases while showing negligible effect on the other gases and subsequently enhancing the gas selectivity for the CO_2 and C_3H_6 [23]. The presence of IL also reduced the surface area and partially blocked the pores which may also further reduce the permeability of the un-wanted gases (N_2, CH_4 and C_3H_8) through the pores of R-ZIF, thus further improving CO_2 and C_3H_6 selectivity.

The difference in the gas separation efficiency of MMMs with different ILs in this work is speculated to be affected by the gas transport properties of each IL. As previously mentioned, the IL layer plays the role of "gas carrier", improving the gas permeability through the MMMs. While also exhibiting enhancement in gas selectivity for CO_2/N_2, CO_2/CH_4 and C_3H_6/C_3H_8, PR/IL2 MMMs expressed a lower gas permeability compared to the PR/IL1 MMMs. This comparatively inferior gas permeability of PR/IL2 MMMs may be due to the superior occupation of IL2 on surface and in the near-surface pores of R-ZIF. [Bmim][Tf_2N] molecules possess longer alkyl chains, which may reduce the gas diffusivity through the ZIF channels more than that of the [Emim][Tf_2N]. This hypothesis is in agreement with previous reports in literature [24,25]. This result is also compatible with the ideal gas selectivity data previously discussed, as the R/IL2 showed lower gas adsorption capacity at 30°C compared to the R/IL1.

The separation performance of PR/IL MMMs for the 50:50 CO_2/CH_4 mixed-gas was also investigated and the results are shown in Fig. 5.8. Compared to the single gas permeation, a reduction in CO_2 permeability is observed along with slight decline in CO_2/CH_4 selectivity for all PR20/IL MMMs. The reduction is less pronounced for the PR/IL2 MMM. This phenomenon is likely due to the competitive sorption of CO_2 and CH_4 in both the filler, ILs and the polymer

matrix.The presence of CH_4 in the gas mixture might obstruct adsorption of CO_2 on R-ZIF fillers and prevent the extra condensation of CO_2, leading to the decrease in CO_2 solubility [26]. The impact of the competitive sorption is less for IL2 in comparison to IL1, which is likely due to the increased CO_2 and decreased CH_4 sorption capacity of the IL. In other words the IL allowed less CH_4 into the IL and subsequently the R-ZIF, so the impact of CH_4 on the transport phenomena was reduced. Compared to the single gas separation performance of the neat polymer membrane and the PR MMMs, the PR/IL MMMs still showed higher CO_2/CH_4 selectivity in mixed-gas with slight reduction in CO_2 permeability. This result indicated that IL immobilization on the surface of R-ZIF is an effective method to enhance the gas separation efficiency of the MMMs.

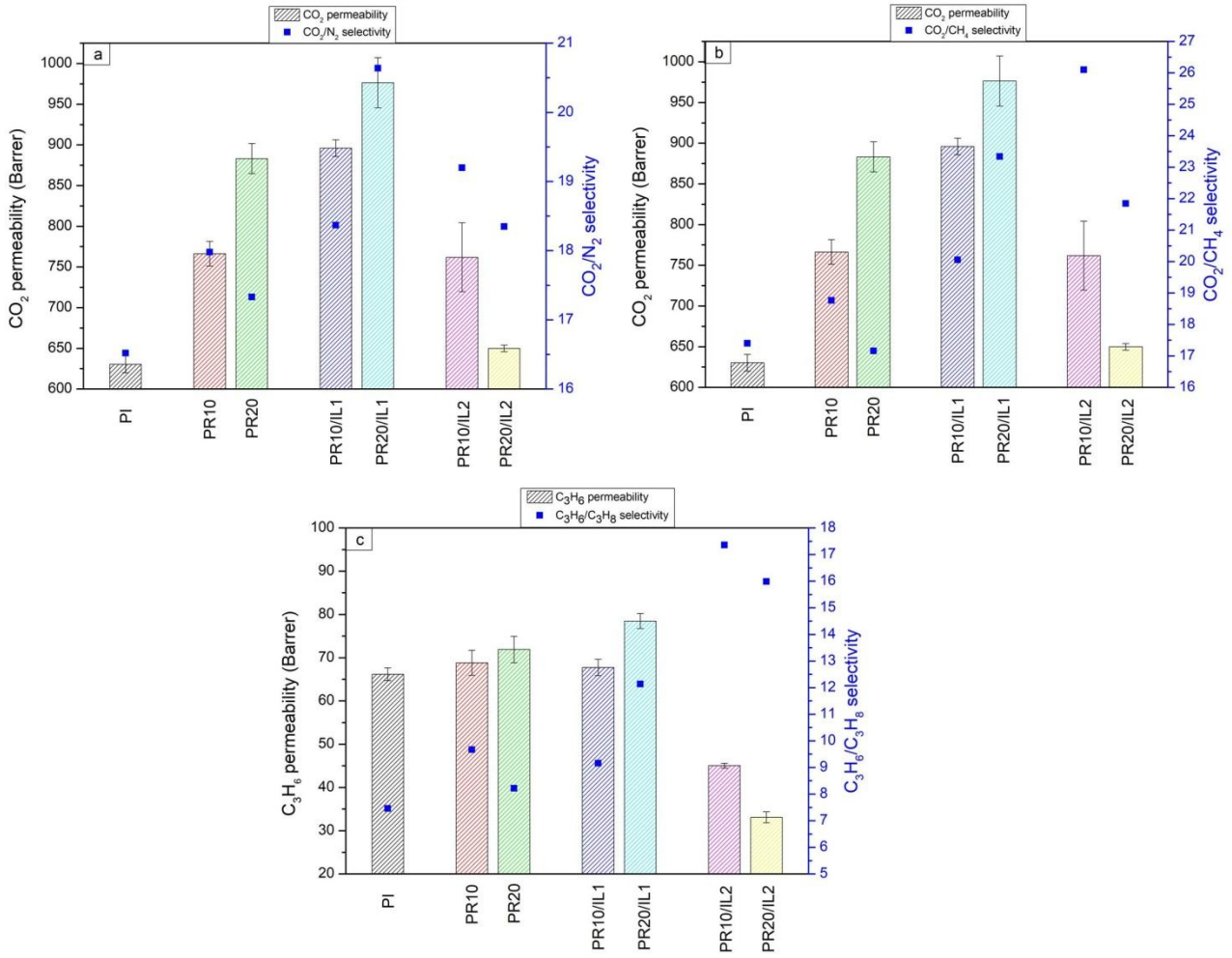

Figure 5.7. Gas permeability and selectivity of orginal PI membrane, PR MMM and PR/IL MMMs: (a) CO_2/N_2, (b) CO_2/CH_4 and (c) C_3H_6/C_3H_8 (at 30°C, 2 bar)

Table 5.3. Gas permeability and selectivity of pure 6FDA-durene membrane, PZ MMM and PZ/IL MMM

Sample	Permeability (barrer)					Selectivity		
	CO_2	N_2	CH_4	C_3H_6	C_3H_8	CO_2/N_2	CO_2/CH_4	C_3H_6/C_3H_8
PI	630.25±10.33	38.15±0.87	36.08±0.73	66.18±1.45	8.87±0.17	16.52	17.4	7.46
PR10	766.390±15.22	42.630±1.79	40.82±1.12	68.826±2.91	7.048±0.15	17.98	18.77	9.67
PR20	883.203±18.46	50.95±2.21	51.47±2.56	71.914±3.06	8.75±0.21	17.33	17.16	8.22
PR10/IL1	896.063±10.24	48.77±1.23	44.671±1.21	67.73±1.87	7.39±0.11	18.37	20.06	9.16
PR20/IL1	1035.615±30.78	44.80±1.28	44.341±1.67	78.472±1.73	6.451±0.22	23.12	23.36	12.14
PL10/IL2	761.86±42.25	38.42±0.46	29.18±1.52	45.04±0.56	2.59±0.23	19.83	26.1	17.36
PL20/IL2	649.89±4.06	35.43±0.77	29.74±0.36	33.09±1.29	2.04±0.78	18.35	21.85	15.99

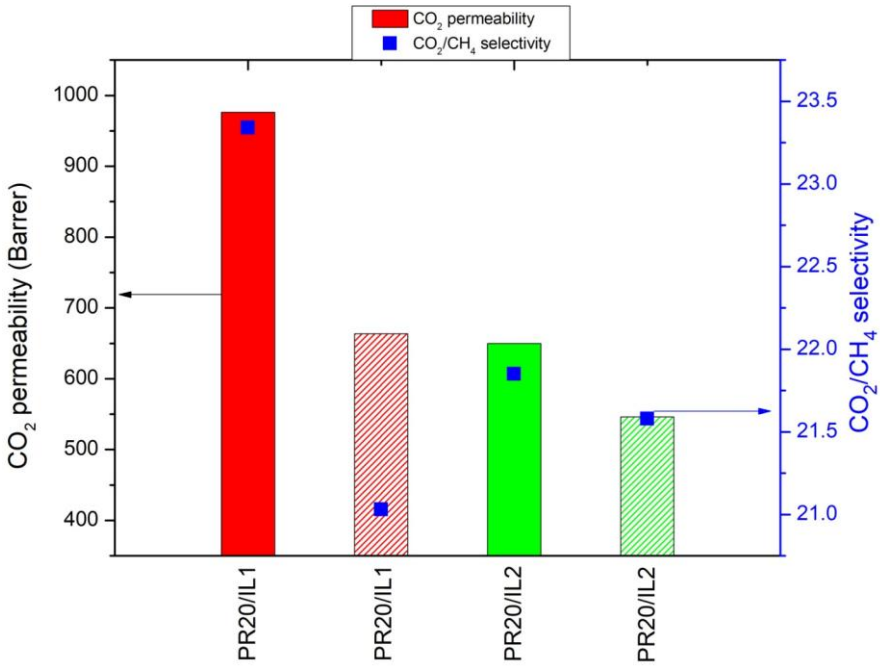

Figure 5.8. Gas permeability and selectivity for CO_2/CH_4 as single gas and gas mixture (50/50 vol) of PR20/IL MMMs (at 30°C, 2 bar) (Filled bar: single gas, patterned bar: gas mixture)

5.4. Conclusion

In this chapter, ionic liquids have been successfully immobilized on the surface of R-ZIF in a mixed matrix membrane and characterised for gas separation. The presence of an IL layer effectively improved the interfacial interaction between R-ZIF and the polymer matrix due to the favourable ZIF-IL-polymer bridging interaction. This in turn led to an enhancement in gas separation performance of the PR/IL MMMs. With these results, using ILs as the binding component in MMMs can be considered an effective approach to improve the filler/polymer interfacial adhesion in order to achieve better gas-separation performance in mixed matrix membranes.

References

[1] R. Lin, L. Ge, H. Diao, V. Rudolph, Z. Zhu, Ionic Liquids as the MOFs/Polymer Interfacial Binder for Efficient Membrane Separation, ACS Appl Mater Interfaces. 8 (2016) 32041–32049.

[2] H. An, S. Park, H.T. Kwon, H.K. Jeong, J.S. Lee, A new superior competitor for exceptional propylene/propane separations: ZIF-67 containing mixed matrix membranes, J. Membr. Sci. 526 (2017) 367–376.

[3] S.R. Venna, M. Lartey, T. Li, A. Spore, S. Kumar, H.B. Nulwala, D.R. Luebke, N.L. Rosi, E. Albenze, Fabrication of MMMs with improved gas separation properties using externally-functionalized MOF particles, J. Mater. Chem. A. 3 (2015) 5014–5022.

[4] H. Zhu, L. Wang, X. Jie, D. Liu, Y. Cao, Improved Interfacial Affinity and CO2Separation Performance of Asymmetric Mixed Matrix Membranes by Incorporating Postmodified MIL-53(Al), ACS Appl. Mater. Interfaces. 8 (2016) 22696–22704.

[5] S.N. Wijenayake, N.P. Panapitiya, S.H. Versteeg, C.N. Nguyen, S. Goel, K.J. Balkus, I.H. Musselman, J.P. Ferraris, Surface cross-linking of ZIF-8/polyimide mixed matrix membranes (MMMs) for gas separation, Ind. Eng. Chem. Res. 52 (2013) 6991–7001.

[6] M. Askari, T.S. Chung, Natural gas purification and olefin/paraffin separation using thermal cross-linkable co-polyimide/ZIF-8 mixed matrix membranes, J. Membr. Sci. 444 (2013) 173–183.

[7] B. Seoane, V. Sebastián, C. Téllez, J. Coronas, Crystallization in THF: The possibility of one-pot synthesis of mixed matrix membranes containing MOF MIL-68(Al), CrystEngComm. 15 (2013) 9483–9490.

[8] R. Lin, L. Ge, S. Liu, V. Rudolph, Z. Zhu, Mixed-matrix membranes with metal-organic framework-decorated CNT fillers for efficient CO_2 separation, ACS Appl. Mater. Interfaces. 7 (2015) 14750–14757.

[9] R. Lin, L. Ge, L. Hou, E. Strounina, V. Rudolph, Z. Zhu, Mixed matrix membranes with strengthened MOFs/polymer interfacial interaction and improved membrane performance, ACS Appl. Mater. Interfaces. 6 (2014) 5609–5618.

[10] Z. Dai, R.D. Noble, D.L. Gin, X. Zhang, L. Deng, Combination of ionic liquids with membrane technology: A new approach for CO_2 separation, J. Membr. Sci. 497 (2016) 1–20.

[11] Y.C. Hudiono, T.K. Carlisle, A.L. LaFrate, D.L. Gin, R.D. Noble, Novel mixed matrix membranes based on polymerizable room-temperature ionic liquids and SAPO-34 particles to improve CO_2 separation, J. Membr. Sci. 370 (2011) 141–148.

[12] C. Casado-Coterillo, M. Del Mar Lopez-Guerrero, A. Irabien, Synthesis and Characterisation of ETS-10/Acetate-based Ionic Liquid/Chitosan Mixed Matrix Membranes for CO_2/N_2 Permeation, Membr. 4 (2014) 287–301.

[13] H. Li, L. Tuo, K. Yang, H.K. Jeong, Y. Dai, G. He, W. Zhao, Simultaneous enhancement of mechanical properties and CO_2 selectivity of ZIF-8 mixed matrix membranes: Interfacial toughening effect of ionic liquid, J. Membr. Sci. 511 (2016) 130–142.

[14] L. Ge, Z. Zhu, F. Li, S. Liu, L. Wang, X. Tang, V. Rudolph, Investigation of gas permeability in carbon nanotube (CNT)-polymer matrix membranes via modifying CNTs with functional groups/metals and controlling modification location, J. Phys. Chem. C. 115 (2011) 6661–6670.

[15] S.A.S.C. Samarasinghe, C.Y. Chuah, Y. Yang, T.H. Bae, Tailoring CO2/CH4 separation properties of mixed-matrix membranes via combined use of two- and three-dimensional metal-organic frameworks, J. Membr. Sci. 557 (2018) 30–37.

[16] F. Yang, H. Mu, C. Wang, L. Xiang, K.X. Yao, L. Liu, Y. Yang, Y. Han, Y. Li, Y. Pan, Morphological Map of ZIF-8 Crystals with Five Distinctive Shapes: Feature of Filler in Mixed-Matrix Membranes on C_3H_6/C_3H_8 Separation, Chem. Mater. 30 (2018) 3467–3473.

[17] K. Hanke, M. Kaufmann, G. Schwaab, M. Havenith, C.T. Wolke, O. Gorlova, M.A. Johnson, B.P. Kar, W. Sander, E. Sanchez-Garcia, Understanding the ionic liquid $[NC_{4111}][NTf_2]$ from individual building blocks: an IR-spectroscopic study, Phys. Chem. Chem. Phys. 17 (2015) 8518–8529.

[18] Y.S. Ye, M.Y. Cheng, J.Y. Tseng, G.-W. Liang, J. Rick, Y.J. Huang, F.C. Chang, B.J. Hwang, New proton conducting membranes with high retention of protic ionic liquids, J. Mater. Chem. 21 (2011) 2723.

[19] B. Koyuturk, C. Altintas, F.P. Kinik, S. Keskin, A. Uzun, Improving Gas Separation

Performance of ZIF-8 by [BMIM][BF_4] Incorporation: Interactions and Their Consequences on Performance, J. Phys. Chem. C. 121 (2017) 10370–10381.

[20] P. Krokidas, M. Castier, S. Moncho, D.N. Sredojevic, E.N. Brothers, H.T. Kwon, H.-K. Jeong, J.S. Lee, I.G. Economou, ZIF-67 Framework: A Promising New Candidate for Propylene/Propane Separation. Experimental Data and Molecular Simulations, J. Phys. Chem. C. 120 (2016) 8116–8124.

[21] J. Ahn, W.J. Chung, I. Pinnau, M.D. Guiver, Polysulfone/silica nanoparticle mixed-matrix membranes for gas separation, J. Membr. Sci. 314 (2008) 123–133.

[22] S. Raeissi, C.J. Peters, A potential ionic liquid for CO_2 - separating gas membranes: selection and gas solubility studies, Green Chem. 11 (2009) 185–192.

[23] S. n. v. k. Aki, B.R. Mellein, E.M. Saurer, J.F. Brennecke, High-pressure phase behavior of carbon dioxide with imidazolium-based ionic liquids, J, Phys. Chem. B. 108 (2004) 5–20365.

[24] Z. Lei, C. Dai, B. Chen, Gas solubility in ionic liquids, Chem. Rev. 114 (2014) 1289–1326.

[25] J.L. Anthony, J.L. Anderson, E.J. Maginn, J.F. Brennecke, Anion effects on gas solubility in ionic liquids, J. Phys. Chem. B. 109 (2005) 6366–6374.

[26] C. Zhang, Y. Dai, J.R. Johnson, O. Karvan, W.J. Koros, High performance ZIF-8/6FDA-DAM mixed matrix membrane for propylene/propane separations, J. Membr. Sci. 389 (2012) 34–42.

CHAPTER 6. EFFECT OF IONIC LIQUIDS ON MOFS/POLYMER INTERFACIAL ENHANCEMENT IN MIXED MATRIX MEMBRANES

Contribution to field

Strong interfacial interactions between the filler(s) and the chosen polymer in mixed matrix membranes (MMMs) is a crucial factor in obtaining high gas separation efficiency. However, it is challenging to obtain excellent filler/polymer contact simply by direct incorporation of micron-sized metal-organic frameworks (MOFs) into a polymer matrix without modification. This chapter continues the investigation into the enhancement of micron-sized ZIF particles using a thin layer of three different ionic liquids (ILs). However, in contrast to Chapter 5 which used R-ZIF particles which already displayed good but not perfect interfacial adhesion, the ZIF particles in this chapter are polyhedral in shape (P-ZIF). These were chosen for IL coating as Chapter 4 showed they had the worst interfacial adhesion of the 3 ZIF morphologies. Hence this represents a more challenging test for the hypothesis that coating with IL is an effective method for enhancing filler dispersion, reducing filler aggregation and improving MMM performance. The coated P-ZIF particles were incorporated into 6FDA-durene polymer at different loadings to fabricate MMMs for gas separation. Playing the role of interfacial binder, all ILs effectively enhanced the polymer/ZIF adhesion, minimizing the formation of non-selective interfacial defects, which was evidenced by the scanning electron microscopy (SEM) as well as by the focus ion beam scanning electron microscopy (FIB-SEM), leading to an increment in CO_2/N_2, CO_2/CH_4 and C_3H_6/C_3H_8 selectivity. The contribution of this chapter then is that the successful combination of P-ZIF/IL is further confirmed as an effective method to overcome interfacial issues in MMMs, particularly in the application of larger micron-sized fillers. The work in this Chapter has been submitted to the Journal of Membrane Science.

6.1. Introduction

Gas separation is one of the most challenging and energy intensive steps for many industrial processes such as in hydrogen purification (H_2/N_2, H_2/CO_2, H_2/hydrocarbon), air separation (N_2/O_2), natural gas sweetening (CO_2/CH_4), flue gas cleaning and CO_2 capture (CO_2/N_2) and hydrocarbon

separation (olefins/paraffins) [1]. Many of the separations are achieved through conventional distillation although wet gas scrubbing, pressure swing adsorption, and membranes also play an important role. Membrane-based technologies are potentially an attractive alternative due to a relatively high energy efficiency, low capital cost and ease of operation [2,3]. Whilst a diverse mix of materials have been extensively studied, only polymeric membranes have been widely applied as they are relatively inexpensive and easy to scale up. Conventional polymeric membranes, however, suffer from a trade-off between the desire for high flux and high selectivity for the chosen gas [4]. Furthermore, due to the vulnerability of polymeric membranes to chemical degradation and thermal processing, their application has been narrowed to where reactive gases, high humidity and high temperature are not present [3,5].

Mixed matrix membranes (MMMs), wherein a highly selective inorganic filler is embedded into a low cost and easily processable polymeric matrix, have been developed as a way to overcome the above limitations [4,6,7]. Metal-organic frameworks (MOFs) are a recent group of nanoporous materials that have attracted considerable attention both for membrane applications as well as other gas separation processes due to their large surface areas, well-defined and tunable pore structures, good thermal and chemical stability [2,8]. Zeolite imidazolate frameworks (ZIFs), a subfamily of MOFs, fabricated using transition metals (Zn, Co) and imidazolate linkers have been intensively investigated in mixed matrix membranes in recent years, with mixed success [9]. Bushell et al. [10] investigated the ZIF-8 incorporated PIM-1 MMM which demonstrated an increase in CO_2/CH_4 selectivity from 14.2 to 18.6 while the CO_2 permeability slightly decreased from 4390 to 4270 Barrer. High propylene/propane selectivity was also obtained in the work of Zhang et al. [11] by embedding ZIF-8 into a polyimide matrix. MMMs that contain ZIF-90 filler particles in Ultem, Matrimid and 6FDA-DAM polyimide were fabricated by the Bae group, of which the highest selectivity for CO_2/CH_4 and CO_2/N_2 was achieved with ZIF-90/6FDA-DAM membranes [12]. ZIF-7 was also investigated by Yang and co-workers as they embedded ZIF-7 into polybenzimidazole (PBI) and observed higher permeability and selectivity for H_2/CO_2 compared to the neat PBI and ZIF-7 membranes [13]. Work by Kwon et al. [14] demonstrated that the separation performance of propylene/propane could be enhanced by growing ZIF-67 on ZIF-8 seed layers. According to the authors, ZIF-67 might be more efficient than ZIF-8 in propylene/propane separation as the Co-N bond in ZIF-67 is stiffer than the Zn-N bond in ZIF-8. This result was also confirmed through dynamics simulation carried out by Krokidas et al. [15]. Very recently, An et. al. [4] also investigated the C_3H_6/C_3H_8 separation performance of nano-size ZIF-67 contained MMMs, which

showed considerable improvement in both propylene permeability and propylene/propane selectivity.

Despite the many advantages of using ZIFs in MMMs and success at improving the ideal selectivity of various gas pairs, the non-ideal interfacial adhesion and morphology between the polymer matrix and filler still represent a great challenge. The most prominent of the issues are filler agglomeration and interfacial voids caused by poor interaction between the filler and polymer matrix during fabrication [4,8]. Several techniques have been studied in order to improve the interfacial interaction between polymers and inorganic fillers such as: grafting functional groups onto the filler surface [16,17], modification of the polymeric matrix [18,19], in situ synthesis of the filler in polymer solution before casting [20], coating the surface of the filler with a compatibilising compound and using composite fillers which are combination of different types of fillers [21,22]. Among these methods, using ionic liquids (ILs) to improve the gas separation performance of MMMs show great potential since ILs might increase the permeability of targeted gas species through the membranes whilst also offering improved interfacial wetting between the polymer matrix and filler particles [23]. Hudiono et al. [24] showed that by coating IL onto the surface of the SAPO-34 particles, the compatibility of polymer matrix and the zeolite particles was enhanced. Additionally, the ILs created a selective layer around the SAPO-34 particles, which then improves the CO_2 permeability and selectivity over CH_4 and N_2. More recently, acetate based ILs were used in titanosilicate ETS-10/chitosan MMMs which showed sharply increment in both permeability and selectivity for CO_2/N_2 separation. Moreover, the ILs increased the flexibility of polymer segments in MMMs, thus improving the processability [25]. However, directly introducing ILs into polymers with large free volume may result in reducing the gas permeability of the membranes. This behaviour is hypothesized to result from the free volume of the polymer being occupied by the ILs, therefore decreasing the gas diffusion through the membranes. In order to overcome these issues, researchers have sought new ways to incorporate ILs. Hao et.al. [26] coated the ZIF-8 particle surface with ILs before incorporation into a Pebax matrix. This resulted in both an enhancement of polymer/filler compatibility as well as CO_2/N_2 and CO_2/CH_4 gas separation performance. More recently, Lin et.al [8] applied ILs onto the surface of HKUST-1 effectively eliminating the interfacial void formed between the pure HKUST-1 and polymer matrix. The selectivity for CO_2/N_2 and CO_2/CH_4 gas pairs also increased compared to the neat MMMs.

The majority of work with ILs has focused on nano-sized MOFs being incorporated into MMMs. Micron-size MOFs are easier and cheaper to synthesize and would be preferred as fillers; however,

poor interfacial interactions with the polymer matrix [8] have meant micron-sized fillers often fail to meet their potential. In this chapter, micron-sized polyhedral shape ZIF (P-ZIF) was chosen as the filler and three kinds of ILs: 1-butyl-3-methylimidazolium tetrafluoroborate ([Bmim][BF_4]), 1-ethyl-3-methylimidazolium bis(trifluoromethanesulfonyl)imide ([Emim][Tf_2N]) and 1-Butyl-3-methylimidazolium bis(trifluoromethanesulfonyl)imide ([Bmim][Tf_2N]) were used as the interfacial binder for the fabrication of 6FDA-durene/P-ZIF MMMs. Based on previous studies and the Chapter 5, [Bmim][BF4] can provide improvement in terms of propylene solubility and selectivity, while both [Emim][Tf_2N] and [Bmim][Tf_2N] are well known for their excellent intrinsic CO_2 solubility [25, 26].

P-ZIF was chosen as Chapter 4 showed it had the worst interfacial adhesion and MMM gas separation performance of the three morphologies tested. The work in Chapter 5 indicates ILs are an effective means of improving MMM properties in this 6FDA-durene system. Therefore enhancement of the polyhedral ZIF represents a greater challenge and more thorough test of the hypothesis from Chapter 5. Furthermore P-ZIF particles are easier to manufacture, so if similar properties can be replicated through the application of ILs, as hypothesized, the resulting membrane will be more industrially significant. The enhancement of interfacial adhesion of P-ZIF with the 6FDA-durene matrix in the presence of ILs was investigated via scanning electron microscopy observation with focused ion beam analysis. Membrane performance was characterized via gas permeability and permselectivity measurements for CO_2, N_2, CH_4, C_3H_6 and C_3H_8, and was complimented by extensive characterization of the IL coated fillers. Gas mixture testing (50:50 mixture of CO_2/CH_4) was also conducted to better closer simulate industrially relevant conditions.

6.2. Experimental

6.2.1. Materials

4, 4'-(hexafluoroisopropylidene) diphthalic anhydride (6FDA), 2,3,5,6-tetramethyl-1,3-phenyldiamine (durene), triethylamine, acetic anhydride N,N-dimethylacetamide (DMAc), and chloroform were supplied by Sigma–Aldrich.

Cobalt nitrate hexahydrate ($Co(NO_3)_2.6H_2O$, 98%, Sigma-Aldrich) and 2-methylimidazole $C_4H_6N_2$, 99%, Sigma-Aldrich) and methanol (Merck) were used for the synthesis of P-ZIF nanoparticles without further purification.

Three types of ionic liquids (ILs): 1-Butyl-3-methylimidazolium bis(trifluoromethanesulfonyl)imide 99.9% ([Bmim][Tf_2N]), 1-ethyl-3-methylimidazolium bis(trifluoromethanesulfonyl)imide 99.9% ([Emim][Tf_2N]), 1-butyl-3-methylimidazolium tetrafluoroborate ([Bmim][BF_4]) were purchased from Sigma-Aldrich.

6.2.2. Preparation of P-ZIF particles

P-ZIF particles were synthesized at room temperature according to a literature procedure [27]. The first solution of cobalt metal source was made of 8.15g of $Co(NO_3)_2.6H_2O$ in 700 mL methanol while the second solution of ligand source included 9.19g of 2-methylimidazole (HmIm) in 700 mL methanol. The first solution was then added dropwise into the second one and the mixed solution was gently stirred at 150 rpm for 18h. The obtained purple mixture was centrifuged at 8000 rpm for 30 min and the purple particles were collected. In order to remove all the residual solvent and unreacted species, the prepared particles were washed in methanol for at least three times and then dried at 100 ^oC under vacuum for 24 h before use.

IL-incorporated P-ZIF samples were prepared in the open atmosphere. Firstly, a preset amount of IL was put in an empty vial and weigh with the balance. Based on the amount of IL in the vial, the quantity of P-ZIF was calculated to make the ratio of P-ZIF/IL = 95/5. 15 mL of chloroform was poured in the vial and stir to dissolve the IL then the P-ZIF was added into the solution and the resulting mixture was stirred continuously at 25 °C while leaving expose to air until most of the solvent evaporated. The resulting sample was consequently dried in a vacuum oven at 100 ^oC for 24 h. The ratios of P-ZIF/IL were made at 95/5 wt.%. The obtained samples were labeled as Z/IL1, Z/IL2 and Z/IL3 considering the ILs ([Emim][Tf_2N]), ([Bmim][Tf_2N]) and ([Bmim][BF_4]), respectively.

6.2.3. 6FDA-durene synthesis

6FDA-durene polyimide was synthesized (Figure 6.1) based on work reported elsewhere [19,28]. Briefly, polyamic acid was formed by polymeric reaction between equimolar of durene (1.426 g) and 6FDA (3.861 g) in DMAc. The mixture was stirred under nitrogen at room temperature for 24 h. After that, a mixture of triethylamine (3.2 mL) and acetic anhydride (1.2 mL) was added to the former solution. The mixture was stirred under nitrogen at room temperature for another 24 h to form polyimides. The obtained polymer was precipitated in methanol, washed several times with

methanol, and dried at 180 °C under vacuum for 18 h. The as-prepared polyimide is referred as 6FDA-durene.

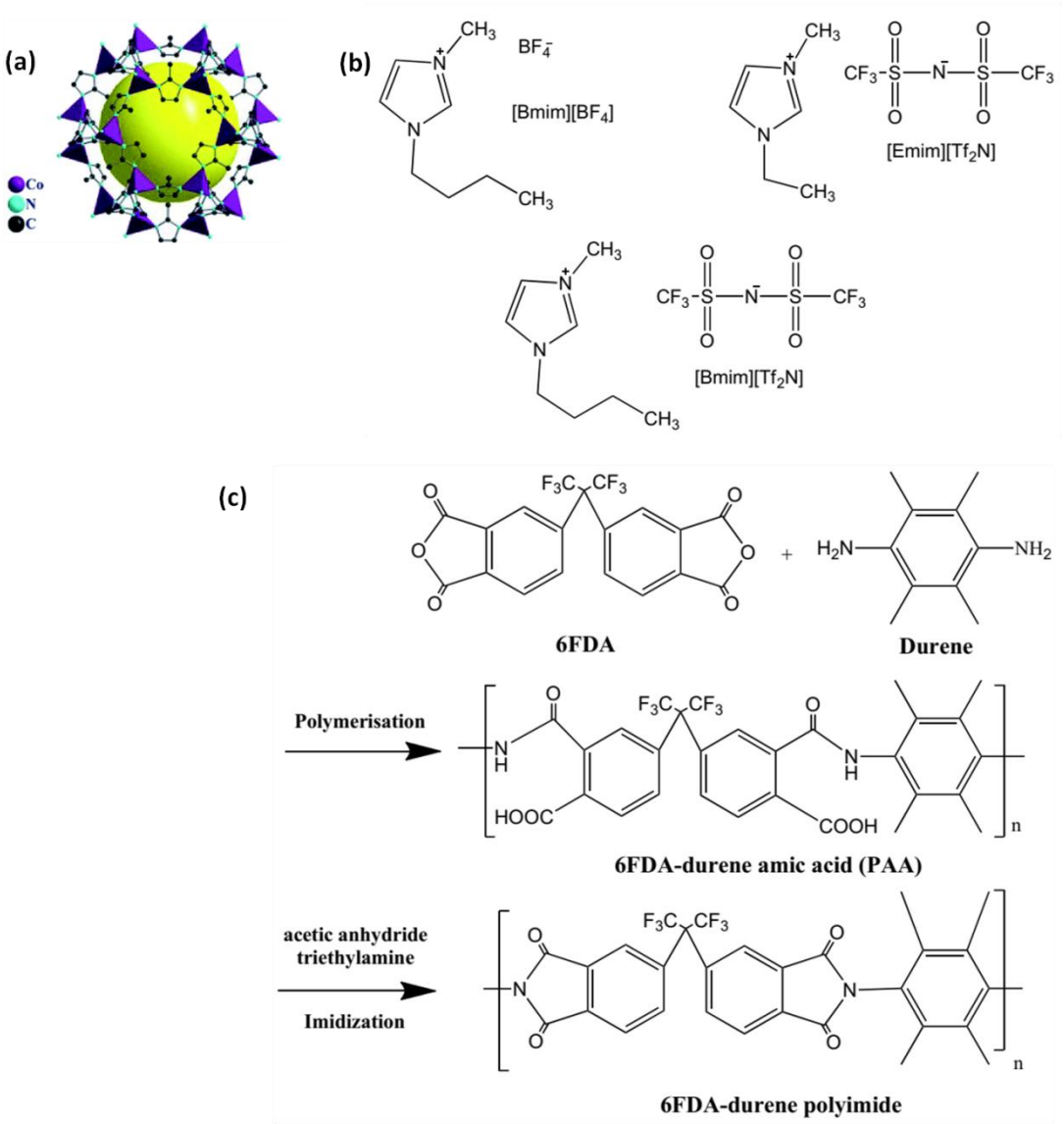

Figure 6.1. Structure of (a): P-ZIF, (b) ionic liquids and (c) 6FDA-durene polyimide synthesis process

6.2.4. Fabrication of MMMs

For the pure 6FDA-durene membrane, 0.45 g 6FDA-durene was dissolved into 3 mL chloroform and then cast onto a clean glass plate with a doctor blade at gap setting of 300 µm and covered to slowly dry at room temperature for 24 h. After that, the membrane was dried at 100 ^{o}C for 24 h under vacuum. The thickness of the final membranes is about 40-50 µm.

For the MMMs, a calculated amount of as-synthesized P-ZIF was dispersed in chloroform under sonication. 0.45 g 6FDA-durene was dissolved into this suspension further stirred for 12 h. The resulting mixture was cast on glass plate with a doctor blade at gap setting of 300 µm and dried at room temperature for 24 h, followed by drying at 100 ^{o}C for 24 h under vacuum. The obtained membranes have the thickness of 40-50 µm. The loading of P-ZIF in MMMs were 10 wt.% and 20 wt.% calculated based on equation below:

$$\Phi = \frac{m_{filler}}{m_{filler} + m_{6FDA-durene}} \times 100\ (\%)$$

where Φ is the filler loading (%), m_{filler} and $m_{6FDA\text{-}durene}$ are the mass of P-ZIF or Z/IL and mass of polymer in the MMMs, respectively. Samples used in this study were named as in Table 6.1:

Table 6.1. Sample names and nomenclature in this chapter

Sample	**Pure 6FDA-durene membrane**	**6FDA-durene/P-ZIF membrane**	**6FDA-durene/P-ZIF/IL membrane**	**P-ZIF/IL particles**
Nomenclature	PI	PZ (x) x: P-ZIF weight percent	PZ(x)/IL(y) x: P-ZIF weight percent y: type of IL	Z/IL(y) y: type of IL

6.2.5. Characterization

The XRD, FTIR, N_2 adsorption isotherm analyses as well as the cross-sectional morphologies of the samples were carried out at the same conditions as mentioned in section 4.2.4 in chapter 4.

XPS elemental analysis was conducted on the KRATOS Axis Ultra using 4 keV argon ions at an ion source extractor current of 630 nA. The sputter rates were in the region of 2 nm min^{-1} and the analyzed surface was an area of 0.8 mm x 0.3 mm centered in a sputter area of 4 x 4 mm. The samples were prepared by dispersing P-ZIF/IL particles in n-hexane and add several small droplets

onto the 10 x 10 mm silica wafer to form a layer of P-ZIF/IL. The samples were then dried at 100°C for 24h before XPS analysis.

Focused ion beam scanning electron microscopy (FIB-SEM) observation was carried out in a FEI SCIOS FIB/SEM dual beam system to determine the contact of the inorganic phase and polymeric matrix. A trench was firstly milled on the surface of the membrane with a Ga+ focused ion beam (FIB) (Fig 6.2). Numbers of slices with fixed thickness were cut from the specimen by the Ga+ FIB at 30kV and 3nA, while a series of exposed cross-section SEM images were collected in back-scattered electron (BSE) mode at 2kV. The segmentation of the individual phases (e.g. polymer, filler, voids) was conducted by image thresholding based on their different grayscale [29,30]. The whole stack of these SEM images was aligned and reconstructed in three-dimensions using Avizo software (FEI Visualization Sciences Group).

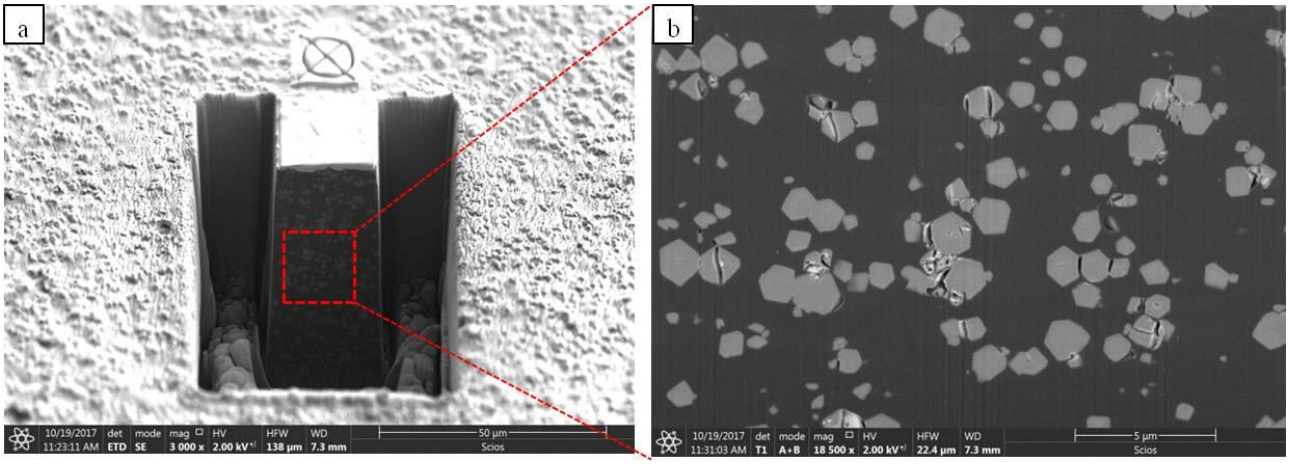

Figure 6.2. Typical FIB-SEM images of PZ20/IL MMMs: (a) FIB milling trend and (b) cross-sectional image in BSE mode

6.2.6. Gas permeation test

6.2.6.1. Single gas permeation test

The single gas permeation test was conducted with the same conditions as described in section 3.3.1, chapter 3 as well as showed in the Appendix.

6.2.6.2. Mix gas permeation test

The mix-gas permeation test was carried out with the same conditions mentioned in section 5.2.4.2 and the test procedure was described in detail in the Appendix.

6.3. Results and Discussion

6.3.1. P-ZIF preparation and characterization

The XRD patterns of P-ZIF and Z/IL are displayed in Fig. 6.3. The diffraction patterns of all IL-coated P-ZIF are well-matched with the neat P-ZIF, which implies that the crystallinity of P-ZIF is maintained after coating with the ILs. Fig. 6.4 shows the SEM images of the pure P-ZIF and the IL-treated P-ZIF. The cubic P-ZIF particles show sodalite (SOD) topology with polyhedral shapes and most of them are sized from 0.6 to 1.3 µm. In this work, the ILs were incorporated onto P-ZIF using chloroform based solutions to avoid over-occupation of the IL in the P-ZIF pore entrances which might hinder gas transportation and reduce the gas separation performance of the related MMMs. As can be seen in Fig. 6.3(c, d) the morphology of P-ZIF remains intact after the coating, indicating that the solvent and ionic liquid have little effect on the structure of P-ZIF.

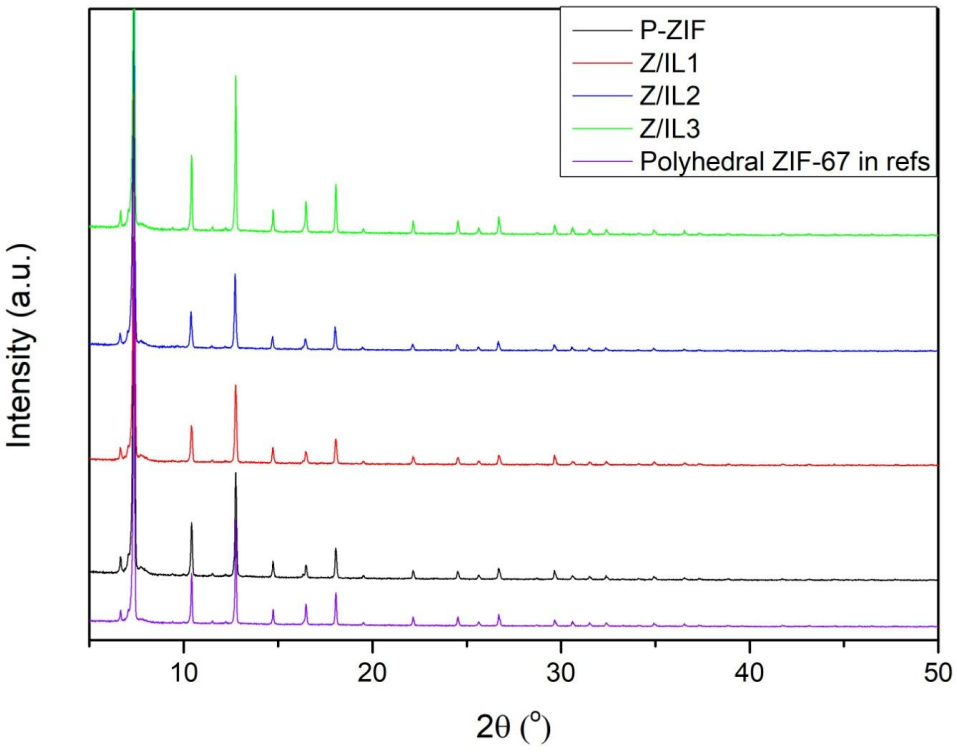

Figure 6.3. XRD patterns of P-ZIF and Z/IL

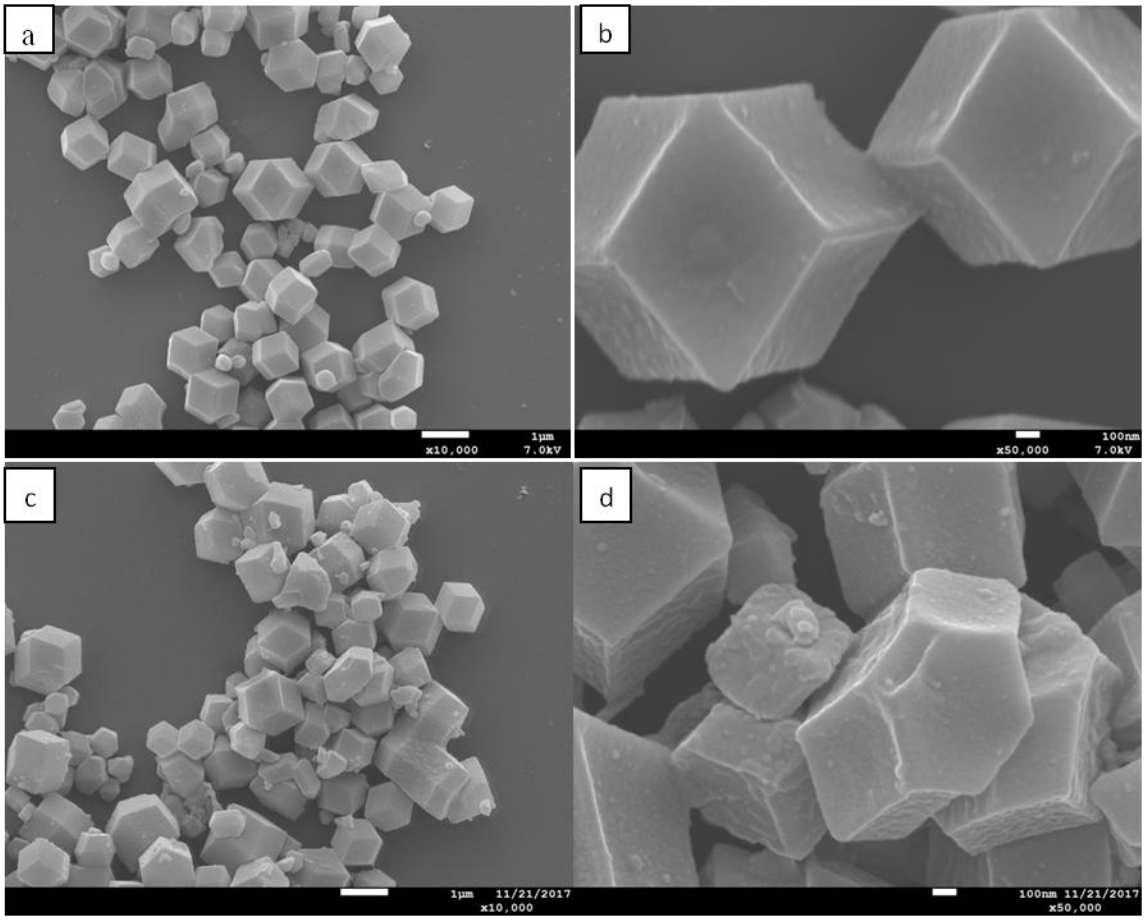

Figure 6.4. SEM images of P-ZIF: (a, b) and Z/IL3: (c, d)

XPS analysis was also conducted in order to confirm the successful introduction of ILs on P-ZIF particles. The XPS spectra of the Z/IL2 in Fig. 6.5 shows the F^{1s} and S^{2p} at 680-690 eV and 160-170 eV binding energy which indicate the presence of the anion $[Tf_2N]^-$ of IL on the surface of P-ZIF particles and confirms the successful incorporation of IL onto P-ZIF particles. The change in elemental composition of Z/IL2 along the depth from the surface was characterized by the XPS depth-profile, which is shown in Fig. 6.6. In this method, the ratios of unique elements in Z/IL particles at different depth from the surface were measured. As the scanning depth increased, the F^{1s} and S^{2p} ratio gradually reduced, while in contrast, the Co^{2p} ratio has a sharp increase at the depth of 3 nm. The existence of F^{1s} and S^{2p} at the further depth than 3 nm may be due to the IL occupation in the pores and cavities near the interface region. Due to the fact that it is difficult to obtain a perfect single layer of P-ZIF as well as the XPS sputter could not focus on a single P-ZIF crystal but a large area of sample, the change in element ratios may not be used to estimate the exact thickness of IL

layer on P-ZIF surface. However, the trend of changing elemental ratios indicated that a thin layer of IL was successfully decorated on the surface of P-ZIF particles [32].

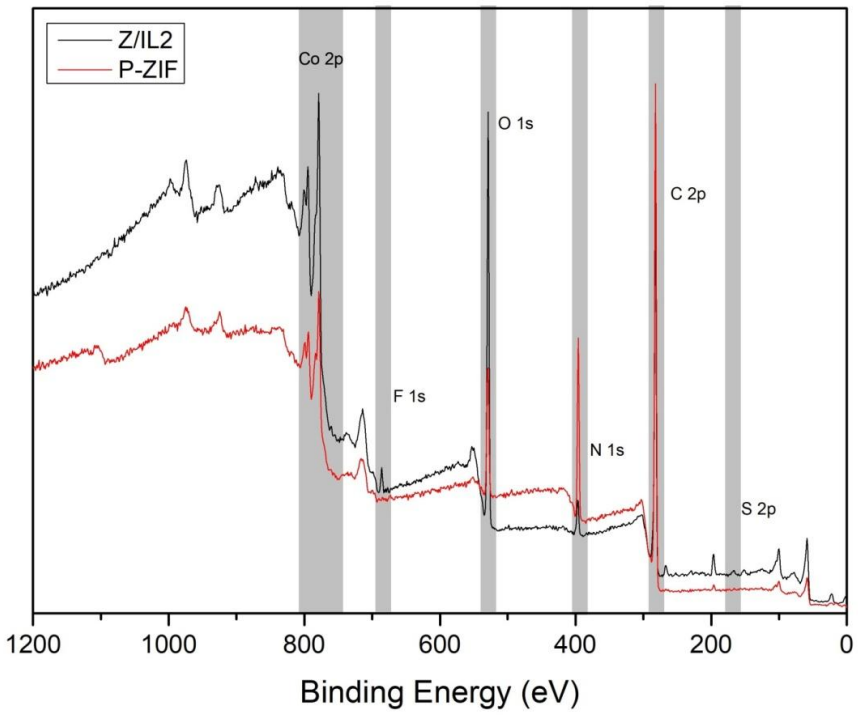

Figure 6.5. XPS spectra of P-ZIF and Z/IL2 samples

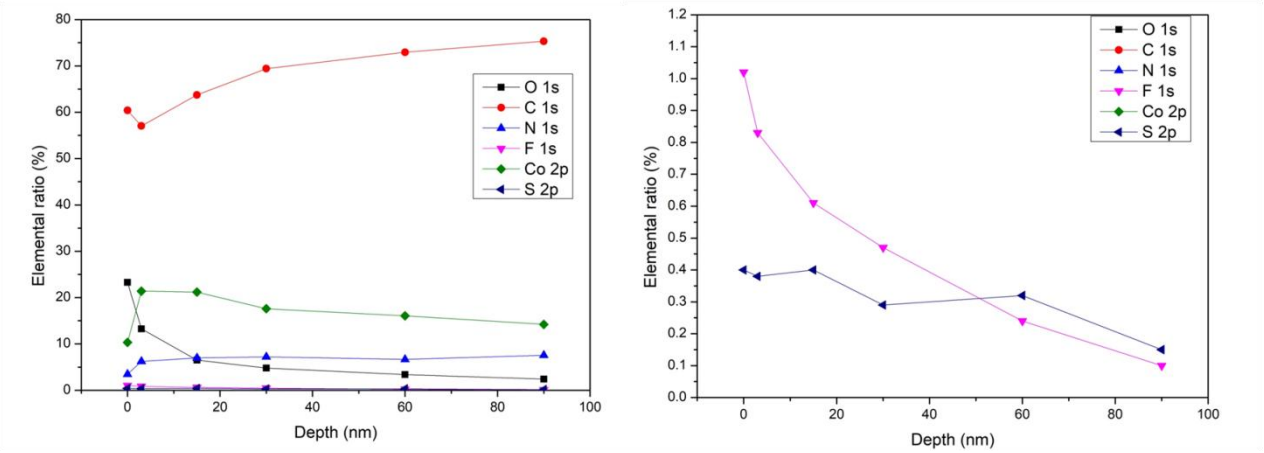

Figure 6.6. XPS depth profile analysis of Z/IL2

The FTIR spectra of as-synthesized P-ZIF and Z/IL are shown in Fig. 6.7. The bands at 680-760 cm^{-1} and between 900-1350 cm^{-1} correspond to the out of plane and in-plane bending of the imidazole ring of P-ZIF. The peaks at ~1650 cm^{-1} are assigned to the stretching and bending vibration of the N-H group in the imidazole ring while the bands at 1350-1500 cm^{-1} are associated

with the entire ring stretching. Similar peaks were observed in the spectra of IL1 and IL2 as previously discussed in Chapter 5, while the band at 754 cm^{-1} in IL3 spectra corresponds to the vibrations of the B-F bond in $[BF_4]^-$, relating to the structure of the anion [33,34]. For the spectra of P-ZIF/ILs, new peaks are observed at 1065 cm^{-1} which correspond to the stretching vibration of the $[Tf_2N]^-$ or asymmetric vibration of $[BF_4]^-$ anions. This result indicated the successful incorporation of the ionic liquid onto the P-ZIF framework [8,26,33–35].

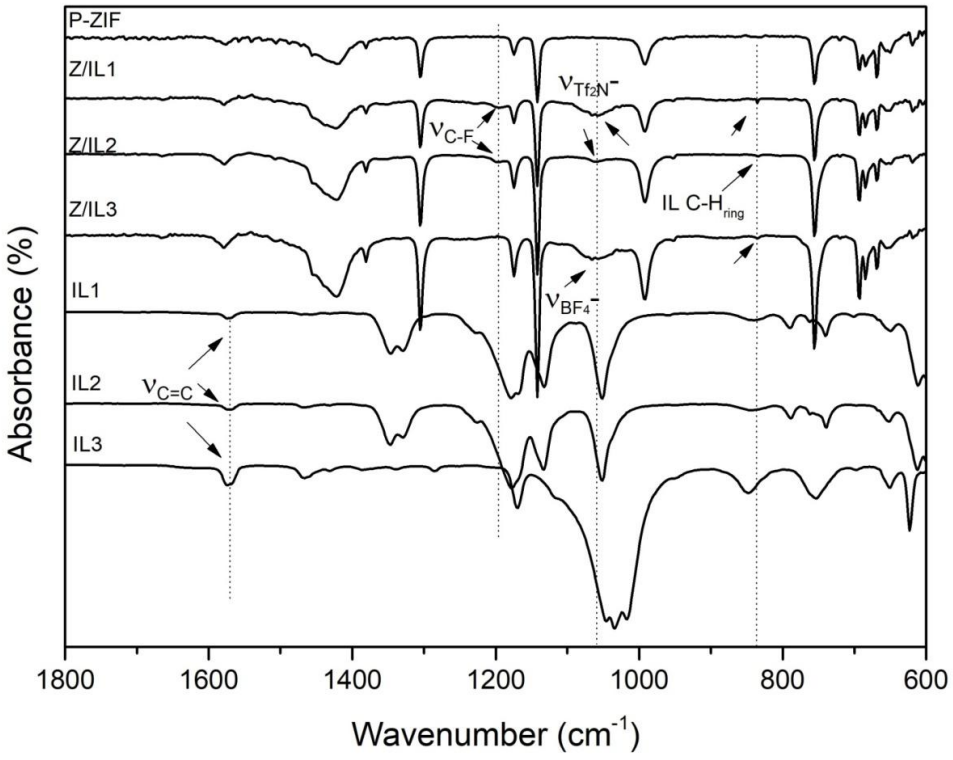

Figure 6.7. FTIR spectra of P-ZIF, ILs and Z/IL

N_2 adsorption at 77K of both the neat P-ZIF and Z/IL particles gave type I isotherms where a sharp increase adsorption at low relative pressures was observed (Fig. 6.8). Notably, the introduction of the ionic liquids caused a significant reduction in amount of N_2 adsorbed, with the BET surface area reduced from 1402 ± 30 m^2g^{-1} for the neat P-ZIF to 950 ± 36 $m^2g^{-1}$with the introduction of IL1, 895 ± 22 $m^2g^{-1}$with the introduction of IL2 and 990 ± 26 $m^2g^{-1}$with the introduction of IL3 (all at 5 wt.% loading of ionic liquid). This phenomenon is attributed to the occupation of pore space in the P-ZIF, leading to the reduction in BET surface area and N_2 adsorption amount. Similar phenomenon was also observed in other literature [8,26].

The adsorption of CO_2, N_2, CH_4, C_3H_6 and C_3H_8 at 303K for P-ZIF and Z/IL was also conducted (isotherms are displayed in Fig 6.9). Similar trends were observed as the introduction of ILs reduced the gas adsorption capacity of P-ZIF. Notably, the propane adsorption capacity of P-ZIF and Z/IL was higher than the propylene adsorption amount at pressures below 400 mmHg while the reverse was observed at pressures higher than 400 mmHg (Fig. 6.9(c)). This result suggested that the C_3H_6/C_3H_8 adsorption selectivity of P-ZIF and Z/IL may become more significant at higher pressures. Similar results have also been reported in previous studies in the literature [15,36]. Based on the isotherms, the ideal gas selectivities of IL-incorporated P-ZIF at 1 bar was calculated and is shown in Table 6.2. The presence of ILs, while decreasing the gas permeability due to the surface area occupation of ZIF as previously mentioned, clearly improves the ideal gas selectivity of CO_2/N_2, CO_2/CH_4 and C_3H_6/C_3H_8 gas pairs at 1 bar. These improvements are attributed to the higher sorption affinity of ILs toward CO_2 and C_3H_6 compared to N_2, CH_4 and C_3H_8 which have been discussed in the literature [37]. It was also suggested by Brennecke and coworkers that the combination of fluoroalkyl and S=O groups in the $[Tf_2N]^-$ could contributed to the higher solubility of CO_2 compared to the $[BF_4]^-$ anion, leading to the higher ideal selectivity of CO_2/N_2 and CO_2/CH_4 [38].

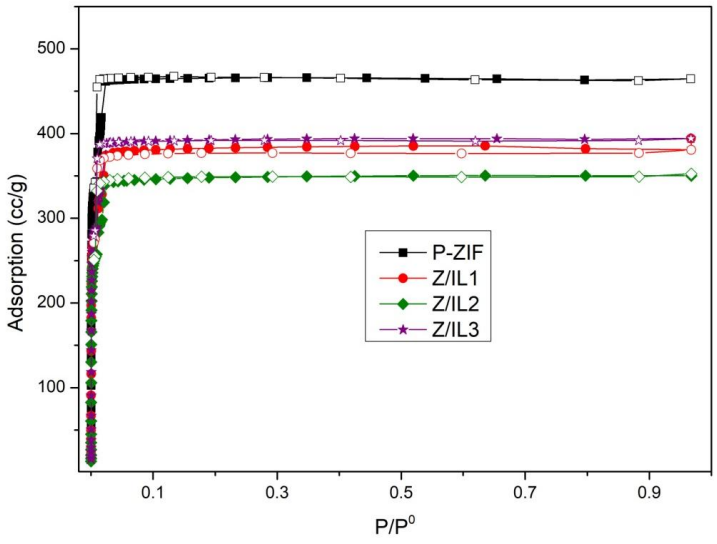

Figure 6.8. N_2 adsorption isotherm of P-ZIF and Z/IL at 77K (Solid: adsorption, hollow: desorption)

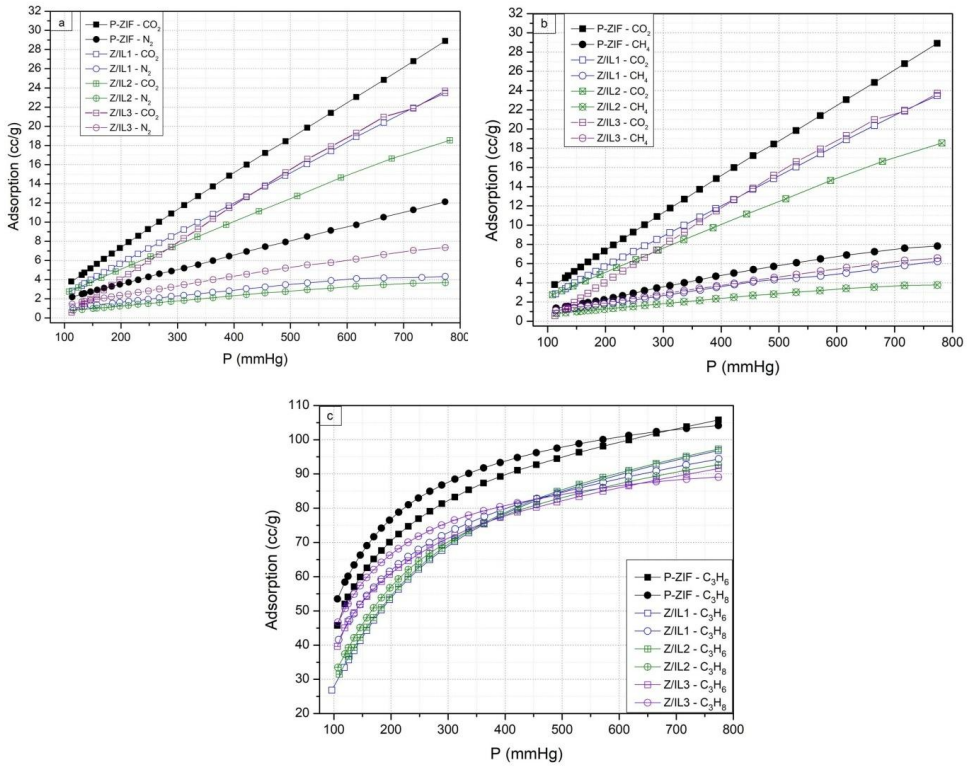

Figure 6.9. Gas adsorption isotherm of P-ZIF and Z/IL at 303K: (a): CO_2/N_2, (b) CO_2/CH_4 and (c) C_3H_6/C_3H_8

Table 6.2. Ideal selectivity of pristine P-ZIF and IL-modified P-ZIF at 1 bar

Samples	Gas adsorption at 1 bar (cc/g)					Ideal selectivity at 1 bar		
	CO_2	N_2	CH_4	C_3H_6	C_3H_8	CO_2/N_2	CO_2/CH_4	C_3H_6/C_3H_8
P-ZIF	28	12	8	105	104	2.33	3.50	1.009
Z/IL1	23	6.5	6	96	95	3.54	3.83	1.011
Z/IL2	18	3.8	4	96	94	4.74	4.5	1.021
Z/IL3	23	7	6.5	91	89	3.29	3.54	1.022

6.3.2. Mixed matrix membrane characterization

As the gas separation performance of MMMs is highly dependent on the dispersion and adhesion between the filler and the polymer matrix, the interfacial morphology of PZ MMMs and PZ/IL MMMs were investigated by FESEM techniques and the images are displayed in Fig. 6.10 while the high magnification images are shown in Fig. 6.11. As indicated in Chapter 4, P-ZIF showed poor adhesion with polymer matrix, as the interfacial voids between the filler and polymer phases can be clearly observed [41,42].

For the PZ/IL MMMs (Fig. 6.10(c)-(h) and Fig. 6.11(c)-(h)), a significantly improved interface between filler and polymer matrix is observed. The dispersion of P-ZIF in the polymer matrix is more uniform and there are fewer interfacial voids observed. This improved filler/polymer interface is attributed to the excellent adhesion of Z/IL particles with the polymer. Even at higher loading of P-ZIF/IL (20 wt.%), the interfacial voids observed is less than for the pure P-ZIF, which provides further evidence of better interactions between the P-ZIF and polymer matrix due to the presence of the ILs. These results clearly indicate that the introduction of IL contributes to the improvement of the filler/polymer interfacial adhesion, as well as in the prevention of filler agglomeration in the MMMs. Overall it provides strong evidence that the idea of IL coating in Chapter 5 is an effective method for this ZIF / 6FDA-durene system.

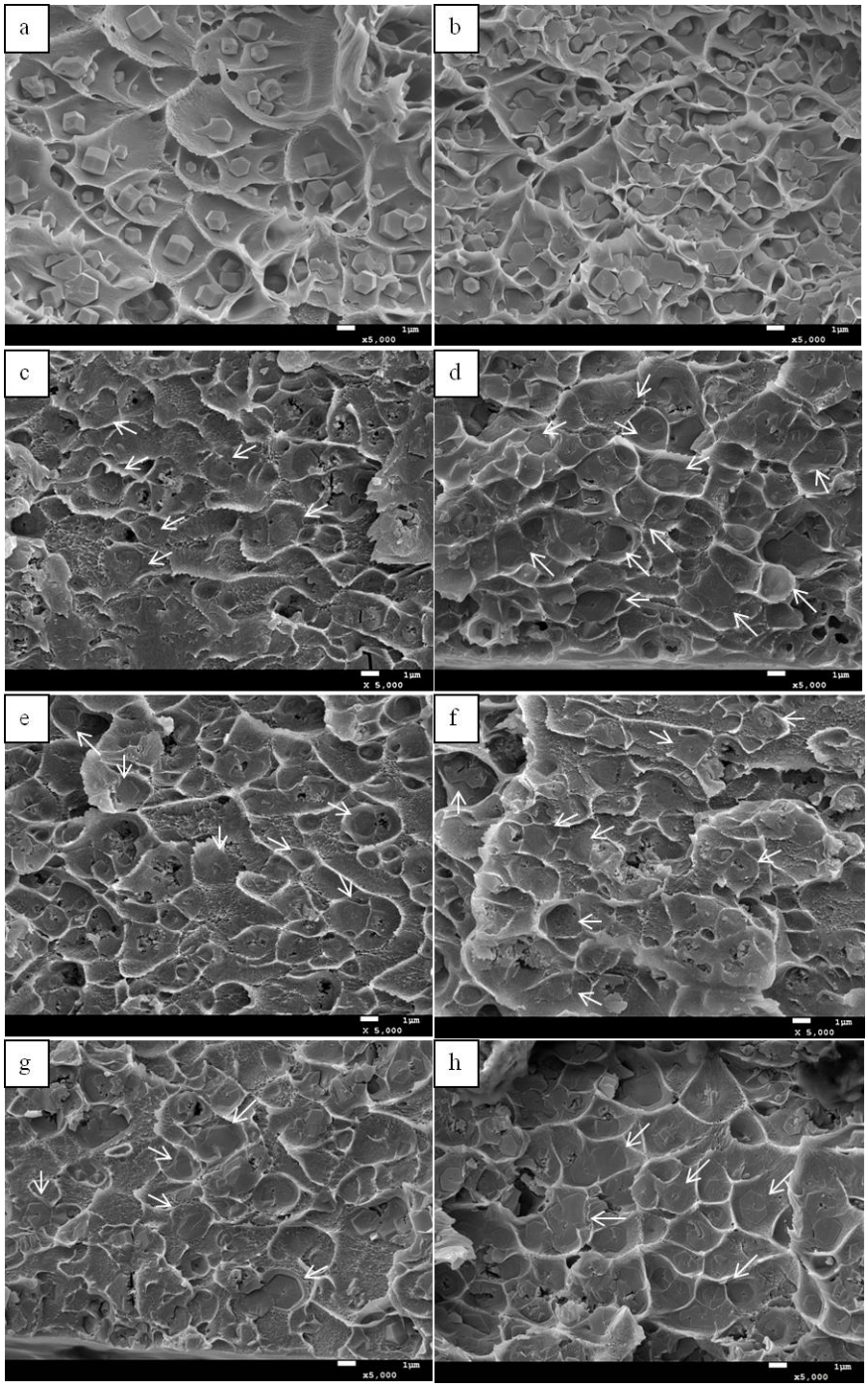

Figure 6.10. SEM images of PZ MMMs and PZ/IL MMMs: (a) PZ10, (b) PZ20, (c) PZ10/IL1, (d) PZ20/IL1, (e) PZ10/IL2, (f) PZ20/IL2, (g) PZ10/IL3 and (h) PZ20/IL3 (Arrows point to the P-ZIF embedded in polymer matrix)

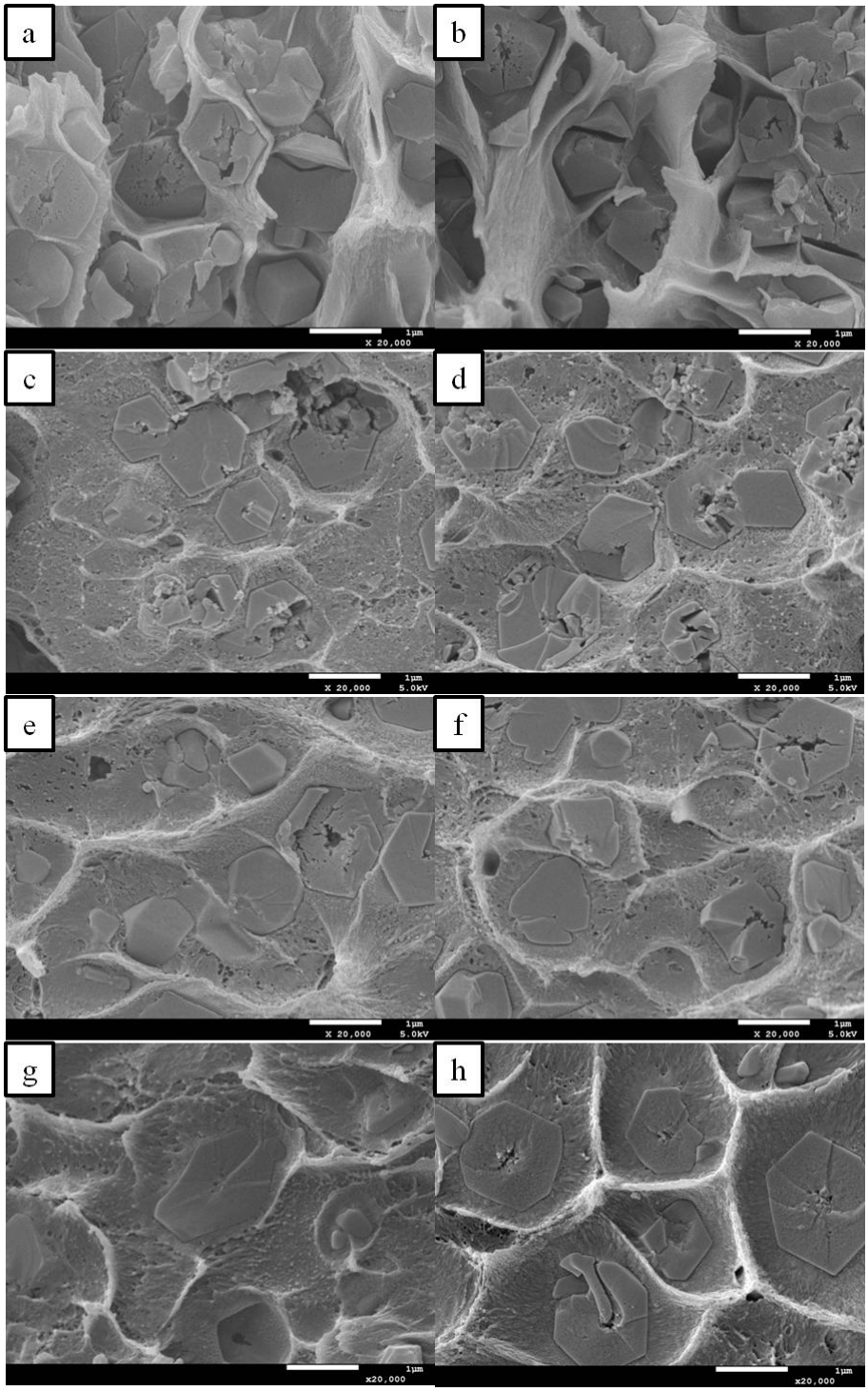

Figure 6.11. SEM images of PZ and PZ/IL MMM (high magnification): (a) PZ10, (b) PZ20, (c) PZ10/IL1, (d) PZ20/IL1, (e) PZ10/IL2, (f) PZ20/IL2, (g) PZ10/IL3 and (h) PZ20/IL3

In order to further investigate the distribution of fillers, polymer and void space in MMMs, the internal structure of the composite membranes was studied by using FIB-SEM via image thresholding. The volume fractions of filler, polymer and voids in MMM were also quantified. Fig

6.12, 6.13, 6.14 and 6.15 show the 3D representation of the interface and distribution of the fillers and voids in PZ MMM and PZ/IL MMM samples. The P-ZIF particles are of polyhedral shape and were identified in agreement with the SEM images in Fig 6.10 and Fig 6.11. The volume fractions of the filler, polymer phase and voids were calculated based on 3D image analysis and reported in Table 6.3. The volume fraction of the voids in MMMs are 1.17 % without IL and reduced to, 0.35%, 0.33% and 0.49 %with the incorporation of 5wt.% loading of IL1, IL2 and IL3, respectively. The coating of IL onto the P-ZIF surface significantly reduces the formation of voids in the MMMs which indicates that the ionic liquids are playing a vital role in eliminating interfacial voids as well as improving the filler/polymer adhesion in the MMMs. This enhancement is due to the high compatibility and strong interaction between the IL and the polymer which has been reported in previous polymer/IL composite membranes studies [43–45] and observed in Chapter 5 of this thesis. Even at high loading of P-ZIF (20 wt.%), less agglomeration was observed in the FIB image of PZ/IL MMM compared to the PZ MMM due to the presence of ILs, which indicated better dispersion of P-ZIF in the membranes and showed agreement with the conventional SEM results.

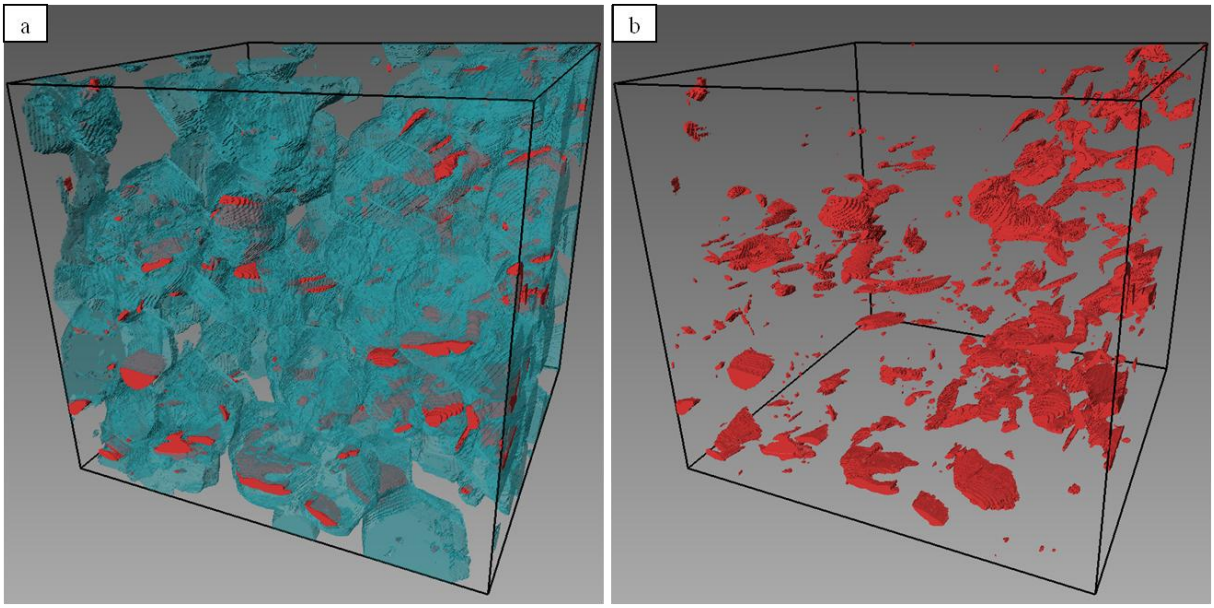

Figure 6.12. FIB surface rendered view of PZ20 MMM: (a) Fillers and voids, (b) Voids. Filler appear in blue and voids are in red. Box size: (7.5x7.3x6.8 µm)

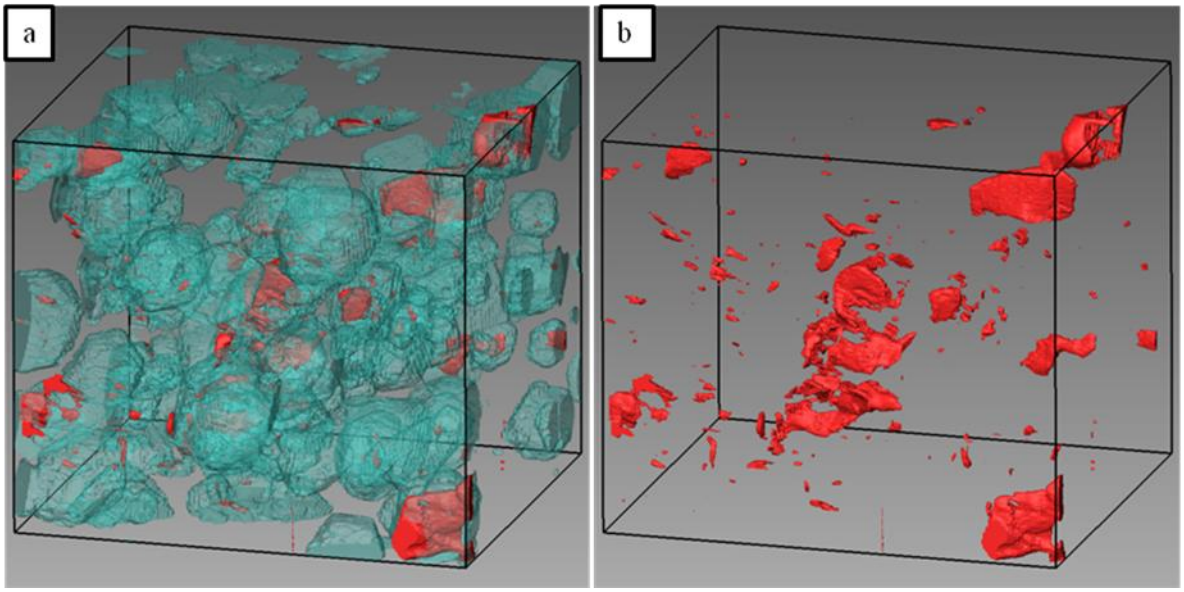

Figure 6.13. FIB surface rendered view of PZ20/IL1 MMM: (a) Fillers and voids, (b) Voids. Filler appear in blue and voids are in red. Box size: (7.5x7.3x6.8 µm)

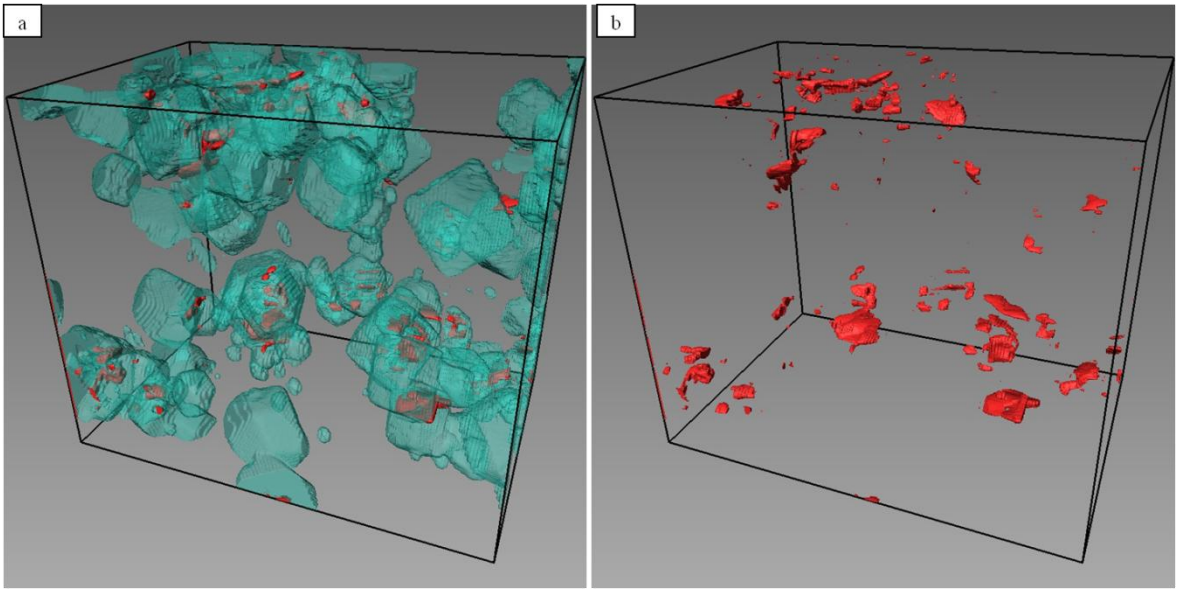

Figure 6.14. FIB surface rendered view of PZ20/IL2 MMM: (a) Fillers and voids, (b) Voids. Filler appear in blue and voids are in red. Box size: (7.5x7.3x6.8 µm)

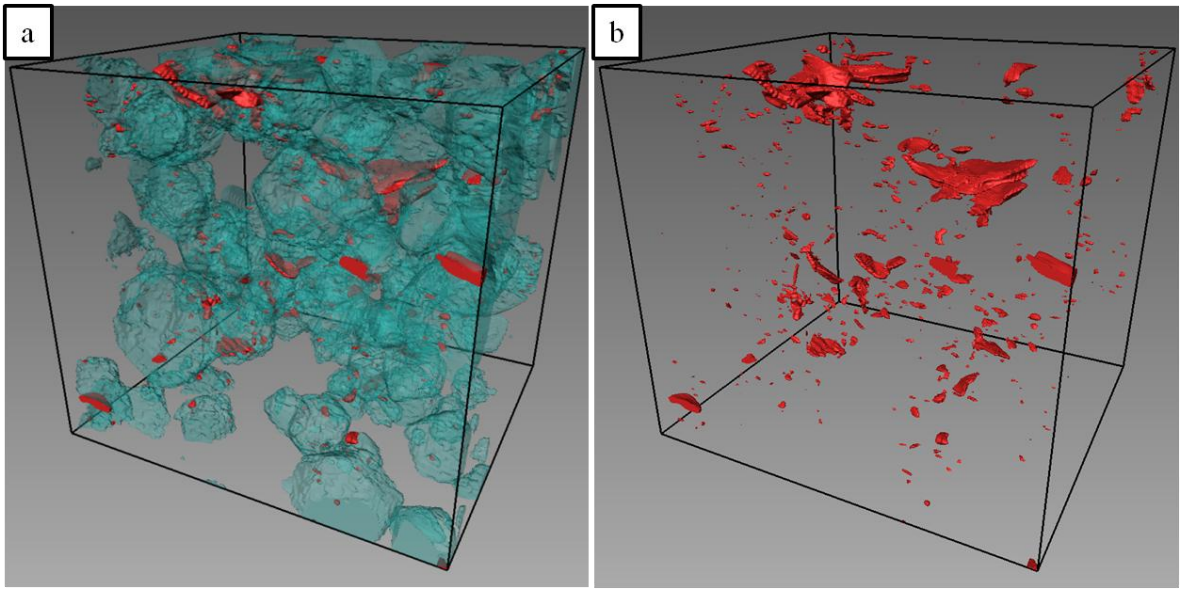

Figure 6.15. FIB surface rendered view of PZ20/IL3 MMM: (a) Fillers and voids, (b) Voids. Filler appear in blue and voids are in red. Box size: (7.5x7.3x6.8 µm)

Table 6.3. Calculated - phase volume in PZ20 MMM and PZ20/IL MMMs based on FIB analysis

Sample	**PZ20**		**PZ20/IL1**		**PZ20/IL2**		**PZ20/IL3**	
	Vol (nm^3)	%	Vol (nm^3)	%	Vol (nm^3)	%	Vol (nm^3)	%
Void	3.56×10^{9}	1.17	8.60×10^{8}	0.35	6.13×10^{8}	0.33	1.26×10^{9}	0.49
Filler	1.06×10^{11}	35.03	5.38×10^{10}	21.85	3.12×10^{10}	16.90	5.54×10^{10}	21.30
Polymer	1.94×10^{11}	63.80	1.91×10^{11}	77.80	1.53×10^{11}	82.77	2.03×10^{11}	78.21

6.3.3. Gas separation performance

The ideal gas separation performance of the PZ MMMs and PZ/IL MMMs was investigated through single gas permeability measurements. Fig. 6.16 (a, b, c) and Table 6.4 shows the CO_2 and C_3H_6 permeability and the gas selectivity for CO_2/N_2, CO_2/CH_4 and C_3H_6/C_3H_8 gas pairs of neat PI membrane, PZ MMM and PZ/IL MMM. The presence of P-ZIF in MMM increased the permeability for CO_2 and C_3H_6 with lower CO_2/N_2, CO_2/CH_4 and C_3H_6/C_3H_8 selectivity compared to the pure 6FDA-durene membrane as previously mentioned in Chapter 4.

In the case of MMMs incorporating IL-coated P-ZIF, the presence of ILs considerably enhances both the CO_2 and C_3H_6 permeability and gas selectivity for CO_2/N_2, CO_2/CH_4 and C_3H_6/C_3H_8 gas pairs. Furthermore the increased permeability and selectivity for the desired gases (CO_2 and C_3H_6) increases with increased filler loading. The introduction of ILs significantly improved the interfacial interaction between the P-ZIF particles and polymer matrix, which helps eliminating the non-selective voids and enhances the filler dispersion in the polymer matrix, thus leading to the better gas separation performance of the MMM. Furthermore, the thin IL layer cover around the P-ZIF surface may eventually act as a "gas carrier agent" which further increases the sorption affinity of the filler toward CO_2 and C_3H_6 gases while showing negligible effect on the other gases and subsequently enhancing the gas selectivity for the CO_2 and C_3H_6 [23]. In addition, the surface area reduction and pore-blockage caused by the presence of IL may also further reduce the sorption and diffusivity of the non-desired gases (N_2, CH_4 and C_3H_8) through the pores of P-ZIF, leading to further improvement in CO_2 and C_3H_6 selectivity.

In order to further confirm the role of ILs in MMM in this work, additional samples were made by simply mixing ILs with the 6FDA-durene (maintaining the same ratio of polymer/IL without the presence of P-ZIF particles). As shown in Table 6.5, the permeability for all tested gases was significantly reduced, while the changes in gas selectivity for CO_2/N_2, CO_2/CH_4 and C_3H_6/C_3H_8 are negligible, both of which strongly indicate occupation of the polymer free volume by the IL. It is worth noting that excess usage of IL may lead to the blockage of polymer free volume which decreases the gas permeability of the membrane [47,48]; by contrast, an insufficient amount of IL in the MMM may not be able to make any impact in improving the gas separation performance of the MMM. The results presented in this study strongly suggest that the combination of pre-coating P-ZIF filler particles with thin layer of IL is a more effective method to improve the gas separation performance of the ZIF/polymer MMMs.

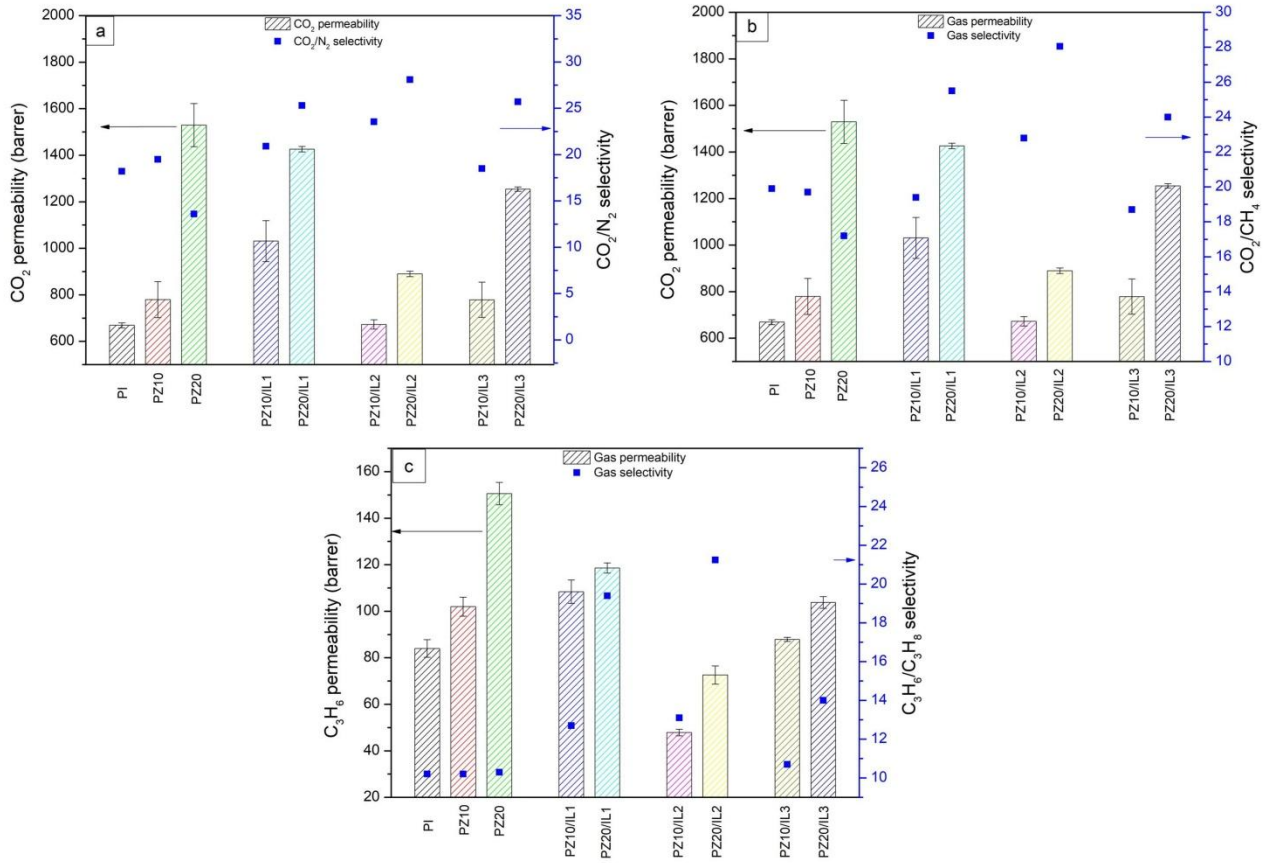

Figure 6.16. Gas permeability and selectivity of PZ MMM and PZ/IL MMMs: (a) CO_2/N_2, (b) CO_2/CH_4 and (c) C_3H_6/C_3H_8

Table 6.4. Gas permeability and selectivity of pure PI membrane, PZ MMM and PZ/IL MMM

Sample	Permeability (barrer)					Selectivity		
	CO_2	N_2	CH_4	C_3H_6	C_3H_8	CO_2/N_2	CO_2/CH_4	C_3H_6/C_3H_8
PI	669.12±10.24	36.72±0.90	33.64±1.66	84.03±3.80	8.23±1.74	18.22	19.89	10.21
PZ10	779.51±77.25	40.07±4.09	39.52±13.56	101.96±4.09	9.99±0.64	19.45	19.72	10.21
PZ20	1529.86±92.71	112.45±14.92	89.10±1.88	150.56±4.78	14.55±0.61	13.60	17.17	10.35
PZ10/IL1	1030.96±88.08	49.39±5.91	53.13±12.96	108.39±5.03	8.53±0.95	20.87	19.40	12.71
PZ20/IL1	1426.12±11.95	56.42±12.69	55.94±7.43	118.61±2.17	6.13±0.22	25.28	25.49	19.35
PZ10/IL2	672.79±20.37	28.58±4.35	29.55±7.00	47.87±1.45	3.65±0.39	23.54	22.77	13.12
PZ20/IL2	889.87±11.66	31.68±1.32	31.72±2.79	72.58±3.93	3.42±0.17	28.09	28.05	21.24
PZ10/IL3	779.01±75.59	42.15±0.75	41.53±17.95	87.87±0.88	8.22±1.30	18.48	18.76	10.69
PZ20/IL3	1254.64±9.26	48.81±1.20	52.28±2.66	103.79±2.54	7.40±1.10	25.70	24.00	14.03

Table 6.5. Gas permeability and selectivity of P/IL MMMs

Sample	Permeability (barrer)					Selectivity		
	CO_2	N_2	CH_4	C_3H_6	C_3H_8	CO_2/N_2	CO_2/CH_4	C_3H_6/C_3H_8
P/IL1	300.56	18.17	15.34	19.21	2.34	16.54	19.59	8.21
P/IL2	277.87	15.21	14.11	16.57	1.57	18.26	19.69	10.55
P/IL3	295.13	16.43	16.14	18.70	1.65	17.96	18.29	11.33

The difference in the gas separation performance of MMMs using different ILs in this work is hypothesized to be the result of the differing gas solubility of each IL. As discussed above, the IL layer may act as the "gas carrier agent", promoting the gas transfer through MMMs by a solution-diffusion mechanism. The nature of both the cation and anion in the IL impact this process; however, the anion is known to be the more dominating factor [37]. Work by Brennecke et. al. [49] and Wang et. al. [50] found that the CO_2 and C_3H_6 solubility values in ILs are in the order of anions: $[BF_4]^-$ < $[Tf_2N]^-$, which matches well with the results of this study, with the PZ/IL1 demonstrating better CO_2 and C_3H_6 permeability as well as CO_2/N_2, CO_2/CH_4 and C_3H_6/C_3H_8 selectivity compared to the PZ/IL3 MMM. As discussed in Chapter 5, the PZ/IL2 exhibited highest CO_2/N_2, CO_2/CH_4 and C_3H_6/C_3H_8 selectivity among the three ILs, but lower CO_2 and C_3H_6 permeability than both PZ/IL1 and PZ/IL3 samples. Besides, it is hypothesized that the longer alkyl chain and larger size of the [Bmim][Tf_2N] molecules compared to [Emim][Tf_2N] and [Bmim][BF_4] may reduce the gas diffusion through the ZIF channels, more than that of the other two ILs [51,52]. This result is also in agreement with the ideal gas selectivity data mentioned above, in which the Z/IL2 showed the highest gas selectivity value along with the lowest gas permeability among the all three ILs being tested.

The gas separation performance of PZ/IL MMMs for the 50:50 CO_2/CH_4 mixed-gas was also investigated and the results are shown in Fig. 6.17. Both CO_2 permeability and CO_2/CH_4 selectivity decreased in the gas mixture compared to the single gas results for the PZ20/IL1 and PZ20/IL2 MMMs. As discussed in Chapter 5, the competitive sorption and diffusion of CO_2 and CH_4 through both the fillers and the polymer matrix could contribute to this reduction. The larger size of CH_4 molecules in the gas mixture might obstruct the adsorption of CO_2 on P-ZIF surface and pores as

well as compete with CO_2 molecules in the diffusion pathway, leading to the decrease in CO_2 permeability. However, the PZ/IL MMMs still exhibited higher CO_2/CH_4 selectivity in mixed-gas compared to the single gas CO_2/CH_4 separation performance of the neat polymer membrane and the PR MMMs.

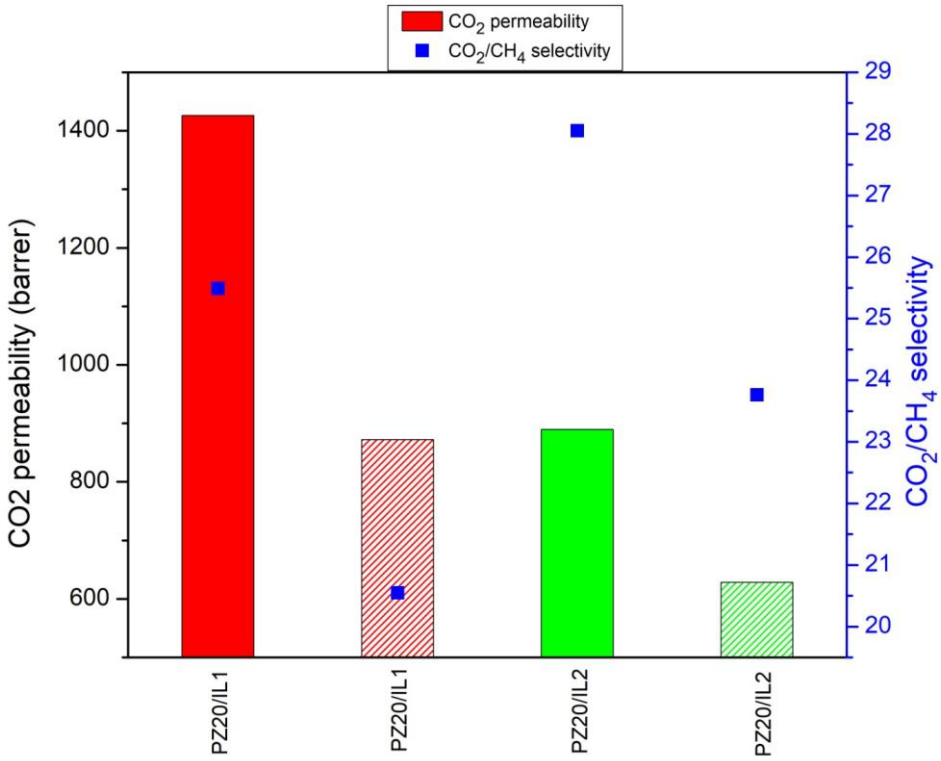

Figure 6.17. Gas permeability and selectivity for CO_2/CH_4 as single gas and gas mixture (50/50 vol) of PZ20/IL MMMs (at 30°C, 2 bar) (Filled bar: single gas, patterned bar: gas mixture)

6.3.4. Comparison with the Robeson Upper Bound

Fig 6.18 shows the performance of MMMs in this work when plotted with the CO_2/N_2, CO_2/CH_4 and C_3H_6/C_3H_8 Robeson upper bound [5] and in comparison with other previous studies in the literature (Appendix Table S1, S2, S3) [4,11,12,18,19,39,47,53-62]. At 20 wt.% loading, all of the PZ20/IL MMM offer substantial enhancement in both permeability and selectivity over the pure 6FDA-durene. Furthermore, the gas separation performance of the PZ20/IL MMM for the CO_2/CH_4 also clearly surpasses the upper bound and show improvement in comparison with other MOFs-based MMMs in the literature. Such a result demonstrates the effectiveness of the IL coating

method in simultaneously improving permeability and selectivity of CO_2 and C_3H_6 and the potential for applying a micron-sized filler/polymer membrane system for achieving better gas separation performance. The fact it showed the greatest performance enhancement of the worst filler morphologies from Chapter 4, is both confirmation of its effectiveness as a strategy and an indication of the impact of poor interfacial adhesion and aggregation on MMM performance.

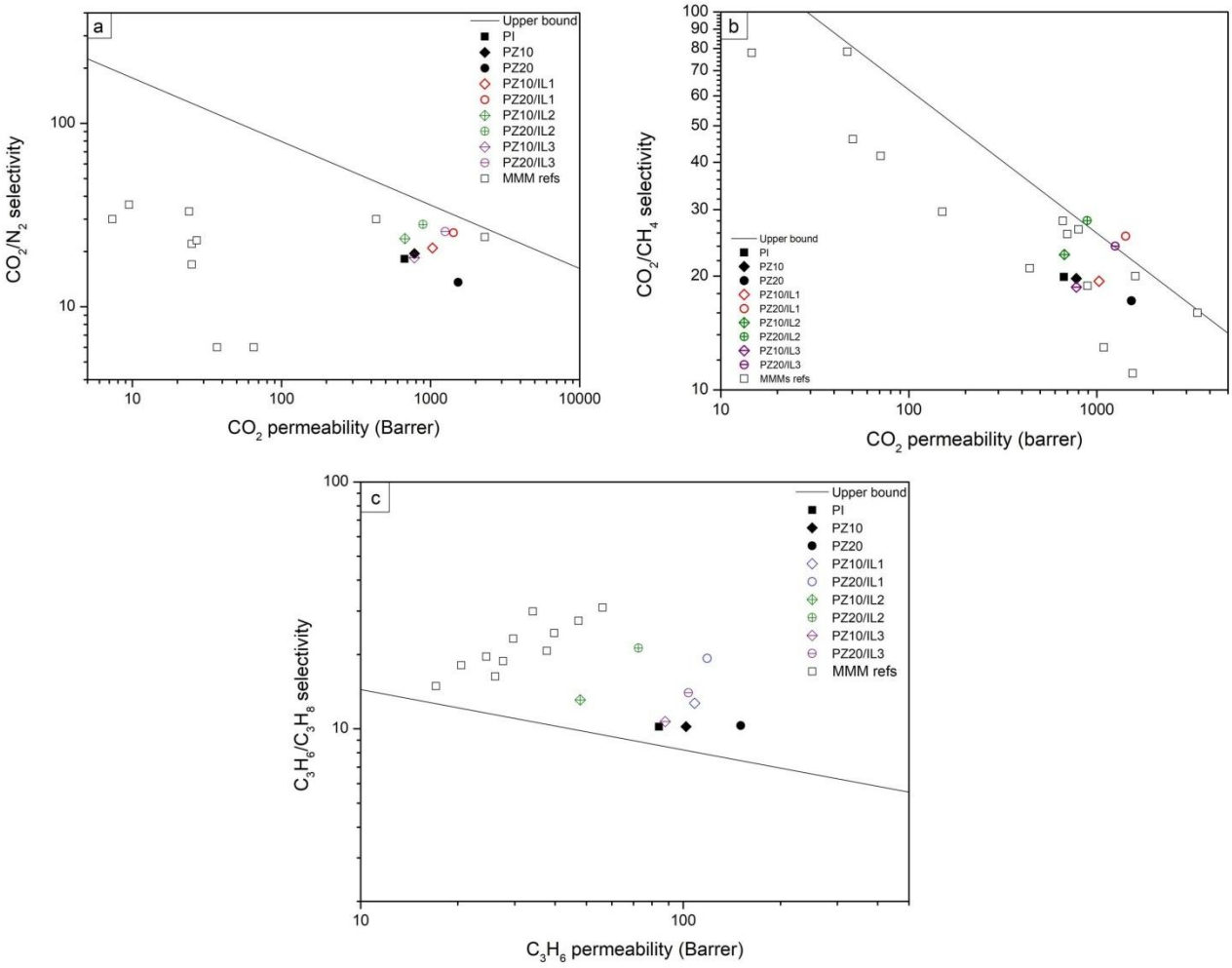

Figure 6.18. Gas separation performance of PZ MMM and PZ/IL MMMs in respect with Robeson trade-off line: (a) CO_2/N_2, (b) CO_2/CH_4 and (c) C_3H_6/C_3H_8

6.4. Conclusion

In this study, the surface modification of micron-sized P-ZIF has been successfully carried out by coating with a thin layer of IL for membrane fabrication. The presence of the IL layer has been proven to effectively reduce the non-selective interfacial defects in the MMM and enhance the

polymer/P-ZIF adhesion due to the favourable ZIF-IL-polymer bridging interaction. In comparison with the pristine PZ MMM, the vol.% of interfacial voids has been reduced from 1.17% to 0.49%, 0.35% and 0.33% with the PZ/IL1, PZ/IL2 and PZ/IL3 MMM, respectively, leading to a significant improvement in gas separation performance, particularly with the CO_2/CH_4 separation performance surpassing the 2008 upper bound. With these results, the IL-coating method can be considered an effective modification approach, especially for large-sized fillers, to solve the filler/polymer interfacial issues in order to achieve better gas-separation performance in mixed matrix membranes.

References

[1] Z. Kang, L. Fan, D. Sun, Recent advances and challenges of metal–organic framework membranes for gas separation, J. Mater. Chem. A 5 (2017) 10073–10091.

[2] I. Erucar, G. Yilmaz, S. Keskin, Recent Advances in Metal-Organic Framework-Based Mixed Matrix Membranes, Chem. Asian J. 8 (2013) 1692–1704.

[3] R. Nasir, H. Mukhtar, Z. Man, D.F. Mohshim, Material Advancements in Fabrication of Mixed-Matrix Membranes, Chem. Eng. Technol. 36 (2013) 717–727.

[4] H. An, S. Park, H.T. Kwon, H.K. Jeong, J.S. Lee, A new superior competitor for exceptional propylene/propane separations: P-ZIF containing mixed matrix membranes, J. Membr. Sci. 526 (2017) 367–376.

[5] L.M. Robeson, The upper bound revisited, J. Membr. Sci. 320 (2008) 390–400.

[6] R. Lin, L. Ge, H. Diao, V. Rudolph, Z. Zhu, Propylene/propane selective mixed matrix membranes with grape-branched MOF/CNT filler, J. Mater. Chem. A 4 (2016) 6084–6090.

[7] R. Lin, B. Villacorta, L. Ge, Z. Zhu, Metal organic framework based mixed matrix membranes: An overview on filler/polymer interface, J. Mater. Chem. A 6 (2017) 293–312.

[8] R. Lin, L. Ge, H. Diao, V. Rudolph, Z. Zhu, Ionic Liquids as the MOFs/Polymer Interfacial Binder for Efficient Membrane Separation, ACS Appl. Mater. Interfaces 8 (2016) 32041–32049.

[9] X. Wu, W. Liu, H. Wu, X. Zong, L. Yang, Y. Wu, Y. Ren, C. Shi, S. Wang, Z. Jiang, Nanoporous P-ZIF embedded polymers of intrinsic microporosity membranes with enhanced gas separation performance, J. Membr. Sci. 548 (2018) 309–318.

[10] A.F. Bushell, M.P. Attfield, C.R. Mason, P.M. Budd, Y. Yampolskii, L. Starannikova, A. Rebrov, F. Bazzarelli, P. Bernardo, J. Carolus Jansen, M. Lanč, K. Friess, V. Shantarovich, V. Gustov, V. Isaeva, Gas permeation parameters of mixed matrix membranes based on the polymer of intrinsic microporosity PIM-1 and the zeolitic imidazolate framework ZIF-8, J. Membr. Sci. 427 (2013) 48–62.

[11] C. Zhang, Y. Dai, J.R. Johnson, O. Karvan, W.J. Koros, High performance ZIF-8/6FDA-DAM mixed matrix membrane for propylene/propane separations, J. Membr. Sci. 389 (2012) 34–42.

[12] T.H. Bae, J.S. Lee, W. Qiu, W.J. Koros, C.W. Jones, S. Nair, A high-performance gas-separation membrane containing submicrometer-sized metal-organic framework crystals, Angew. Chem. Int. Ed. 49 (2010) 9863–9866.

[13] T. Yang, G.M. Shi, T.-S. Chung, Symmetric and Asymmetric Zeolitic Imidazolate Frameworks (ZIFs)/Polybenzimidazole (PBI) Nanocomposite Membranes for Hydrogen Purification at High Temperatures, Adv. Energy Mater. 2 (2012) 1358–1367.

[14] H.T. Kwon, H.K. Jeong, A.S. Lee, H.S. An, J.S. Lee, Heteroepitaxially grown zeolitic imidazolate framework membranes with unprecedented propylene/propane separation performances, J. Am. Chem. Soc. 137 (2015) 12304–12311.

[15] P. Krokidas, M. Castier, S. Moncho, D.N. Sredojevic, E.N. Brothers, H.T. Kwon, H.-K. Jeong, J.S. Lee, I.G. Economou, P-ZIF Framework: A Promising New Candidate for Propylene/Propane Separation. Experimental Data and Molecular Simulations, J. Phys. Chem. C 120 (2016) 8116–8124.

[16] H. Zhu, L. Wang, X. Jie, D. Liu, Y. Cao, Improved Interfacial Affinity and CO_2 Separation Performance of Asymmetric Mixed Matrix Membranes by Incorporating Postmodified MIL-53(Al), ACS Appl. Mater. Interfaces 8 (2016) 22696–22704.

[17] S.R. Venna, M. Lartey, T. Li, A. Spore, S. Kumar, H.B. Nulwala, D.R. Luebke, N.L. Rosi, E. Albenze, Fabrication of MMMs with improved gas separation properties using externally-functionalized MOF particles, J. Mater. Chem. A 3 (2015) 5014–5022.

[18] M. Askari, T.S. Chung, Natural gas purification and olefin/paraffin separation using thermal cross-linkable co-polyimide/ZIF-8 mixed matrix membranes, J. Membr. Sci. 444 (2013) 173–183.

[19] S.N. Wijenayake, N.P. Panapitiya, S.H. Versteeg, C.N. Nguyen, S. Goel, K.J. Balkus, I.H. Musselman, J.P. Ferraris, Surface cross-linking of ZIF-8/polyimide mixed matrix membranes (MMMs) for gas separation, Ind. Eng. Chem. Res. 52 (2013) 6991–7001.

[20] B. Seoane, V. Sebastián, C. Téllez, J. Coronas, Crystallization in THF: The possibility of one-pot synthesis of mixed matrix membranes containing MOF MIL-68(Al), CrystEngComm 15 (2013) 9483–9490.

[21] R. Lin, L. Ge, S. Liu, V. Rudolph, Z. Zhu, Mixed-matrix membranes with metal-organic framework-decorated CNT fillers for efficient CO_2 separation, ACS Appl. Mater. Interfaces 7 (2015) 14750–14757.

[22] R. Lin, L. Ge, L. Hou, E. Strounina, V. Rudolph, Z. Zhu, Mixed matrix membranes with strengthened MOFs/polymer interfacial interaction and improved membrane performance, ACS Appl. Mater. Interfaces 6 (2014) 5609–5618.

[23] Z. Dai, R.D. Noble, D.L. Gin, X. Zhang, L. Deng, Combination of ionic liquids with

membrane technology: A new approach for CO_2 separation, J. Membr. Sci. 497 (2016) 1–20.

[24] Y.C. Hudiono, T.K. Carlisle, A.L. LaFrate, D.L. Gin, R.D. Noble, Novel mixed matrix membranes based on polymerizable room-temperature ionic liquids and SAPO-34 particles to improve CO_2 separation, J. Membr. Sci. 370 (2011) 141–148.

[25] C. Casado-Coterillo, M. Del Mar Lopez-Guerrero, A. Irabien, Synthesis and Characterisation of ETS-10/Acetate-based Ionic Liquid/Chitosan Mixed Matrix Membranes for CO_2/N_2 Permeation, Membranes 4 (2014) 287–301.

[26] H. Li, L. Tuo, K. Yang, H.-K.K. Jeong, Y. Dai, G. He, W. Zhao, Simultaneous enhancement of mechanical properties and CO_2 selectivity of ZIF-8 mixed matrix membranes: Interfacial toughening effect of ionic liquid, J. Membr. Sci. 511 (2016) 130–142.

[27] K.Y.A. Lin, H.A. Chang, Zeolitic Imidazole Framework-67 (P-ZIF) as a heterogeneous catalyst to activate peroxymonosulfate for degradation of Rhodamine B in water, J. Taiwan Inst. Chem. Eng. 53 (2015) 40–45.

[28] Y. Liu, R. Wang, T.-S. Chung, Chemical cross-linking modification of polyimide membranes for gas separation, J. Membr. Sci. 189(2) (2001) 231–239.

[29] T. Rodenas, I. Luz, G. Prieto, B. Seoane, H. Miro, A. Corma, F. Kapteijn, F.X. Llabrés I Xamena, J. Gascon, Metal-organic framework nanosheets in polymer composite materials for gas separation, Nat. Mater. 14 (2015) 48–55.

[30] T. Rodenas, M. Van Dalen, E. García-Pérez, P. Serra-Crespo, B. Zornoza, F. Kapteijn, J. Gascon, Visualizing MOF mixed matrix membranes at the nanoscale: Towards structure-performance relationships in CO_2/CH_4 separation over NH_2-MIL-53(Al)@PI, Adv. Funct. Mater. 24 (2014) 249–256.

[31] L. Ge, Z. Zhu, F. Li, S. Liu, L. Wang, X. Tang, V. Rudolph, Investigation of gas permeability in carbon nanotube (CNT)-polymer matrix membranes via modifying CNTs with functional groups/metals and controlling modification location, J. Phys. Chem. C 115 (2011) 6661–6670.

[32] D. Uhlmann, S. Smart, J.C. Diniz da Costa, H_2S stability and separation performance of cobalt oxide silica membranes, J. Membr. Sci. 380 (2011) 48–54.

[33] K. Hanke, M. Kaufmann, G. Schwaab, M. Havenith, C.T. Wolke, O. Gorlova, M.A. Johnson, B.P. Kar, W. Sander, E. Sanchez-Garcia, Understanding the ionic liquid $[NC_{4111}][NTf_2]$ from individual building blocks: an IR-spectroscopic study, Phys. Chem. Chem. Phys. 17 (2015) 8518–8529.

[34] Y.S. Ye, M.Y. Cheng, J.Y. Tseng, G.-W. Liang, J. Rick, Y.J. Huang, F.C. Chang, B.J. Hwang, New proton conducting membranes with high retention of protic ionic liquids, J. Mater. Chem. 21 (2011) 2723.

[35] B. Koyuturk, C. Altintas, F.P. Kinik, S. Keskin, A. Uzun, Improving Gas Separation Performance of ZIF-8 by [BMIM][BF_4] Incorporation: Interactions and Their Consequences on Performance, J. Phys. Chem. C 121 (2017) 10370–10381.

[36] J. Ahn, W.J. Chung, I. Pinnau, M.D. Guiver, Polysulfone/silica nanoparticle mixed-matrix membranes for gas separation, J. Membr. Sci. 314 (2008) 123–133.

[37] S. Raeissi, C.J. Peters, A potential ionic liquid for CO_2 -separating gas membranes: selection and gas solubility studies, Green Chem. 11 (2009) 185–192.

[38] S. n. v. k. Aki, B.R. Mellein, E.M. Saurer, J.F. Brennecke, High-pressure phase behavior of carbon dioxide with imidazolium-based ionic liquids, J, Phys. Chem. B 108 (2004) 5–20365.

[39] O.G. Nik, X.Y. Chen, S. Kaliaguine, Functionalized metal organic framework-polyimide mixed matrix membranes for CO_2/CH_4 separation, J. Membr. Sci. 413–414 (2012) 48–61.

[40] L. Ge, W. Zhou, V. Rudolph, Z. Zhu, Mixed matrix membranes incorporated with size-reduced Cu-BTC for improved gas separation, J. Mater. Chem. A 1 (2013) 6350.

[41] G. Dong, H. Li, V. Chen, Challenges and opportunities for mixed-matrix membranes for gas separation, J. Mater. Chem. A 1 (2013) 4610.

[42] R. Mahajan, W.J. Koros, Factors controlling successful formation of mixed-matrix gas separation materials, Ind. Eng. Chem. Res. 39 (2000) 2692–2696.

[43] E. Ghasemi Estahbanati, M. Omidkhah, A. Ebadi Amooghin, Preparation and characterization of novel Ionic liquid/Pebax membranes for efficient CO_2/light gases separation, J. Ind. Eng. Chem. 51 (2017) 77–89.

[44] S. Kanehashi, M. Kishida, T. Kidesaki, R. Shindo, S. Sato, T. Miyakoshi, K. Nagai, CO_2 separation properties of a glassy aromatic polyimide composite membranes containing high-content 1-butyl-3-methylimidazolium bis(trifluoromethylsulfonyl)imide ionic liquid, J. Membr. Sci. 430 (2013) 211–222.

[45] L. Liang, Q. Gan, P. Nancarrow, Composite ionic liquid and polymer membranes for gas separation at elevated temperatures, J. Membr. Sci. 450 (2014) 407–417.

[46] M.A. Aroon, A.F. Ismail, T. Matsuura, M.M. Montazer-Rahmati, Performance studies of mixed matrix membranes for gas separation: A review, Sep. Purif. Technol. 75 (2010) 229–242.

[47] R. Shindo, M. Kishida, H. Sawa, T. Kidesaki, S. Sato, S. Kanehashi, K. Nagai, Characterization and gas permeation properties of polyimide/ZSM-5 zeolite composite membranes containing ionic liquid, J. Membr. Sci. 454 (2014) 330–338.

[48] D.F. Mohshim, H. Mukhtar, Z. Man, The effect of incorporating ionic liquid into polyethersulfone-SAPO34 based mixed matrix membrane on CO_2 gas separation performance, Sep. Purif. Technol. 135 (2014) 252–258.

[49] M.J. Muldoon, S.N.V.K. Aki, J.L. Anderson, J.K. Dixon, J.F. Brennecke, Improving carbon dioxide solubility in ionic liquids, J. Phys. Chem. B 111 (2007) 9001–9009.

[50] Y. Wang, T.Y. Goh, P. Goodrich, M. Atilhan, M. Khraisheh, D. Rooney, J. Thompson, J. Jacquemin, Impact of ionic liquids on silver thermoplastic polyurethane composite membranes for propane/propylene separation, Arabian J. Chem. (2017).

[51] Z. Lei, C. Dai, B. Chen, Gas solubility in ionic liquids, Chem. Rev. 114 (2014) 1289–1326.

[52] J.L. Anthony, J.L. Anderson, E.J. Maginn, J.F. Brennecke, Anion effects on gas solubility in ionic liquids, J. Phys. Chem. B. 109 (2005) 6366–6374.

[53] Z. Wang, D. Wang, S. Zhang, L. Hu, J. Jin, Interfacial Design of Mixed Matrix Membranes for Improved Gas Separation Performance, Adv. Mater. 28 (2016) 3399–3405.

[54] B. Seoane, C. Téllez, J. Coronas, C. Staudt, NH_2-MIL-53(Al) and NH_2-MIL-101(Al) in sulfur-containing copolyimide mixed matrix membranes for gas separation, Sep. Purif. Technol. 111 (2013) 72–81.

[55] S. Japip, H. Wang, Y. Xiao, T.S. Chung, Highly permeable zeolitic imidazolate framework (ZIF)-71 nano-particles enhanced polyimide membranes for gas separation, J. Membr. Sci. 467 (2014) 162–174.

[56] X.Y. Chen, H. Vinh-Thang, D. Rodrigue, S. Kaliaguine, Amine-functionalized MIL-53 metal-organic framework in polyimide mixed matrix membranes for CO_2/CH_4 separation, Ind. Eng. Chem. Res. 51 (2012) 6895–6906.

[57] A. Sabetghadam, B. Seoane, D. Keskin, N. Duim, T. Rodenas, S. Shahid, S. Sorribas, C. Le Guillouzer, G. Clet, C. Tellez, M. Daturi, J. Coronas, F. Kapteijn, J. Gascon, Metal Organic Framework Crystals in Mixed-Matrix Membranes: Impact of the Filler Morphology on the Gas Separation Performance, Adv. Funct. Mater. 26 (2016) 3154–3163.

[58] A. Ito, T. Yasuda, T. Yoshioka, A. Yoshida, X. Li, K. Hashimoto, K. Nagai, M. Shibayama, M. Watanabe, Sulfonated Polyimide/Ionic Liquid Composite Membranes for CO_2 Separation: Transport Properties in Relation to Their Nanostructures, Macromolecules 51

(2018) 7112–7120.

[59] M. Waqas Anjum, B. Bueken, D. De Vos, I.F.J. Vankelecom, MIL-125(Ti) based mixed matrix membranes for CO_2 separation from CH_4 and N_2, J. Membr. Sci. 502 (2016) 21–28.

[60] S. Basu, A. Cano-Odena, I.F.J. Vankelecom, MOF-containing mixed-matrix membranes for CO_2/CH_4 and CO_2/N_2 binary gas mixture separations, Sep. Purif. Technol. 81 (2011) 31–40.

[61] J. Hu, H. Cai, H. Ren, Y. Wei, Z. Xu, H. Liu, Y. Hu, Mixed-matrix membrane hollow fibers of $Cu_3(BTC)_2$MOF and polyimide for gas separation and adsorption, Ind. Eng. Chem. Res. 49 (2010) 12605–12612.

[62] M. Etxeberria-Benavides, O. David, T. Johnson, M.M. Łozińska, A. Orsi, P.A. Wright, S. Mastel, R. Hillenbrand, F. Kapteijn, J. Gascon, High performance mixed matrix membranes (MMMs) composed of ZIF-94 filler and 6FDA-DAM polymer, J. Membr. Sci. 550 (2018) 198–207.

CHAPTER 7. CONCLUSIONS AND RECOMMENDATIONS

7.1. Conclusions

This thesis outlines the development of mixed matrix membranes for high performance gas separation. This thesis focuses on developing effective methods for tailoring the filler/polymer interface and eliminating filler/polymer interfacial defects. Based on the work in this thesis, the following conclusions are made:

(1) Surface modification of non-porous fillers by grafting a compatible polymer can effectively improve both the interfacial adhesion and dispersion of the filler in the polymer matrix. Being grafted onto the surface of nanodiamond particles, the low-molecular weight polyethyleneimine (PEI) acts as the "interfacial bridge", improving the compatibility between nanodiamond and the Pebax polymer matrix. The introduction of PEI also significantly improved the ideal selectivity of CO_2/N_2 due to the "CO_2 carrier" role of the PEI, paving the pathway for CO_2 to improve its permeation through the membrane, as well as resisting the diffusion of N_2. This method of modification provides the potential for applying inexpensive, non-porous fillers into membrane gas separation.

(2) The morphology and dimension of a filler can significantly impact the interfacial adhesion and gas separation performance of the resultant MMM. MMMs based on conventional polyhedral ZIF67 (P-ZIF) showed improvement in gas permeability but a decline in gas selectivity when compared to the pure polymer membrane because of the poor interfacial adhesion between P-ZIF and the polymer matrix. Both ZIF nanorod (R-ZIF) and leaf shaped nanosheet (L-ZIF) exhibited better interfacial adhesion with the polymer matrix compared to the P-ZIF, leading to the improvement in membrane gas separation efficiency. Compared to R-ZIF MMMs, L-ZIF MMMs showed higher gas selectivity while sacrificing gas permeability. Based on the results, ZIF nanorod and nanosheet can be consider as superior filler candidates for the gas separation MMM application.

(3) Introducing ionic liquid as the third component is an effective method in tailoring the polymer/filler interface in the MMMs. The IL-immobilized rod-shape ZIF (R/IL) displayed improved adhesion with the polymer matrix compared to the original R-ZIF. The MMMs containing R/IL exhibited improvement in both CO_2 and C_3H_6 permeability as well as the CO_2/N_2, CO_2/CH_4 and C_3H_6/C_3H_8 selectivity compared to the R-ZIF MMMs without IL incorporation. This was also true for 50:50 gas mixtures of CO_2/CH_4. Importantly, this IL decoration method can be

applied to MMMs with micron sized fillers. Compared to the unmodified micron sized P-ZIF, the IL-decorated P-ZIF showed much better adhesion with the polymer matrix, while the PZ/IL MMMs exhibited significant improvement in gas separation performance. The volume fraction of non-selective voids in MMMs were significantly reduced after the incorporation of IL, which was clearly indicated in the FIB-SEM observations.

In summary, mixed matrix membranes show great potential to overcome or at least improve the trade-off between permeability and selctivity seen in pure polymer membranes. Surface-grafting a compatible polymer, selecting a filler with an appropriate morphology and dimensions, and applying ionic liquid as the interfacial binder are effective methods to address the issue of improper interfacial adhesion between fillers and polymers in MMM fabrication.

7.2. Recommendations for future work

(1) The effects of water vapour on gas separation performance and the polymer/filler interface of MMMs can be further studied. The presence of water vapour can decrease the gas permeability and selectivity of the MMMs because of the competitive sorption and free volume occupation in the membranes [1,2]. In industrial mixed-gas separation, the presence of water vapour is unavoidable, thus understanding the transport mechanism of water vapour through MMMs is necessary in order to prevent or even utilize water vapour for maintaining the gas permeability as well as selectivity.

(2) Modifying the polymer matrix with methods such as crosslinking, grafting, blending, copolymerization, in order to design a desirable polymer structure for better interaction with the fillers in the MMM fabrication. In comparison with filler modification, there are more varied options available in polymer modification. Altering the molecular structure of the polymer can affect the packing and rigidity, which will tailor the diffusivity of gases through the membrane and achieve improvement in gas separation efficiency.

(3) Plasticization of the membrane occurs when the polymeric membrane is operated under high pressure or high concentration of CO_2 for long periods of time, causing the increase in free volume and mobility of molecular segments, leading to the deterioration in gas selectivity [3,4]. It is worth investigating this phenomenom as it relates to the long term stability of the membrane in gas separation. Interfacial modification methods will have positive effects in supressing the plasticization as the incorporation of filler and the improvement in polymer/filler interaction can restrict the mobility of the polymer chains.

(4) Development of asymmetric membrane or hollow fiber membrane which contains an ultrathin selective-layer of mixed matrix membrane on a porous support is worth studying. Fabricating such a thin film is currently extremely challenging due to the polymer/filler incompatibility, hence effective aproaches for eliminating interfacial defects and maintaining the mechanical strength of the membrane will be required.

References

[1] G.Q. Chen, S. Kanehashi, C.M. Doherty, A.J. Hill, S.E. Kentish, Water vapor permeation through cellulose acetate membranes and its impact upon membrane separation performance for natural gas purification, J. Membr. Sci. 487 (2015) 249–255.

[2] G.Q. Chen, C.A. Scholes, C.M. Doherty, A.J. Hill, G.G. Qiao, S.E. Kentish, Modeling of the sorption and transport properties of water vapor in polyimide membranes, J. Membr. Sci. 409–410 (2012) 96–104.

[3] J.K. Adewole, A.L. Ahmad, S. Ismail, C.P. Leo, Current challenges in membrane separation of CO_2 from natural gas: A review, Int. J. Greenh. Gas Control. 17 (2013) 46–65.

[4] M.M. M. Roussenova A. Alam, J. Ubbink, Plasticization, antiplasticization, and molecular packing in amorphous carbohydrate-glycerol matrices, Biomacromolecules. 11 (2010) 3237–3247.

Appendix

Table S1. CO_2/N_2 separation data for selected MOFs based MMMs reported in literature

MMMs	Loading (wt.%)	Pressure	Temperature (°C)	P_{CO2}	$\alpha_{CO2/N2}$	Ref
IL/6FDA-TeMPD	33	-	30	7.33	30	[1]
IL/6FDA-TeMPD	75	-	30	431	30	[1]
-NH_2-MIL-125(Ti)/Matrimid	15	9 bar	35	9.5	36	[2]
-NH_2-MIL-125(Ti)/Matrimid	30	9 bar	35	24	33	[2]
CuBTC/Polyimide	3	10 bar	25	65	6	[3]
CuBTC/Polyimide	6	10 bar	25	37	6	[3]
ZIF-94/6FDA-DAM	40	4 bar	25	2310	24	[4]
ZIF-8/Matrimid	10	10 bar	35	25	17	[5]
ZIF-8/Matrimid	20	10 bar	35	25	22	[5]
ZIF-8/Matrimid	30	10 bar	35	27	23	[5]

Table S2. CO_2/CH_4 separation data for selected MOFs based MMMs reported in literature

MMMs	Loading (wt.%)	Pressure	Temperature (°C)	P_{CO2}	$\alpha_{CO2/CH4}$	Ref
NH_2-MIL-53/6FDA-ODA	32	10 bar	35	14.6	78	[6]
NH_2-MIL-101/6FDA-durene-SDA	10	3 bar	35	151	29.6	[7]
NH_2-MIL-101/6FDA-DSDA-durene-SDA	10	3 bar	35	70.9	41.6	[7]
ZIF-8/6FDA-durene	20	10 bar	35	1090	12.96	[8]
ZIF8/6FDA-durene-	20	10 bar	35	892	18.84	[8]

DABA(9/1)						
ZIF-8/6FDA-durene-DABA(7/3)	20	10 bar	35	698	25.84	[8]
ZIF-8/6FDA-durene	33.3	3.5 bar	35	1552	11.06	[9]
ZIF-90/6FDA-DAM	15	2 bar	25	800	26.6	[10]
UiO-66/6FDA-ODA	25	10 bar	35	50.4	46.1	[11]
NH_2-MIL-53/6FDA-DAM-HAB(1/1)	10	150 psi	35	47.1	78.5	[12]
ZIF-71/6FDA-durene	10	3.5 bar	35	1606	20	[13]
ZIF-71/6FDA-durene	20	3.5 bar	35	3435	16	[13]
NH_2-MIL-53(Al)/6FDA-DAM	20	3 bar	25	660	28	[14]
ZSM-5/IL/6FDA-durene	Zeolite: 15% of polymer; IL: 9% of polymer	1 bar	35	441	21	[15]

Table S3. C_3H_6/C_3H_8 separation data for selected MOFs based MMMs reported in literature

MMMs	**Loading (wt.%)**	**Pressure**	**Temperature (°C)**	$\mathbf{P_{C3H6}}$	$\boldsymbol{\alpha_{C3H6/C3H8}}$	**Ref**
ZIF-67/6FDA-durene	10	2 bar	35	24.52	19.6	[16]
ZIF-67/6FDA-durene	20	2 bar	35	34.14	29.9	[16]
ZIF-8/6FDA-durene	10	2 bar	35	26.10	16.3	[16]
ZIF-8/6FDA-durene	20	2 bar	35	37.73	20.7	[16]
ZIF-8/6FDA-durene/DABA	10	3.5 bar	35	17.1	14.9	[8]
ZIF-8/6FDA-durene/DABA	20	3.5 bar	35	20.5	18.1	[8]
ZIF-8/6FDA-durene/DABA	30	3.5 bar	35	29.7	23.3	[8]
ZIF-8/6FDA-durene/DABA	40	3.5 bar	35	47.3	27.4	[8]

ZIF-8/6FDA-DAM	16.4	2 bar	35	27.6	18.8	[17]
ZIF-8/6FDA-DAM	28.7	2 bar	35	39.8	24.4	[17]
ZIF-8/6FDA-DAM	48	2 bar	35	56.2	31.0	[17]

Single gas permeation test

The single gas permeation test was conducted as described in Figure S1. The membranes were held in a stainless steel cell under vacuum for 30 min to achieve a steady state before being exposed to the selected gas. The test was held at 30 ^{o}C, 2 atm feed pressure. Each single gas was fed in the retentate side of the membrane cell and the change of gas pressure in the permeate side was recorded continuously every 3 seconds over 2 hours. The test for each gas was repeated no less than 3 times with each sample to confirm the reproducibility of the results.

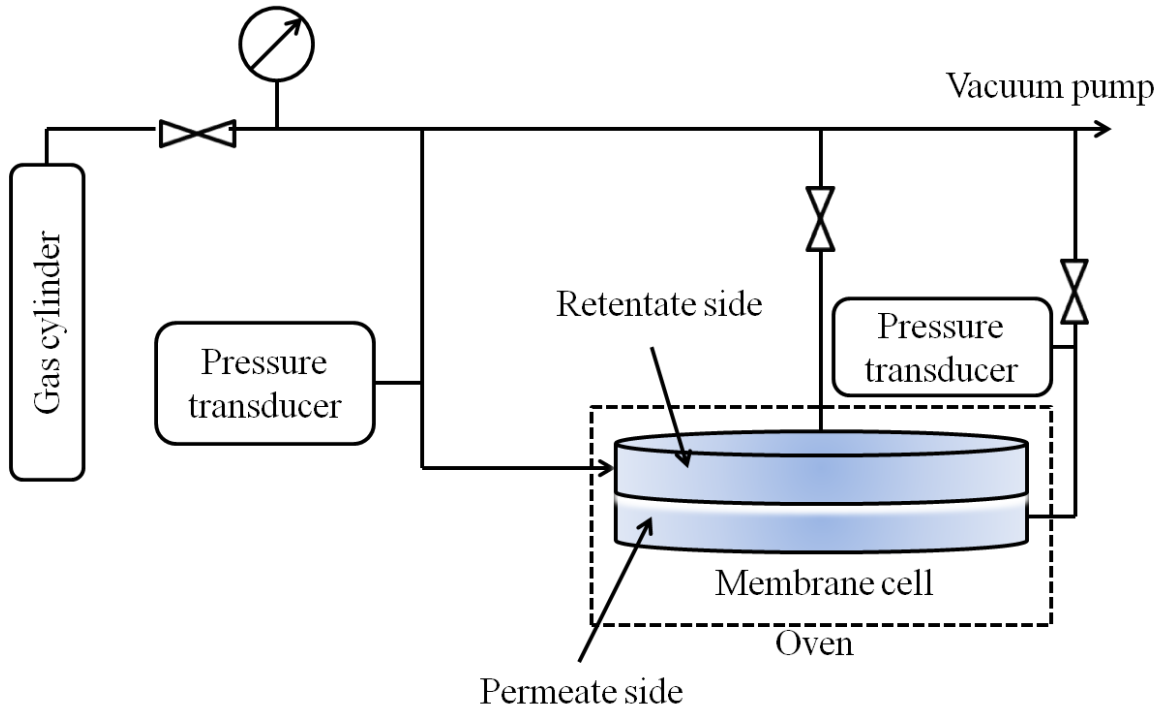

Fig. S1. Schematic diagram of the single gas permeation test

The permeation coefficient is calculated using the following equation:

$$P = \frac{273.15\times10^{10}}{760\mathrm{AT}} \frac{VL}{\frac{P_0\times76}{14.7}} \frac{\mathrm{d}p}{\mathrm{d}t}$$

where P is the permeation coefficient in barrer (1 barrer =1×10^{-10} cm^3 (STP) cm cm^{-2} s^{-1} cm Hg^{-1}), A is the effective area of the membrane (cm^2), T is the absolute temperature (K), V is the dead-volume of the downstream chamber (cm^3), L is the membrane thickness (cm), P^0 is the feed pressure (psi), and dp/dt is the steady rate of pressure increase in the downstream side (mm Hg s^{-1}).

The ideal selectivity for two gases is determined as:

$$\alpha = \frac{P_A}{P_B}$$

where P_A and P_B are the permeation coefficients of pure gas A and B, respectively.

Mixed gas permeation test

The mix-gas permeation test was carried out with a CO_2/CH_4 (50/50) mixture gas provided by Coregas Pty Ltd. The membrane sample was firstly fixed onto the membrane cell and the whole system was vacuumed to remove residual gases. The temperature of the permeation system was kept at 30°C by the oven. The feed gas was inserted to the upstream chamber at 3 bar, and the gas at the permeate side was swept by Argon (1 bar). The composition of gas in the permeate chamber was collected and analyzed by gas chromatography (Shimazu) to calculate the permeability of each components. The measurements was repeated no less than 3 times to confirm the reproducibility of the results.

In order to build up the calibration curves for the GC with CO_2 and CH_4 gases, each single gas cylinder of CO_2 and CH_4 was used instead of the CO_2/CH_4 mixed gas cylinder. The GC calibration curve was built based on the peak intensity ratios of CO_2/CH_4 achieved at different flow rate ratios controlled by MFC.

For the mixed gas, the intensities of both CO_2 and CH_4 gases were collected and the intensity ratios were calculated. These values were compared with the calibration curve to identify the CO_2/CH_4 ratios in the permeate side of the membrane cell, thus achieved the CO_2/CH_4 mixed gas selectivity of the MMMs.

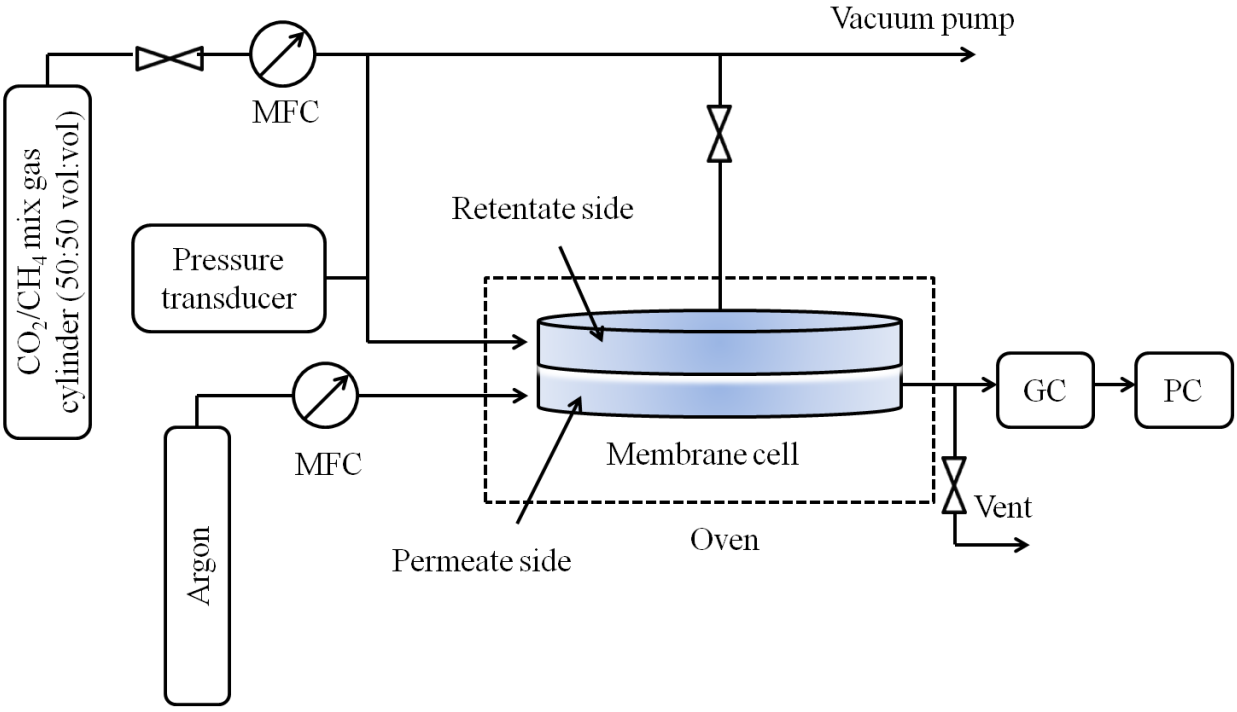

Fig. S2. Schematic diagram of the mixed gas permeation test

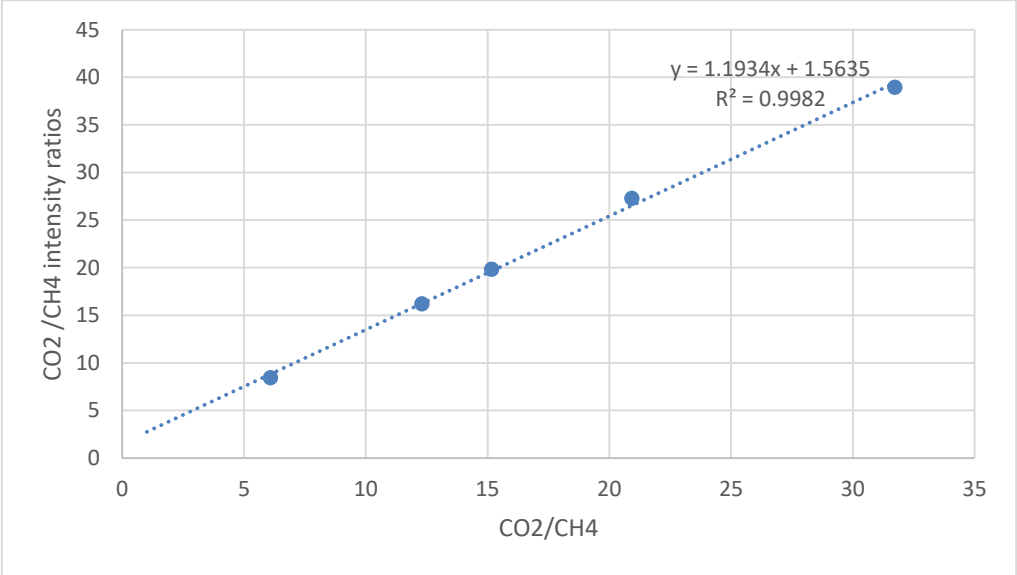

Fig. S3. Calibration curve of GC with CO_2 and CH_4 gas

References

[1] A. Ito, T. Yasuda, T. Yoshioka, A. Yoshida, X. Li, K. Hashimoto, K. Nagai, M. Shibayama, M. Watanabe, Sulfonated Polyimide/Ionic Liquid Composite Membranes for CO_2 Separation: Transport Properties in Relation to Their Nanostructures, Macromolecules. 51 (2018) 7112–7120.

[2] M. Waqas Anjum, B. Bueken, D. De Vos, I.F.J. Vankelecom, MIL-125(Ti) based mixed matrix membranes for CO_2 separation from CH_4 and N_2, J. Membr. Sci. 502 (2016) 21–28.

[3] J. Hu, H. Cai, H. Ren, Y. Wei, Z. Xu, H. Liu, Y. Hu, Mixed-matrix membrane hollow fibers of $Cu_3(BTC)_2$ MOF and polyimide for gas separation and adsorption, Ind. Eng. Chem. Res. 49 (2010) 12605–12612.

[4] M. Etxeberria-Benavides, O. David, T. Johnson, M.M. Łozińska, A. Orsi, P.A. Wright, S. Mastel, R. Hillenbrand, F. Kapteijn, J. Gascon, High performance mixed matrix membranes (MMMs) composed of ZIF-94 filler and 6FDA-DAM polymer, J. Membr. Sci. 550 (2018) 198–207.

[5] S. Basu, A. Cano-Odena, I.F.J. Vankelecom, MOF-containing mixed-matrix membranes for CO_2/CH_4 and CO_2/N_2 binary gas mixture separations, Sep. Purif. Technol. 81 (2011) 31–40.

[6] X.Y. Chen, H. Vinh-Thang, D. Rodrigue, S. Kaliaguine, Amine-functionalized MIL-53 metal-organic framework in polyimide mixed matrix membranes for CO_2/CH_4 separation, Ind. Eng. Chem. Res. 51 (2012) 6895–6906.

[7] B. Seoane, C. Téllez, J. Coronas, C. Staudt, NH_2-MIL-53(Al) and NH_2-MIL-101(Al) in sulfur-containing copolyimide mixed matrix membranes for gas separation, Sep. Purif. Technol. 111 (2013) 72–81.

[8] M. Askari, T.S. Chung, Natural gas purification and olefin/paraffin separation using thermal cross-linkable co-polyimide/ZIF-8 mixed matrix membranes, J. Membr. Sci. 444 (2013) 173–183.

[9] S.N. Wijenayake, N.P. Panapitiya, S.H. Versteeg, C.N. Nguyen, S. Goel, K.J. Balkus, I.H. Musselman, J.P. Ferraris, Surface cross-linking of ZIF-8/polyimide mixed matrix membranes (MMMs) for gas separation, Ind. Eng. Chem. Res. 52 (2013) 6991–7001.

[10] T.H. Bae, J.S. Lee, W. Qiu, W.J. Koros, C.W. Jones, S. Nair, A high-performance gas-separation membrane containing submicrometer-sized metal-organic framework crystals, Angew. Chemie - Int. Ed. 49 (2010) 9863–9866.

[11] O.G. Nik, X.Y. Chen, S. Kaliaguine, Functionalized metal organic framework-polyimide mixed matrix membranes for CO_2/CH_4 separation, J. Membr. Sci. 413–414 (2012) 48–61.

[12] N. Tien-Binh, H. Vinh-Thang, X.Y. Chen, D. Rodrigue, S. Kaliaguine, Polymer functionalization to enhance interface quality of mixed matrix membranes for high CO_2/CH_4 gas separation, J. Mater. Chem. A. 3 (2015) 15202–15213.

[13] S. Japip, H. Wang, Y. Xiao, T.S. Chung, Highly permeable zeolitic imidazolate framework (ZIF)-71 nano-particles enhanced polyimide membranes for gas separation, J. Membr. Sci. 467 (2014) 162–174.

[14] A. Sabetghadam, B. Seoane, D. Keskin, N. Duim, T. Rodenas, S. Shahid, S. Sorribas, C. Le Guillouzer, G. Clet, C. Tellez, M. Daturi, J. Coronas, F. Kapteijn, J. Gascon, Metal Organic Framework Crystals in Mixed-Matrix Membranes: Impact of the Filler Morphology on the Gas Separation Performance, Adv. Funct. Mater. 26 (2016) 3154–3163.

[15] R. Shindo, M. Kishida, H. Sawa, T. Kidesaki, S. Sato, S. Kanehashi, K. Nagai, Characterization and gas permeation properties of polyimide/ZSM-5 zeolite composite membranes containing ionic liquid, J. Membr. Sci. 454 (2014) 330–338.

[16] H. An, S. Park, H.T. Kwon, H.K. Jeong, J.S. Lee, A new superior competitor for exceptional propylene/propane separations: ZIF-67 containing mixed matrix membranes, J. Membr. Sci. 526 (2017) 367–376.

[17] C. Zhang, Y. Dai, J.R. Johnson, O. Karvan, W.J. Koros, High performance ZIF-8/6FDA-DAM mixed matrix membrane for propylene/propane separations, J. Membr. Sci. 389 (2012) 34–42.